2699/3

CRACK GROWTH PROCESSES AT ELEVATED TEMPERATURES IN ADVANCED MATERIALS

By

David L. Davidson
Kwai S. Chan
James Lankford

AFOSR FINAL REPORT

This research was sponsored by the Air Force Office of Scientific Research,
Electronic and Materials Sciences Directorate
Under Contract F49620-89-C-0032

Approved for release; distribution unlimited

*Original contains color plates: All DTIC reproductions will be in black and white.

February 1992

SOUTHWEST RESEARCH INSTITUTE
SAN ANTONIO HOUSTON
DETROIT WASHINGTON, DC

DISCLAIMER NOTICE

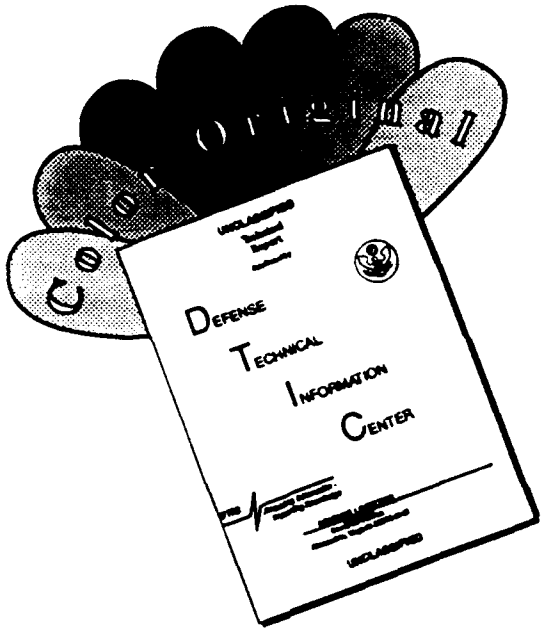

THIS DOCUMENT IS BEST QUALITY AVAILABLE. THE COPY FURNISHED TO DTIC CONTAINED A SIGNIFICANT NUMBER OF COLOR PAGES WHICH DO NOT REPRODUCE LEGIBLY ON BLACK AND WHITE MICROFICHE.

UNCLASSIFIED

SECURITY CLASSIFICATION OF THIS PAGE

REPORT DOCUMENTATION PAGE

Form Approved OMB No. 0704-0188 Exp.Date: Jun 30, 1986

1a. REPORT SECURITY CLASSIFICATION UNCLASSIFIED	1b. RESTRICTIVE MARKINGS
2a. SECURITY CLASSIFICATION AUTHORITY	3. DISTRIBUTION/AVAILABILITY OF REPORT Approved for public release; distribution unlimited
2b. DECLASSIFICATION/DOWNGRADING SCHEDULE	
4. PERFORMING ORGANIZATION REPORT NUMBER(S) 06-2699/3	5. MONITORING ORGANIZATION REPORT NUMBER(S) F49620-[illegible]-0082 AFOSR-TR- 92 0241
6a. NAME OF PERFORMING ORGANIZATION Southwest Research Institute 6b. OFFICE SYMBOL *(If applicable)*	7a. NAME OF MONITORING ORGANIZATION Air Force Office of Scientific Research
6c. ADDRESS *(City, State, and ZIP)* 6220 Culebra Road San Antonio, TX 78228-0510	7b. ADDRESS *(City, State, and ZIP Code)* Department of the Air Force Bolling Air Force Base Washington, DC 20332
8a. NAME OF FUNDING/SPONSORING ORGANIZATION AFOSR 8b. OFFICE SYMBOL *(If applicable)* NC	9. PROCUREMENT INSTRUMENT IDENTIFICATION NUMBER F49620-89-C-0032
8c. ADDRESS *(City, State, and ZIP)* Department of the Air Force Bolling Air Force Base Washington, DC 20332	10. SOURCE OF FUNDING NUMBERS PROGRAM ELEMENT NO. 61102F; PROJECT NO. 2306; TASK NO. A5; WORK UNIT ACCESSION NO.

11. TITLE *(Include Security Classification)*

Crack Growth Processes at Elevated Temperatures in Advanced Materials

12. PERSONAL AUTHOR(S)

D. L. Davidson, K. S. Chan, and J. Lankford

13a. TYPE OF REPORT	13.b TIME COVERED	14. DATE OF REPORT *(Year, Month, Day)*	15. PAGE COUNT
Annual	FROM 1/1/91 TO 1/1/92	92/01/31	

16. SUPPLEMENTARY NOTATION

17. COSATI CODES			18. SUBJECT TERMS *(Continue on reverse if necessary and identify by block number)*
FIELD	GROUP	SUB-GROUP	Key Words: titanium aluminide alloy, fatigue crack growth, fracture toughness

19. ABSTRACT *(Continue on reverse if necessary and identify by block number)*

Research in this program during the past 3 years has emphasized fracture studies on intermetallic alloys. Most of the work was focused on alloys based on the intermetallic compounds Ti_3Al and TiAl, but some work to characterize alloys based on Nb_3Al was also accomplished. The mechanisms controlling fatigue and fracture toughness of these new materials have been determined and compared to similar knowledge for other alloys.

For a TiAl alloy with lamellar microstructure, fatigue cracks grew 10 times slower at 800°C in vacuum, and the threshold for the crack growth was higher than for 25°C in air. Growth was intermittent and crack tip opening alternated between blunt and sharp, just as found for other alloys. Crack growth was influenced by the direction of the lamellae relative to the loading axis, especially at low stresses. For crack growth perpendicular to the lamella direction, crack advance was linked to the width of the lamellae. Fatigue crack closure was about the same as for other alloys. Because of the similarity of crack growth behavior between this and other titanium alloys, a crack tip geometric model previously used for other materials was applied.

Fatigue crack growth of alloys based on Nb_3Al was difficult to measure because of the extreme resistance of the material to cracking. Great variability was found in material depending on heat treatment. Threshold for fatigue crack growth was estimated to be about $\Delta K = 5.5\ MPa\sqrt{m}$; valid fracture toughness tests were not accomplished.

20. DISTRIBUTION/AVAILABILITY OF ABSTRACT			21. ABSTRACT SECURITY CLASSIFICATION
[X] UNCLASSIFIED/UNLIMITED	[ ] SAME AS RPT.	[ ] DTIC USERS	UNCLASSIFIED

22a. NAME OF RESPONSIBLE INDIVIDUAL	22b. TELEPHONE *(Include Area Code)*	22c. OFFICE SYMBOL
Lt Dan Voss	[illegible]	NC

92 4 15 [illegible]

DD FORM 1473 84 MAR

83 APR edition may be used until exhausted.
All other editions are obsolete.

SECURITY CLASSIFICATION OF THIS PAGE

UNCLASSIFIED

DD FORM 1473 (cont'd)

ABSTRACT (cont'd)

The source of fracture toughness and the role of loading rate and environment in the fracture process of a lamellar TiAl-alloy were studied. A new toughening mechanism, dubbed shear ligament toughening due to the formation of intact ligaments in the crack wake, was identified in TiAl-base alloys. The toughening process was modeled and extended to treat roughness-induced toughness in these alloys. In addition, tensile ductility of TiAl-alloys was found to be inversely related to fracture toughness because of opposite dependence on grain (or colony) size. Both tensile ductility and fracture toughness were adversely affected by a high loading rate at 25 and 800°C, but tensile ductility was influenced by the test environment at 800°c only under a slow strain rate.

Studies of microstructure/property relationships in Ti-24Al-11Nb and Ti-47Al-2.6Nb-2(Cr + V) in this program revealed that two-phase Ti_3Al- and TiAl-alloys derive some of their fracture toughness from the ductile phase in the microstructure through a variety of toughening mechanisms including ductile-phase accommodation, blunting, bridging, crack-path tortuosity, ligament toughening, microcrack toughening, and growing crack singularity. The details and effectiveness of these mechanisms, however, vary in individual microstructures, alloys, and temperature. These toughening mechanisms were reviewed in order to elucidate microstructure/fracture toughness relationships in two-phase titanium aluminides. Possible influence of microstructure on toughening mechanisms in Ti_3Al- and TiAl-alloys is discussed, with particular emphasis on the need to control the microstructure in order to achieve the desired mechanical properties.

Table of Contents

Table of Contents (continued)

Crack Growth Processes at Elevated Temperatures in Advanced Materials

Introduction

This final report to AFOSR is unusual in that it considers a broader range of subjects than is usually covered. This report discusses in detail only the research done during 1991, with primary information on earlier work on this program given through a listing of the resulting publications. An unusual section - entitled "Perspectives on Fatigue and Fracture" - is included to present an overview of the many years of work we have expended on these subjects. That section, of course, also includes results from this and previous year's work, research from previous programs, and information taken from the literature.

Research Objectives

The primary goal of this research has been to experimentally establish the mechanisms controlling fracture and measure the parameters needed to describe the fatigue and fracture toughness characteristics of alloys and fiber reinforeced composites used in aerospace engineering applications. A longer range goal has been to use these mechanisms and measurements to create models with which to predict the fracture characteristics of new alloys based on mechanical properties and a description of the microstructure. For the composites, the goal has been similar, except that the characteristics of the reinforcing fibers and the matrix-fiber interface must also be included in characterization of the material and in mathematical models.

Background

The research results of the last three years are given in the context of previous work on fatigue and fracture toughness characteristics of many materials, starting 20 years ago with the conventional aerospace materials then in use, conventional aluminum and titanium alloys, and then moving to materials being developed for future use. The emphasis of this research has been on blending conventional methods of investigation with newly developed techniques to identify and quantify the mechanisms of fatigue crack growth and fracture toughness. Models describing those

results may then be derived from that understanding.

By comparing results from many different materials, it has been possible to gain a broader perspective on fracture than would be available from experiments made on only a few materials. Modeling of the mechanisms identified as applicable to these materials has been used to assist in increasing the breadth of results and to provide the basis for a predictive capability. The breadth of microstructures investigated may be seen from a listing, **Table 1**, of the numerous materials and composites studied to date.

Table 1
Materials and Composites Studied
at SwRI

C = conventional, A = advanced, E = Experimental

No.	Material	Category	Description
Monolithic Alloys			
1	7075	C	large, pancake grained, ingot
2	7091	A	micrograined, P/M
3	Lo C steel	C	large grained ferrite, ingot
4	304 stainless	C	large grained austenite, ingot
5	Ti-6Al-4V	C	equiaxed α-β, recryst. annealed, ingot
6	CORONA-5	C	lamellar α-β, ingot
7	Al-Fe-X	A	dispersion strengthed, P/M
8	Super α2	A	equiaxed α-β, ingot
9	2411	A	equiaxed α-β, ingot
10	TiAl-based	A	equiaxed and lamellar $\alpha_2+\gamma$, ingot
11	Nb_3Al-based	E	ultrafine lamellar/dendritic, ingot
Composites			
	Matrix	Fiber	Fiber Coating
1	Ti-6Al-4V	boron	boron carbide
2	magnesium	alumina	none
3	aluminum	alumina	none
4	aluminum	aramid	fibers in epoxy
5	Ti-6Al-4V	SiC	carbon and SiC (SCS-6)

The techniques used to study the fracture characteristics of these materials have ranged from the conventional to the unique:

- Cyclic laboratory loading machines (with vacuum capability),
- SEM for fractography and microstructure,
- TEM for microstructure and replicas,
- Electron channeling for crystallography and plasticity,
- SEM cyclic loading stages for detailed mechanismistic studies, and
- Stereoimaging to quantify crack tip micromechanical parameters such as crack opening displacements and strains.
- Fractograpy by STM and AFM.

Research during the last 3 years has emphasized fracture studies on materials No. 9-11; also a detailed investigation of fatigue crack closure on an aluminum alloy was completed. The mechanisms controlling fatigue and fracture toughness of these new materials have been determined and compared to similar knowledge for other alloys. The modeling effort has examined the applicability and adequacy of previously developed models, expanded these models to incorporate new results, and developed new models based on experimental findings.

This research has emphasized experimentation on new materials while modeling has attempted to tie together results from previous work, where possible, and extend the applicability of the experimental results. The goal of this research, as with previous work, is to predict fracture properties from microstructural characteristics, at least conceptually, for new materials and to extend our knowledge of fracture processes in conventional alloys. The broader perspectives on fatigue and fracture gained during the course of this and previous programs is included in another section of this report.

SUMMARY OF RESEARCH RESULTS FOR 1991

Introduction

During the past 3 years, the main emphasis has shifted from aluminum and titanium alloys to those based on the intermetallic compounds Ti_3Al (α_2) and TiAl (γ). Most of the research on the Ti_3Al-based alloys was concluded prior to 1991, and those results have been published or are in press. The major results obtained during 1991 were for the TiAl-based alloys. Some work was also accomplished on a new alloy system based on the intermetallic compound Nb_3Al, but that work was abbreviated due to a lack of reliable material. This section summarizes research on these two alloy systems.

Fatigue crack growth at 25 and 800°C through a lamellar microstructure TiAl alloy

Introduction

The mechanisms and micromechanics of fatigue crack growth at ambient temperature through two $\alpha+\beta$ titanium alloys, Ti-6Al-4V (RA) [1] and CORONA-5, [2] and two $\alpha_2+\beta$ titanium aluminide alloys, Super Alpha 2, [3] and 2411, have been examined and compared [4]. The mechanisms of fatigue crack growth through these alloys were typified more by their similarity than by their differences. In all cases, for crack growth near threshold, a large number of cycles (ΔN) was required before crack advance (Δa). The sequence of events accompanying crack extension was observed to be similar to that found for aluminum alloys; a sharp crack blunted as the number of cycles increased, followed by crack extension and resharpening. For the $\alpha+\beta$ alloys, slip lines were observed to form at the crack tip during the blunting process, and crack advance occurred by breakdown of this slip line. For the $\alpha_2+\beta$ alloy 2411, crack blunting was observed also, but often an α_2 particle near the crack tip broke, and crack advance occurred by linking of this broken particle with the main crack tip.

All the alloys examined to date have consisted of approximately equiaxed α or α_2 particles with varying amounts of β phase in the microstructure. This section of the report covers research on fatigue crack growth through titanium alloys with a fundamentally different microstructure: a TiAl-based alloy having a mixture of $\alpha_2+\gamma$ phases. The nominal composition of the alloy tested was Ti-47Al-0.9Cr-0.8V-2.6Nb (in at.%). Processing resulted in a microstructure of $\alpha_2+\gamma$ lamellae with some regions of equiaxed γ. Dissolved oxygen was measured as 700 ppm (weight). This alloy composition with a lamellar microstructure has demonstrated useful ductility and toughness over other microstructures [5,6]. Results of a detailed investigation of fatigue crack growth at 25 and 800°C are reported.

Material and Microstructure

The microstructure of this alloy, supplied by Dr. Kim of the Metcut

Materials Research Group, is complex, and must be described on several scales. Large, approximately equiaxed regions, which appear to be grains, are visible to the unaided eye on etched samples, as seen in **Fig. 1**(a). In Fig. 1(b), these regions are seen to be colonies of lamellae. Average size of the colonies was 1.2 mm. When a mixed acid etch was used [7], some of these platelets etched and some did not, as seen in Fig. 1(c). Transmission electron microscopy (TEM), Fig. 1(d) revealed a very complex structure consisting of many wide and narrow lamellae.

From the alloy composition and the phase diagram [8], the microstructure should consist of a mixture of Ti_3Al (α_2, DO_{19}) and TiAl (γ, $L1_0$); thus, each of the lamella is one of these two phases, but it is difficult to determine the phase of each lamella. The alloy composition requires more γ than α_2, suggesting that wide lamellae are γ and some of the narrow lamellae are α_2. However, identification of individual phases is complicated by the fact that boundary lines on the phase diagram are not vertical, which means additional lamella are formed as the material cools. The work of Shong, et al. [9], on a Ti-43 at%Al alloy indicates that α, the high temperature phase, first transforms to an ordered α_2. Continued cooling causes precipitation of γ as lamellae, but Umakoshi, et al. [10], describe the transformation for a Ti-48 at.% Al process as γ forming first, followed by precipitation of α_2 lamellae. These studies indicate that the route to final microstructure very sensitive to aluminum content; cooling rate is also known to be important.

A number of TEM studies have been made of these two phase alloys to examine of the orientation relationships between the phases. The most recent report [11] indicates that four different orientation variants can form both between TiAl and adjacent Ti_3Al lamella as well as between two adjacent TiAl lamellae. The reason for this complexity is hypothesized as being due to the ability of different variants to accommodate the strain induced by transformation. Boundaries between lamellae may separate two crystallographic orientations of the same phase, or two different phases. The interfaces between adjacent lamellae, studied by Zhao and Tangri [12] using TEM, were found to contain many misfit dislocations. Twinning is one mechanism by which two adjacent γ lamellae may exist. In interfaces of

this type, three types of defect may exist. Within Ti_3Al lamellae, antiphase domain boundaries appear without preferential crystallographic orientation.

For the material used in this study, the lamellar microstructure has been characterized from secondary electron SEM images at the same magnification as shown in Fig. 1(c), assuming that α_2 etched, and γ did not. The widths of the lamellae were measured at three locations, two within the same colony. As seen from **Table 1**, the area fractions (same as volume fractions) measured were different depending on both the location within one grain and between different grains. If single phase grains of either phase exist, the volume fraction is small.

Table 1
Microstructural Characterization

Colony	1	2	2
Location	1	1	2
Fraction γ	0.44	0.65	0.45
Fraction α_2	0.56	0.35	0.55

The information in Table 1 indicates that the volume fraction of the two phases can vary between colonies as well as within a single colony. This result would agree with interpreting changes in SEM secondary electron image contrast within a single colony, shown in Fig. 1(a), as being due to differences in composition (it was determined, by translating the specimen, that the contrast was not due to electron channeling effects).

When all of the lamellae width data are considered together, the average α_2 lamella width appears to be between 0.6 and 1.4 μm, with the weight of the laths being about 1.4 μm wide. The widest γ plates are wider than the widest α_2 plates. These data should be interpreted within the context of the limited resolution of secondary electron images from etched samples, which does not allow counting of plates less than about 0.3 μm, and the other limitation of small sample size. Even with these considerations, it is clear the bulk of the lamella are less than 2 μm wide and that there is a large variation in lamellae widths. Measured lamellae dimensions of our alloy may be compared with those of Soboyejo, Deffeyes and Aswath [13]. Their material had a colony size of approximately 18 μm,

with an typical lamellae width of 0.26 μm.

At ambient temperature, tensile modulus for this material is 1.75×10^5 MPa and tensile yield was measured by Chan [14] as approximately 400 MPa (at 0.2% strain), which is typical of other measurements made for this material [5]. Strain to fracture was 0.9% (at $\approx 10^{-3}$/sec). At 800°C, modulus is 1.45×10^5 MPa, and yield was measured as 280 MPa in air, but 330 MPa in argon, at a strain rate of 1×10^{-3} /sec. [14]. Strain to fracture ranged from 1 to 9%. Work hardening coefficients at both temperatures were ≈ 0.12 at higher strains, as determined by Chan, but Rao and Tangri [15] give values of ≈ 0.09 and ≈ 0.04 at ambient and 800°C for a Ti-48 at.% alloy.

Specimen surfaces were prepared for experiments using a variety of techniques. The objective was to produce details on a fine scale in the microstructure so that measurements could be made from SEM secondary electron images, while exposing as many microstructural details as possible. Most of the specimens were polished using common metallographic proceedures, followed by etching with the previously mentioned solution [7].

In fracture studies of the type reported here, it was desirable to know the relationship between the crack plane and the crystallography of the material through which the crack is growing, but the microstructure is so fine and the crystallography so complex that no method of identifying the phase and orientation of individual lamella was found.

Experimental Methods

Fatigue cracks were grown at ambient temperatures from notches in two specimen designs: single edge notched (SEN) specimens, having a gauge section 20 mm wide and approximately 3 mm thick, and compact tension (CT) specimens, having a dimension (W) between loading hole and back surface of 16 mm and a thickness of 4.6 mm. Even with this fairly thick specimen, there were only 4-6 colonies of lamellae through the thickness specimen. Elevated temperature tests were conducted using only the SEN specimen design.

The notch from which cracks were initiated, made using a low speed

diamond saw, was approximately 0.5 mm wide and 3 mm deep for the SEN and 6 mm deep for the CT specimen. Cracks were initiated by compression-compression loading at ΔK = 30 MPa$\sqrt{m}$, R = 10 (R = minimum/maximum stress intensity). After crack initiation and some growth, cycling was changed to tension-tension loading, R = 0.1, at 10 Hz. Cracks studied at elevated temperature were initiated and grown at ambient using the same techniques.

Cracks were grown mainly in laboratory fatigue machines under ambient conditions, but transferred to a special loading stage for the SEM [16] for detailed studies. Fatigue cracks grown at 25°C were grown in air (Relative humidity approximately 50%), except for cycles applied using the SEM stage. Cracks were grown at 800°C in both the laboratory machine and the SEM stage in a vacuum of ≈1 mPa.

Results

Fatigue Crack Growth at 25°C

Fatigue crack growth in the lamellar structure is highly dependent on the orientation of the crack to the direction of the lamellae. Near to the threshold stress intensity factor for fatigue crack growth (ΔK_{th}), the application of many (thousands) of loading cycles often did not result in any crack growth. Therefore, the rates of crack growth were difficult to determine and depended strongly on the averaging process used. Furthermore, colony sizes were so large, with only 4-6 colonies through the thickness of the specimen, that observations of crack growth in individual colonies must be considered as essentially tests from single crystals.

All the fatigue crack growth rates, as measured from three specimens, regardless of the orientation between the crack and lamellae directions, is shown in **Fig. 2**, and are compared to results obtained by Soboyejo, et al. [13] under similar conditions.

These data were fit to the correlation

$$da/dN = B\,\Delta K^s \qquad (1)$$

where s = 5.7 and B = 1.9×10^{-14} m/cy. As will subsequently be shown, the

where s = 5.7 and B = 1.9×10^{-14} m/cy. As will subsequently be shown, the wide variation in the data arises, at least partially, from the detailed interaction between microstructure and the crack.

Near Threshold fatigue crack growth (Specimen 1: $4 < \Delta K < 8$ MPa$\sqrt{m}$)

Detailed information on fatigue crack tip mechanics at the lowest growth rates (near threshold) have been confined to only one lamellar orientation to date because of the difficult task of growing a crack at very low rates at various orientations relative to the lamellae. Only a crack growing parallel to lamellae in air at 10 Hz has been observed in detail.

Fatigue crack growth near the threshold has been observed to be intermittent for all of the materials studied thusfar (Al, Ti, and Fe alloys) using similar techniques, and this alloy behaved similarly. However, for the lamellar microstructure, the intermittent nature of crack advance was more exaggerate than has been observed for any other material. Coaxing the crack to grow at near-threshold values of ΔK required extreme patience and was very sensitive to the microstructure and level of ΔK used.

Intermediate crack growth rates (Specimen 2: $8 < \Delta K < 12$ MPa$\sqrt{m}$)

Crack growth in this range of ΔK, although well above the threshold, still required many cycles for crack advance and was very intermittent in growth behavior. Cracks growing approximately parallel to lamellae were mostly observed in this range.

Crack growth near fast fracture (Specimen 3: $12 < \Delta K < 22$ MPa$\sqrt{m}$)

At the high crack growth rates generated at stress intensity factors above about $\Delta K \approx 14$ MPa$\sqrt{m}$, it was possible to advance the crack into a grain where the lamellae were perpendicular to the crack plane and thus obtain data for this crack/lamellae orientation in addition to crack growth approximately parallel to the lamellae.

Crack Growth Perpendicular to Lamellae

The primary knowledge desired for this orientation was a detailed account of crack interaction with the lamellar microstructure. To obtain this

information, the crack tip region was photographed on each successive loading cycle. In order for this procedure to yield meaningful data, the cyclic stress intensity factor was periodically increased until crack growth was achieved in a relatively few number of cycles. This was accomplished by cycling a fixed number of cycles in the laboratory loading frame and then moving the specimen to the loading stage of the scanning electron microscope to continue cycling under high resolution conditions. In this process, it was discovered that the rate of crack growth was sensitive to both the frequency of cyclic loading and the environment. The crack growing at cyclic frequency of 10 Hz in air in the laboratory machine would not grow when cycled in the vacuum of the SEM at 0.3 Hz. This was confirmed by breaking the SEM vacuum and cycling the specimen in the SEM stage in air, followed by evacuation and measurement of the crack length using the secondary electron imaging mode of the SEM.

To examine in detail the mechanisms of crack growth and interaction with the microstructure, the cyclic stress intensity factor was increased in small increments while cycling in a laboratory loading frame at 0.3 Hz in vacuum ($\approx$ 1 mPa) until crack advance was being achieved in only tens of cycles. At this point the specimen was transferred to the SEM loading stage for detailed observation. The description of crack growth observed and photographed under this condition follows.

At the beginning of the detailed observation sequence, the crack at minimum load was tightly shut, as shown in **Fig. 3**(a), while the loaded crack was quite sharp, Fig. 3(b). During the next 5 cycles, the crack tip blunted, Fig. 3(c), although not much when compared to similar crack tip response in other titanium aluminide based alloys. The crack also extended approximately 0.2 μm during these 5 cycles.

On the next loading (cycle 6), the crack grew 0.8 μm and again became sharp. The next 2 cycles caused the crack to grow an additional 1.35 μm across a wide lamella (possibly gamma), resulting in a sharp crack tip, Fig. 3(e). From cycles 8 to 15, the crack tip grew 0.6 μm and blunted, Fig. 3(f), but from cycle 15 to 23, the crack grew 2.4 μm across several narrow lamellae. The crack tip was again very sharp by cycle 23. During the next 2 cycles, the crack grew 0.25 μm and blunted somewhat, and during the next 5 cycles, the crack grew another 0.5 μm and blunted even more, Fig. 3(i). On cycle 31, the crack grew 1.1 μm, resulting in a very sharp crack tip, Fig.

3(j). During the next 4 cycles, the crack branched behind the main crack tip, which ceased to be active, and another crack tip was formed and grew 2.3 μm across 5 or 6 lamella, again leaving a very sharp crack tip, Fig. 3(k). At the end of this sequence, cycle 39, the crack had grown across two wide lamella, was very sharp when loaded and tightly shut when unloaded, Fig. 3(m).

This sequence, taken at a stress intensity factor close to fast fracture, indicates that crack growth is intermittent, even at high ΔK, and that the crack still alternates between being sharp and blunt in different parts of the growth sequence. This same behavior has been observed for a number of other materials, including titanium and titanium aluminide alloys, but the crack tip blunting exhibited by the present material is smaller than for those alloys and required measurement under higher resolution conditions than previously used.

The crack growth sequence of Fig. 3 suggests that the lamellae width may be an important factor in controlling the rate of fatigue crack growth in this alloy. The crack was observed to traverse wide plates (most likely gamma) in one cycles, or at most a few cycles, while crack advance appeared to stop during blunting of the crack tip when the lamella spacing was small (probably a mixture of gamma and alpha 2 plates). However, there are other factors besides lamellae width which could also influence this behavior. The crystallographic orientation between adjacent lamellae may be important in controlling fracture resistance, as may be the sequence of γ and α_2 platelets.

Fatigue Crack Growth Parallel to Lamellae

As the fatigue crack was growing perpendicular to the lamellae direction on one side of the specimen, it was growing almost parallel to the lamellae on the other side. Converse to the behavior illustrated in Fig. 3, the fatigue crack grew on nearly every cycle. This is shown in **Fig. 4** which illustrates the elongation of the crack in just 10 loading cycles. The crack was trying to grow perpendicular to the loading axis, but grew easier in the direction of the lamellae. For the condition shown here, orientation of the lamellae was nearly parallel to the loading axis; thus, the crack jumps back and forth between growth parallel and nearly perpendicular to the lamellae direction. Since ΔK is nearly the same as for Fig. 3, the effects of lamellae

direction on crack growth behavior may be directly compared.

Average fatigue crack growth rate perpendicular to the lamellae direction, shown in Fig. 3, was 2.7×10^{-7} m/cy, while the growth rate approximately parallel to the lamella, Fig. 4, was 7×10^{-7} m/cy. However, crack growth roughly parallel to the lamellae direction is complicated by the formation of multiple crack tips, as shown in the figure. Multiple cracking and the extra energy dissipation mechanisms associated with it slows the rate of crack growth down to approximately that perpendicular to the lamellae direction.

Displacements have been measured for many of the crack tips seen in Figs. 3 and 4. Some of these results will be given in a subsequent section.

Crack Closure

Several measurements of crack opening load were made during these experiments. Measurements were made by directly observing the crack tip in the SEM. Load application caused the crack to open in Mode I near the crack mouth and quickly open in a progressive manner (peeling open) with increasing load until the crack was open near to the tip (10-20 μm). Increasing load then resulted in the crack opening the remainder of the distance to the tip, but more slowly than during initial load application. Similar behavior has been observed many times in other alloys [17], and nothing unique to this alloy was observed in the Mode I crack opening process. The parameter $U = \Delta K_{eff}/\Delta K$ was computed from maximum and minimum and opening loads. Previously, it was found that U correlated with $1/\Delta K$ [18], so the data obtained are thus plotted in **Fig. 5**. The points at U = 0 and 1 were not measured. The measured data for this alloy are sparse, but fit the concept, previously determined for five other metallic alloys and partially stabilized zirconia [19], that

$$U = 1 - K_o/\Delta K \qquad (2)$$

where K_o is the intercept at U = 0. When U = 0, $\Delta K_{eff} = 0$ and $\Delta K = \Delta K_{th}$; therefore, eq. (2) becomes

$$\Delta K_{eff} = \Delta K - \Delta K_{th} \qquad (3)$$

The data point at U = 0 came from the value of ΔK_{th} derived from crack growth tests, and my be seen to be compatible with U determined directly from measured values of opening load.

Since ΔK_{eff} has now been determined, it is possible to rewrite eq. (1) as

$$da/dN = B' \Delta K_{eff}^{s'} \quad (4)$$

Fatigue Crack Growth at 800°C

Most of the cyclic loading at elevated temperature was applied in a laboratory fatigue machine in a vacuum of ≈ 1 mPa (10^{-5} torr). The temperature of testing was achieved by radiation using a resistance heated furnace within the vacuum chamber and was measured with a thermocouple attached to the specimen gauge section.

Specimens were periodically cooled and transferred from the laboratory machine to a special hydraulic cyclic loading frame fitted with resistance heating elements which fit within the SEM, similar to the loading stage used for the ambient temperature. Thus, crack growth was observed for the same conditions of loading and temperature used in the laboratory machine. By working in vacuum, environmental effects on crack growth were minimized. Cyclic loading rates were 10 Hz in the laboratory machine and approximately 0.3 Hz in the SEM. The rate effects (or combination of rate and environmental effects) found at ambient temperature were not noticed during these experiments.

Measured fatigue crack growth rates at 800°C are shown in **Fig. 6**; shown for comparison is a line fit through the ambient data in Fig. 2. Crack growth rates at 800°C are approximately 10 times slower than at ambient temperature, and ΔK_{th} is larger. This behavior is very similar to that observed by Soboyejo, et al. [13] for a similar alloy.

Two direct measurements of the Mode I crack opening load were also made at 800°C, using the same technique as used at ambient temperature. Opening load was used to compute U, and it is graphed vs. $1/\Delta K$ in **Fig. 7**. There is some uncertainty in the opening loads measured, and these are

shown in the figure. The scatter makes it difficult from these data alone to estimate ΔK_{th} - the value derived from crack growth tests was 6.6 ± 1.5 MPa$\sqrt{m}$ - but this helps define the value of crack growth rate at 10^{-10} m/cy shown in Fig. 6. Knowing ΔK_{th}, it is, therefore, possible to determine ΔK_{eff}, eq. (9), and this has been used in subsequent analyses.

A sequence of photographs illustrating crack growth at 800°C was shown in in last year's annual report. Crack growth was found to be intermittant, as it was at ambient temperature.

Crack Tip Analyses

Measurements of crack opening displacements and displacements within the crack tip deformation region were derived from photographs made in the SEM cyclic stages at 25 and 800°C. Photographs made at minimum and maximum load were compared using stereoimaging [20] and displacements were measured with the DISMAP image processing system [21].

As for fatigue cracks in many other materials [2,3], the Mode I crack opening displacement (COD I) was related to the distance behind the crack tip (d) by

$$\text{COD I} = C_o\sqrt{d} \qquad (5)$$

where C_o is a constant. Mode I opening is defined as the opening perpendicular to the local crack path, rather than perpendicular to the loading axis; however, for many of the measurements Mode I openings were coincident with the loading axis. Mode II COD (parallel to the crack path) were also measured, but for this alloy Mode II opening was found to be small - much smaller than for any other metallic alloy studied thusfar. COD II was not found systematically to be dependent on distance from the crack tip.

The gradients of the displacements measured around the crack tip were computed to determine three elements of the in-plane strain tensor, from which the maximum shear strain ($\Delta\gamma_{max}$), the principal strains, and the effective strain ($\Delta\varepsilon_{eff}$) were computed. The Δ is used here to indicate that

these strains are the change from minimum to maximum load.

Micromechanics

Measurements were made from a large number of crack tip photographs. At 25°C, 20 analyses were made for 2.5 < ΔK < 24 MPa$\sqrt{m}$, while at 800°C, 9 analyses were made for 14 < ΔK < 59 MPa$\sqrt{m}$. These data are summarized in **Table 2** for the ambient temperature tests and are summarized in Table 3 for the 800°C measurements. Last year's Annual Report had more detail on the strain distributions for the tests at 800°C.

Table 2
Crack Tip Parameters, 25°C

ΔK MPa$\sqrt{m}$	Envn/freq. Hz	$\Delta\gamma(0)_{max}$	C_o μm
2.5	air/10	0.023	0.02
4.5	air/10	0.029	0.05
6.0	air/10	0.040	0.071
6.0	air/10	0.059	0.170
6.0	air/10	0.026	0.054
7.9	air/10	0.060	0.113
15.7	air/10	0.039	0.107
17.6	air/10	0.105	0.170
17.6	air/0.3	0.124	—
20.9	vac/0.3	0.227	0.58
20.9	vac/0.3	0.255	0.58
20.9	vac/0.3	0.146	0.50
20.9	vac/0.3	0.118	0.43
24.0	vac/0.3	0.30	0.27
24.0	vac/0.3	0.22	0.23
24.0	vac/0.3	0.19	0.19
24.0	vac/0.3	0.090	0.03

Table 3
Crack Tip Parameters, 800°C
(vacuum, 0.3 Hz)

ΔK MPa$\sqrt{m}$	Crack tip strain	C_o μm
14.2	0.0824	0.44
14.2	0.0944	0.51
17.1	0.20	0.90
17.1	0.065	0.63
17.2	0.059	0.38
17.2	0.071	0.071
21.6	0.129	0.55
28.4	0.130	2.44
56.8*	0.513	5.65

* Intense shear band formed approximately parallel to loading axis.

The relationships between C_o (which may also be defined as the CTOD), the crack tip strain, $\Delta\gamma(0)_{max}$, and ΔK_{eff} are shown in **Figs. 8 and 9**. Not all the data given in Table 2 were used in Fig. 8 because some of these measurements were made for special circumstances and were not "typical" of crack growth sequences.

A least squares fit has been made for the correlations between CTOD and crack tip plastic strain and ΔK_{eff} using the following equations. Elastic strain has been subtracted from the values given in the tables to obtain plastic strains. The symbols used are the same as for similar correlations made for other materials [4, 22,23].

$$CTOD = C\Delta K_{eff}^{q} \quad (6)$$

$$\Delta\gamma_p(0) = Ko\ \Delta K_{eff}^{r} \quad (7)$$

and these may be combined to give a relation between the crack tip plastic strain ($\Delta\gamma_p(0)$ or $\Delta\varepsilon_{eff}(0)$) and CTOD

$$\Delta\gamma_p(0) = A\ CTOD^x \qquad (8)$$

Least squares fits were used to determine values of the constants in eqs. (6) - (8), and the values derived are given in **Table 4**. The data correlations are shown in Figs. 8 and 9.

Table 4
Derived parameters for eqs. (6) - (8)

Equation	Parameter	25°C	800°C
6	C	0.0765	0.03
	q	0.282	1.26
7	Ko	0.046	0.016
	r	0.365	0.77
8	A	1.28	0.137
	x	1.29	0.61

Fractography

The fracture surfaces of specimen no. 3, tested at 25°C, were carefully examined by secondary electron contrast in the SEM. A low magnification view of the fracture surface is given in **Fig. 10**(a), which shows a large variety of features, directly related to colony size. The micrographs in Figs. 10(b) and (d) were taken directly below the surface observations of Figs. 3 and 4. These results show that the appearance of the fracture surface is dependent on the orientation of the lamellae relative to the direction of crack growth, just as were the details of crack growth observed directly.

Crack growth approximately perpendicular to the lamellae created the fracture surface shown in Fig 10 (b) and (c). This fracture surface is directly related to the growth sequence shown in Fig. 3. This study reveals that the lamellae were perpendicular to the crack growth direction, but they were at an angle of 60° the surface; thus, lamellae widths shown in Fig. 3 are enlarged by about 15%. The detail shown in Fig. 10(c) shows the same surface features crossing the entire width of a lamella, which

correlates well with the surface observation of cracking across a whole lamella width in only one or two cycles. The direction of local features varies from lath to lath, probably indicating that the local direction of crack growth was variable and depended at least partially on the crystallography of each lamella. These fractographs, together with Fig. 5 are evidence that the growth increment in fatigue is the lamella width.

Fracture features similar to those found in Fig. 10(c) were attributed by Pao, et al. [25], to "following TiAl twin interfaces and Ti_3Al interface" to produce the step-like features seen.

The lamellae widths measured from the fractographs of Fig. 10 indicate two peaks, one between 0 and 0.25 μm and another broad peak between 0.75 and 1.25 μm. These lamella widths agree well with those determined from surface measurements. Stereopairs of the fracture surface, made by tilting, show that it is relatively flat on a microscopic scale.

For crack growth on the other side of the specimen, illustrated in Fig. 10(d), the fracture surface is very rough, as would be surmised from the crack growth sequence shown in Fig. 4. Again, nearly every lamella may be individually seen and has markings which evidence growth across each lamella as one fracture event.

Discussion

It has been shown for this and similar alloy compositions that a lamellar microstructure maximizes crack growth resistance [5]. The main purpose of this research has been to understand how this microstructure controls fatigue crack advance. The direction of crack growth in this material depends on the orientation of the loading axis relative to that of the lamellae. Crack growth, which usually occurs perpendicular to the loading axis for homogeneous materials, was altered as much as 45° by lamellae orientation. This crack growth behavior is similar to that observed in continuous fiber composites; thus, this material might be considered as a class of composites formed by microstructural manipulation.

High resolution observations have shown that crack growth is not a continuous process for this material, much as has been observed for a

number of much more homogeneous microstructures, such as aluminum and titanium alloys and steels. Crack opening displacements are similar to those found for other alloys systems, as are the threshold for fatigue crack growth and crack closure measurements. Thus, the growth of fatigue cracks in this highly anisotropic microstructure has many similarities to crack growth in much more homogeneous materials, and it is logical to extend the description of crack growth physics developed for those alloys to this material.

Previous modeling efforts used to describe fatigue crack advance have been based on the concept that material within the "process zone" at the crack tip could be treated as a low cycle fatigue (LCF) specimen [23,24]. Thus, the relationship between crack tip strain, $\Delta\varepsilon_p$, and cycles to failure, ΔN, is

$$\Delta\varepsilon_p \Delta N^{\beta} = \varepsilon_c \tag{9}$$

where ε_c can be thought of as the cumulative strain required to cause failure in one loading cycle. The parameters β and ε_c can be derived from the descriptions of fatigue crack behavior given by eqs. (4) and (7) together with a relation which describes how crack advance, Δa, depends on ΔK_{eff}. That relationship is

$$\Delta a = A_o \Delta K_{eff}^{n} \tag{10}$$

In most ductile materials, Δa is the same as the striation spacing, but no striations have been detected for this material by fractography. However, direct crack tip observations, Fig. 3, have shown that unit crack advance is approximately the same as lamella width, at least for crack growth perpendicular to the lamellae direction. Thus to a first approximation, Δa is not dependent on ΔK_{eff}; $n \approx 0$. This is not so unusual, because for ductile materials, striation spacing has often been found to be approximately independent of ΔK [26,27] in the near threshold region.

The other relationship necessary to relate the LCF relation to crack tip parameters is the cyclic stress strain curve

$$\Delta\sigma/2 = K_2(\Delta\varepsilon_p/2)^{n'} \tag{11}$$

The cyclic stress-strain behavior can be approximated from the unidirectional stress-strain curve.

The following relationships between the parameters describing crack growth are derived using the model [26,27]:

$$n = n'r \tag{12}$$

$$\beta = r/(s'-n'r) \tag{13}$$

$$\varepsilon_c = K_o(A_o/B')^{\beta} \tag{14}$$

Chan [14] has measured n' ≈ 0.13 at ambient temperature and ≈ 0.15 at 800 °C. The other parameters used in deriving β and ε_c in the LCF equation are listed in **Table 5**.

Table 5
Summary of measured and derived fatigue crack parameters

Parameter	Units	25°C	800°C
n'		0.13	0.15
ΔK_{th}	MPa$\sqrt{m}$	4.2	6.6
B'	m/cy	7.8×10^{-10}	2.1×10^{-13}
s'		2.26	5.72
A_o	μm	0.6 -1.4	0.6 - 1.4
n (eq. 10)		0.05	.12
β (eq. 13)		0.14-0.21	0.12-0.20
ε_c (eq. 14)		0.13-0.17	0.12-0.14

A comparative analysis between the crack tip LCF parameters derived for this material and other alloys based on α_2 (Super α2 and 2411) [4]

indicates that β is about 1/3 the value found for the other alloys, but ε_c is about the same magnitude. This analysis, together with previous work, bridges the phases in the titanium system: $\alpha+\beta+\alpha_2+\gamma$. A more complete comparison between fatigue crack growth through these alloys will be developed elsewhere. Such a comparison is possible only because the mechanism of crack advance is basically the same for all these materials. So far as is known, the physics of crack advance is approximately the same also.

A model has been advanced [28,29] for predicting the threshold stress intensity for crack growth, ΔK_{th}, from microstructural parameters.

$$\Delta K_{th} = \sigma_y \sqrt{2\pi r_s} \qquad (15)$$

where σ_y = the yield stress and r_s is the length of a slip line extending from the crack tip at threshold. The slip line length for this material is limited by the microstructure to approximately the lamella width when the crack is growing perpendicular to the lamellar structure, but what limits slip line length is unknown for cracks growing parallel to lamellae. Using yield stresses and lamellae widths in eq. (15) gives (for ambient temperature) $0.8 < \Delta K_{th} < 1.2$ MPa$\sqrt{m}$, and for 800°C, $0.6 < \Delta K_{th} < 0.9$ MPa$\sqrt{m}$. Comparison with measured values of ΔK_{th} indicates that these values are too small by at least a factor of 5. The inhomogeniety of this material is thought to be the reason for this difference. The values calculated might be close to actual values for single colony materials, but the presence of multiple colonies having different orientations increases ΔK_{th} due to colony boundary effects. For crack growth parallel to the lamellae, slip line lengths are expected to be larger because of the lack of an inherent microstructural barrier, such as the lamellae boundaries provide. A larger slip distance raises the estimate of ΔK_{th} using eq. (15).

Fatigue crack growth rates at ambient temperature, Fig. 2, are somewhat higher than those measured by Soboyejo, et al., [13], mainly at $\Delta K > 10$ MPa$\sqrt{m}$. Their material had a smaller colony size and the lamellae width was smaller than for the material tested in this work. A comparison of crack growth rates at elevated temperature indicates much the same result - the difference in temperature could be the cause of this difference, but

that is less likely because of similar results at ambient temperature. Elevated temperature crack growth rates are about 10 times lower than at 25° for both present work and that of SDA [13].

The difference in crack growth rates at ambient temperature could be due to the difference in technique for measurement of crack length, but the most likely cause is a difference are in strain rate experienced by the material (cyclic frequency), differences in colony size, and in the dimensions of the lamellar microstructure. These differences may be a good indication of just how sensitive crack growth rates are to microstructure. Differences in elevated temperature are probably due to the same factors, but in addition, most of the SDA data were obtained in air at 700°C, while most of the present work was done in vacuum at 800°C. Thus, differences in crack growth rate may be caused by environment as well as microstructural differences.

When the direction of crack growth is approximately the same as the lamellae, has not been possible to discern whether crack was in the interface between two phases or within one of the phases. From studying photographs made from 2000 to 8000X, it appears that crack growth was within one phase in some places and along phase boundaries in others. Both fractography and dynamic observation on the specimen surface showed secondary cracking. Conversely, for crack growth perpendicular to the lamellae direction, neither fractography nor surface observation indicated that cracking occurred either in interlamella boundaries or within specific lamellae. Thus, crack bridging may have had a limited effect on crack growth in the lamellae direction, but no effect for crack growth perpendicular to the lamellae.

The detailed TEM studies of this microstructure by Tangri and coworkers [12, 15,30] has found large numbers of dislocations in the interlamellar boundaries, and these investigators believe that many of these dislocations would be glissile when stressed. They believe that this might lead to extensive cracking in the interlamellar boundaries. The results of the present work have not found much evidence of this type of cracking. However, Tangri, et al. attribute the ductility exhibited by this material to the limitations to slip caused by the lamellae widths; thus, cleavage failure is prevented by extensive slip on a few planes. Meanwhile the existing dislocation structure is activated.

As compared to fatigue cracks in other materials, crack opening displacements at ambient temperature in Mode II for this material were very small, regardless of the level of ΔK. At 800°C the Mode II component was larger. Also, the strain distribution at 25°C was much closer to that derived for a mathematical crack loaded in Mode I, while at elevated temperature, the strain distributions were closer to those observed for other materials cycled at ambient temperature [22]. These differences in strain distribution might be linked to the differences in crack growth rate, with the increase in Mode II being linked to the lower rate. Although there is uncertainty in the crack tip parameters derived using eqs. (13) and (14), as given in Table 5, there is essentially no difference between the values at 25 and 800°C, so the differences in strain distribution do not relate to the parameters used to describe crack advance.

Summary and Conclusions

Fatigue cracks were grown at 25 and 800°C in a titanium aluminide alloy heat treated to give a $\gamma + \alpha_2$ lamellar microstructure. These lamellae, having widths of $\approx$ 0.6 - 1.4 μm, were in colonies approximately 1.2 mm across. Crack growth was observed and photographed under high resolution conditions in the scanning electron microscope. Detailed analyses of crack tip regions were made using stereoimaging. The following results were obtained:

1. Fatigue crack growth rates were approximately a 10 times slower at 800°C in vacuum and the threshold for crack growth was higher than at 25°C in air.

2. Fatigue crack growth was intermittent, as has also been observed for alloys of iron and aluminum alloys and other titanium alloys.

3. Mode I crack tip opening alternated between blunt and sharp. As for other alloys, blunt crack tips had the largest strains. The level of Mode II opening exhibited by crack tips was very small at 25°C, when compared to other alloys, while at 800°C it was more typical of other alloys at ambient temperature.

4. The distributions of strain around cracks at 25°C was more like

computed for a mathematical Mode I loaded crack than for other materials tested. Strain distributions around cracks growing perpendicular to lamellae were not influenced in any noticeable way by the highly anisotropic lamellar structure, but the lamellae direction did have an effect on strain distribution when it was approximately in the same direction as the crack.

5. At low ΔK, the direction of crack growth was greatly influenced by the direction of lamellae boundaries relative to the loading axis, and crack growth was delayed by the presence of colony boundaries. Cracks appeared to grow both within lamella boundaries and inside lamellae.

6. At large ΔK, colony boundaries had much less effect on crack growth rate, and the lamellae orientation was less of an influence on the direction of crack growth. Cracks readily grew across lamellae boundaries.

7. Secondary cracking generally occurred when the crack was growing in the lamella direction at $\approx 45°$ to the loading axis. Usually, only one other crack would form in a nearby lamella, or interface between lamellae. The tip of this crack would eventually become dominant and link to the main crack. This process could retard somewhat the rapid growth of cracks at high ΔK in the lamella direction.

8. For crack growth perpendicular to the lamella direction, the increment of crack advance was linked to the width of the lamellae. Secondary cracking was a rare occurrence.

9. It is concluded from these results and other published work, that lamellae width, which is determined by heat treatment, is likely to have a large influence on fatigue crack growth behavior.

10. Crack tip behavior at 25°C was found to be influenced by environment (air vs. vacuum) and cyclic loading rate (0.3 to 10 Hz).

11. Fatigue crack closure had about the same characteristics as for other alloys. The model used to estimate ΔK_{th} from microstructure was found to be inadequate because of the influences of other microstructural features such as colony boundaries and lamella direction.

12. Because of the similarity of crack growth behavior between this other titanium alloys, a crack tip geometric model previously used for other materials was applied to this material. This model considers material at the crack tip to be failing similar to a low cycle fatigue specimen. Results using this model are compatible with those derived for other alloys.

References

1. D.L. Davidson and J. Lankford "Fatigue Crack Growth Mechanics for Ti-6Al-4V (RA) in Vacuum and Humid Air" *Metallurgical Transactions A*, 1984, v.15A, pp. 1931-1940.

2. D.L. Davidson, D. Eylon, and F.H. Froes "Microstructural and fatigue crack tip characterization of CORONA-5 and powder metallurgy Ti-6Al-4V" in **Microstructure, Fracture Thoughness and Fatigue Crack Growth Rates in Titanium Alloys**, A.K. Chakrabarti and J.C. Chesnutt, eds., TMS, Warrendale, PA, 1987, pp. 19-37.

3. D.L. Davidson, J.B. Campbell, and R.A. Page "The initiation and growth of fatigue cracks in a titanium aluminide alloy" *Metallurgical Transactions A*, 1991, v. 22A, pp. 377-391.

4. D.L. Davidson "Titanium alloys: fatigue crack growth mechanisms and crack tip micromechanics" **Microstructure/Property Relationships in Titanium Aluminides and Alloys**, Y-W. Kim and R.R. Boyer, eds., TMS, Warrendale, PA, 1991, pp. 447-461.

5. Y-W. Kim and D.M. Dimiduk "Progress in the understanding of gamma titanium aluminides" *Journal of Metals*, 1991, v.43, pp. 40-47.

6. K.S. Chan and Y-W. Kim "Fracture processes in a two phase gamma titanium aluminide alloy" **Microstructure/Property Relationships in Titanium Aluminides and Alloys**, Y-W. Kim and R.R. Boyer, eds., TMS, Warrendale, PA, 1991, pp. 179-196.

7. J.B. Campbell "An advance in powder metallugy aluminum alloy etchants" *Metallography*, 1985, v. 18, pp. 413-420.

8. J.A. Graves, L.A. Bendersky, F.S. Biancaniello, J. H. Perepezko, and W.J.

Boettinger "Pathways for microstructural development in TiAl" *Mater. Sci. and Engineering*, 1988, v. 98, pp. 265-268.

9. D.S. Shong, A.G. Jackson, and Y-W. Kim "Formation of Ti_3Al + TiAl lamellar microstructure in cast and heat treated titanium aluminides" in **Titanium Materials, Surfaces and Interfaces**, TMS, Warrendale, PA, 1991 (in press).

10. Y. Umakoshi, T. Nakano, and T. Yamane "Contribution of a single set of lamellae to the plastic behavior of TiAl crystals grown by a floating zone method" *Scripta Met. et Met.*, 1991, v. 25, pp. 1525-1528.

11. Y.S. Yang and S.K. Wu "Orientation relationships between g plates and a2 matrix in a Ti-39 at. % Al alloy" *Scripta Met. et Met.*, 1990, v. 24, pp. 1801-1806.

12. L. Zhao and K. Tangri "Transmission electron microscopy characterization of interfacial boundaries in heat-treated Ti_3Al+TiAl two phase alloy" *Phil. Mag.*, 1991, v. 64, pp. 361-386.

13. W.O. Soboyejo, J.E. Deffeyes and P.B. Aswath "Investigation of room and elevated-temperature fatigue crack growth in Ti-48Al" *Mat. Science and Engineering*, 1991, v. A138, 95-101.

14. K.S. Chan, private communication, 1991.

15. P.P. Rao and K. Tangri "Yielding and workhardening behavior of titanium aluminides at different temperatures" *Mat. Science and Engineering*, 1991, v. A132, 49-59.

16. Andrew Nagy, John B. Campbell and D.L. Davidson"A High Temperature Cyclic Loading Stage for the SEM", *Review of Scientific Instruments*, 1984, v. 55, 778-782.

17. D.L. Davidson "Fatigue Crack Closure"*Engng. Fracture Mech.*, 1991, v. 38, pp. 393-402.

18. S.J. Hudak, Jr. and D.L. Davidson "The dependence of crack closure on fatigue loading variables" **Mechanics of Fatigue Crack Closure**, J.C.

Newman and W. Elber, eds., ASTM STP-982, ASTM, Philidelphia, PA, 1988, pp. 121-138.

19. D.L. Davidson and J.B. Campbell, and J. Lankford "Fatigue crack growth through partially stabilized zirconia at ambient and elevated temperatures" *Acta Metallurgica*, v.39, 1991, pp. 1319-1330.

20. D.R. Williams, D.L. Davidson, and J. Lankford "Fatigue Crack Tip Plastic Strains by the Stereoimaging Technique" *Experimental Mechanics*, 1980, v. 20, pp. 134-139.

21. E.A. Franke, D. Wenzel and D.L. Davidson "Measurement of micro-displacements by machine vision photogrammetry (DISMAP)" *Review of Scientific Instruments* , 1991, v. 62, pp. 1270-1279.

22. D.L. Davidson "The Distribution of Strain within Crack Tip Plastic Zones, *Engineering Fracture Mechanics,* v. 25, 1988, pp. 123-132 .

23. D.L. Davidson "A Model for Fatigue Crack Advance Based on Crack Tip Metallurgical and Mechanics Parameters" *Acta Metallurgica*, v. 32, 707-714, 1984.

24. D.L. Davidson and J. Lankford "The Effects of Aluminum Alloy Microstructure on Fatigue Crack Growth" *Materials Science and Engineering*, v. 74, pp. 189-199, 1985.

25. P.S. Pao, A. Pattmaik, S.J. Gill, D.J. Michel, C.R. Feng and C.R. Crowe "Room temperature fatigue crack propagation in Ti-47Al/TiB_2 composites" *Scripta Met. et Met.*, 1990, v. 24, pp. 1895-1900.

26. N.M. Grinberg "Stage II fatigue crack growth" *Int. J. Fatigue*, 1984, v. 6, pp. 229-242.

27. H.J. Roven and E. Nes "Cyclic deformation of ferritic steel-Stage II crack propagation" *Acta Metal. et Materialia*, 1991, v. 39, pp. 1735-1754.

28. D.L. Davidson "Small and large fatigue cracks in aluminum alloys" *Acta Metallurgica*, 1988, v. 36, pp. 2275-2282.

29. D.L. Davidson "The growth of fatigue cracks through particulate SiC reinforced aluminum alloys" *Engineering Fracture Mechanics*, v. 33, 1989, pp. 965-977.

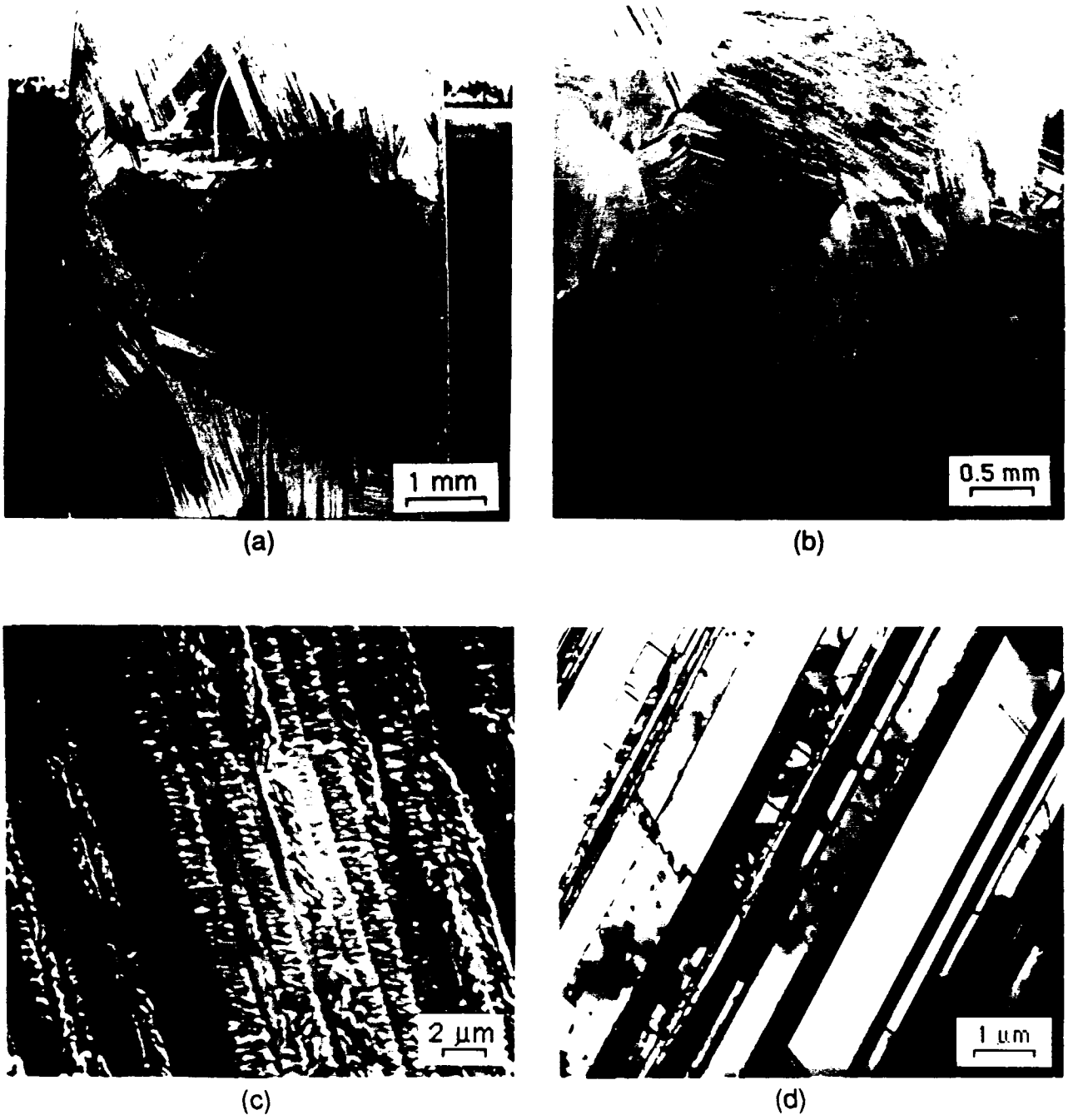

Fig. 1 Microstructure: (a) Cross-sectional view of one of the specimens tested showing large size of colonies, (b) constrast changes across colonies caused by variations in composition, (c) etched section showing lath structure. (a) -(c) are SEM secondary electron images. (d) TEM image showing interior structure of lamella and existance of many, very narrow lamellae not seen with SEM.

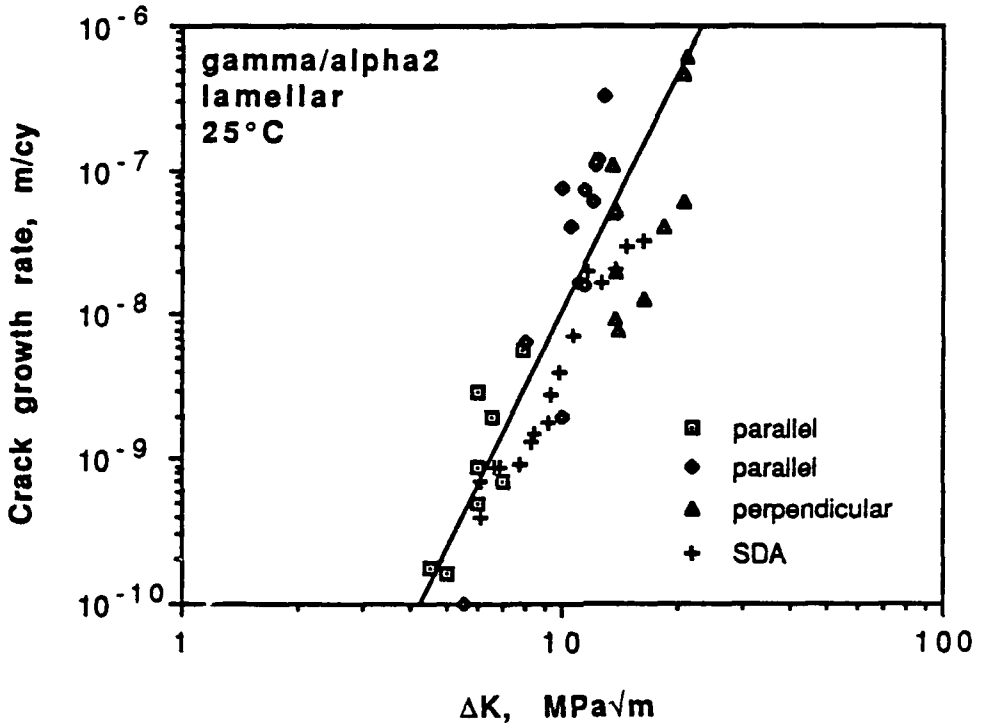

Fig. 2 Crack growth rates at ambient temperature from three specimens. Shown also are data from Soboyejo, Deffeyes and Aswath [13] .

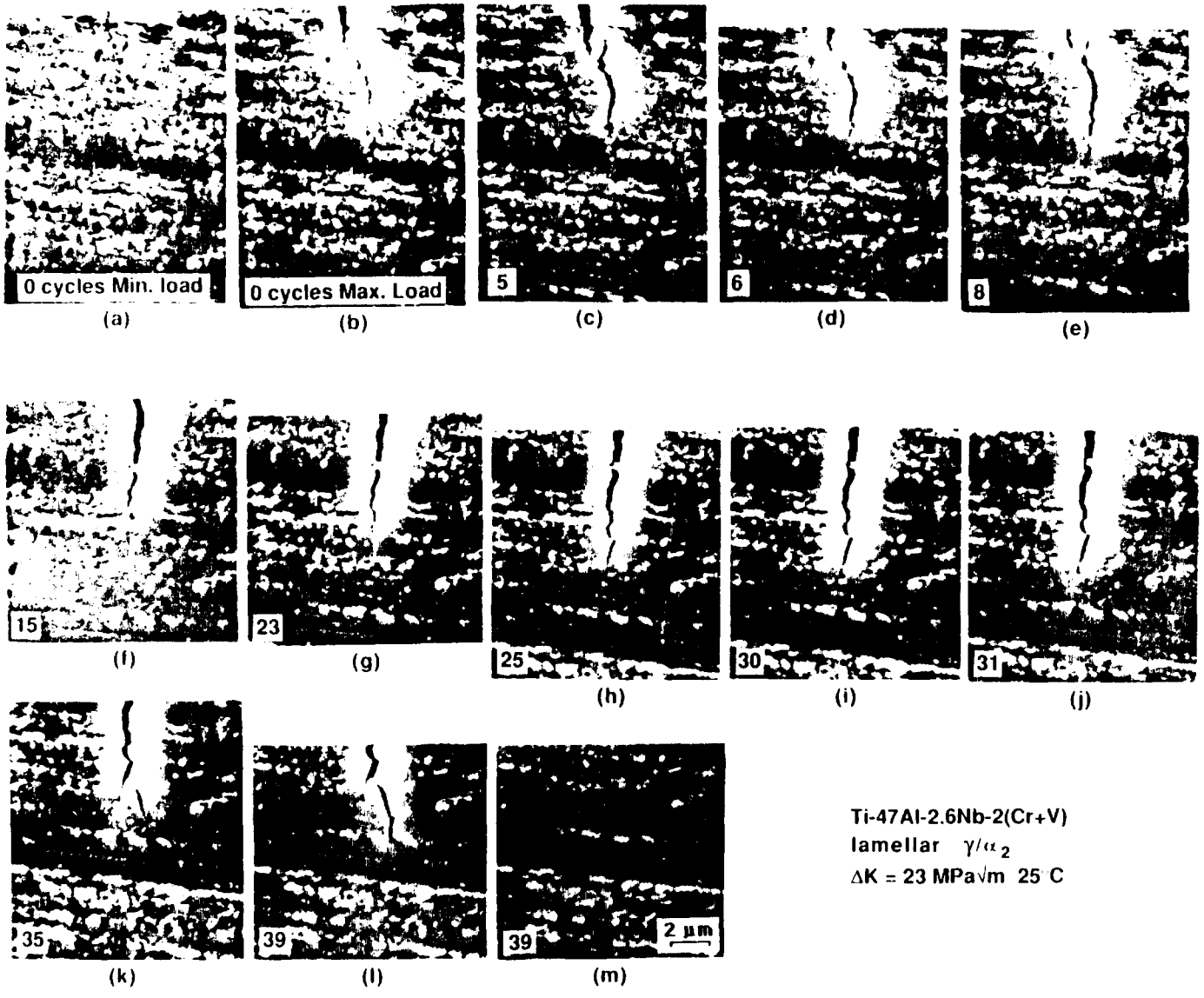

Fig. 3 Crack growth at 25°C, $\Delta K = 23$ MPa$\sqrt{m}$. Lamellae direction is almost in same direction as the loading axis. Crack in (a) is invisible at minimum load. In subsequent cycles, the crack tip progressivelyh blunts for several cycles before growing, which causes formation of a sharp crack tip. The growth increment is linked to lamellae widths.

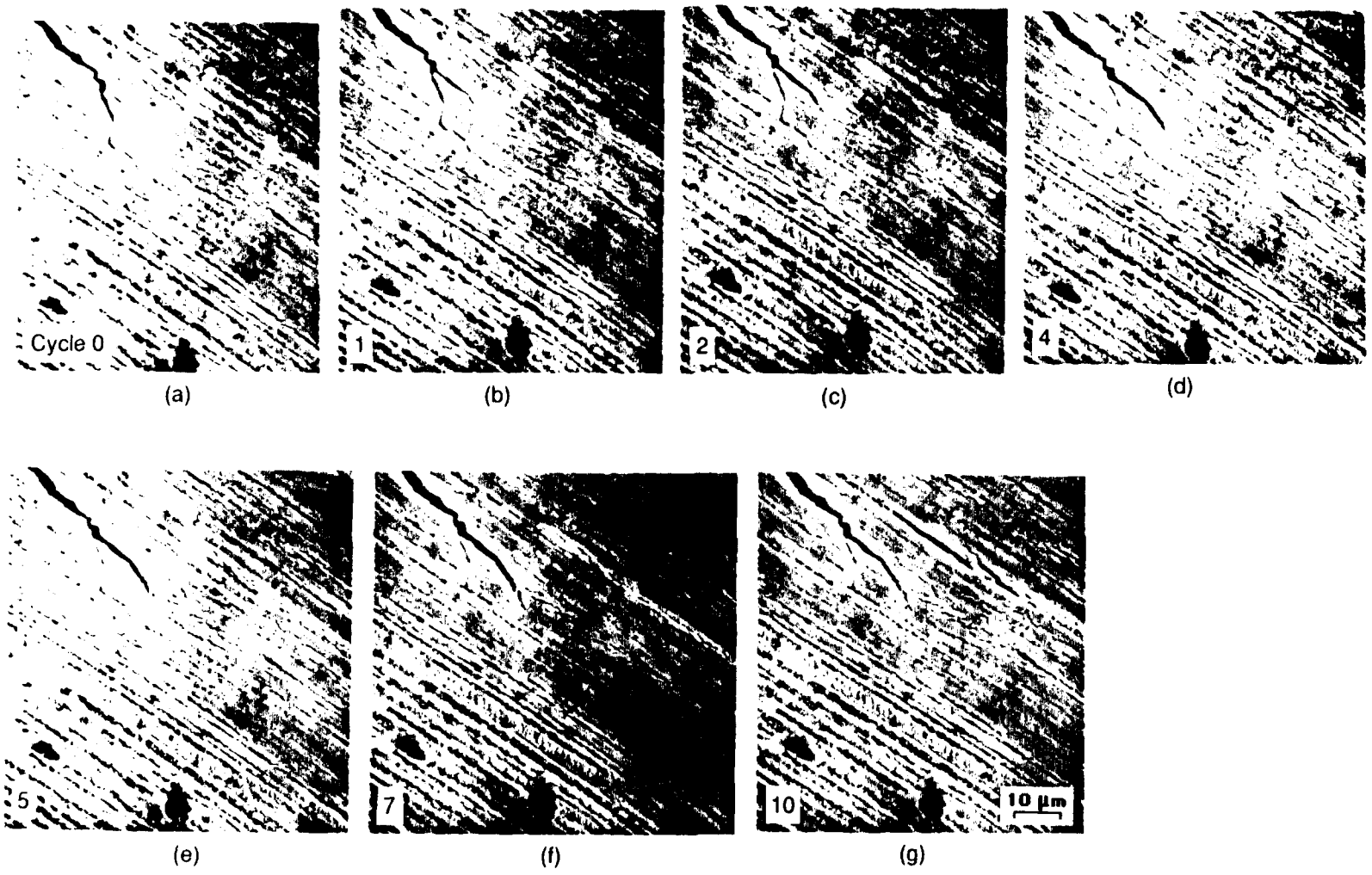

Fig. 4 Crack growth nearly parallel to lamellae direction at ambient temperature, $\Delta K = 23$ MPa$\sqrt{m}$. The angle between loading axis and lamellae direction is approximately 30°. The crack tip in (a) is overtaken by a second crack after 5 cycles, and a new crack appears in an adjacent lamella after 8 cycles.

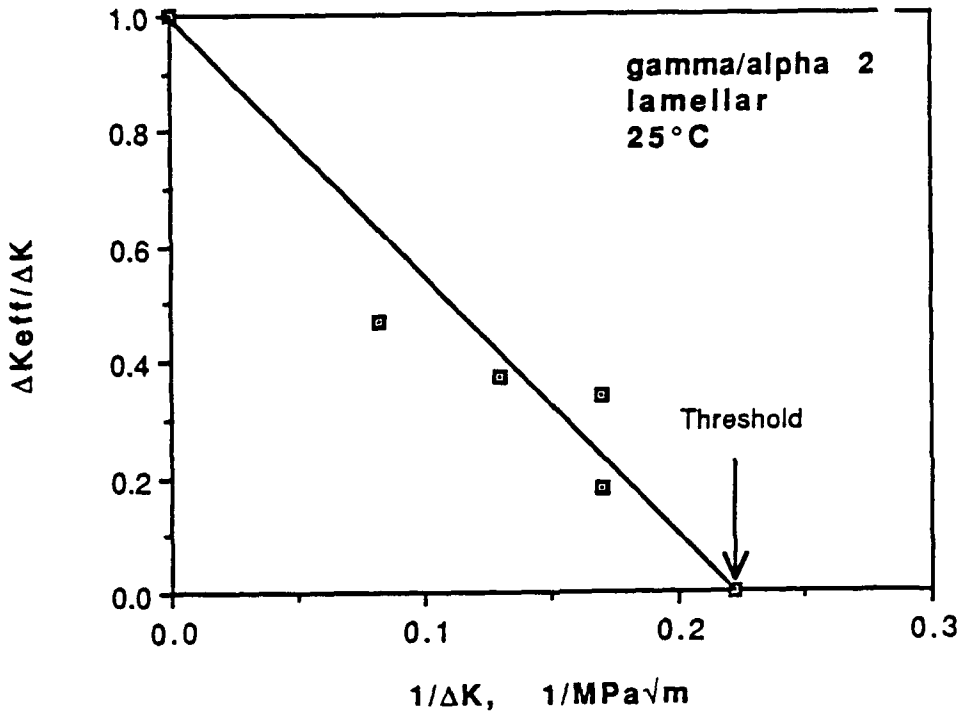

Fig. 5 Crack opening measurements at ambient temperature.

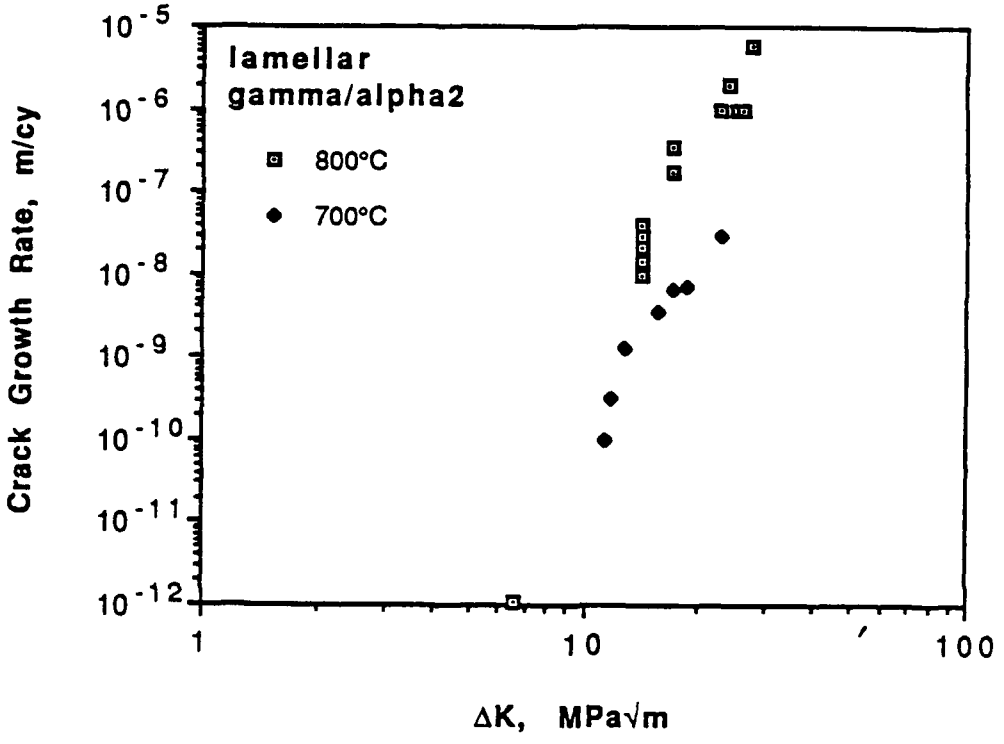

Fig. 6 Crack growth rates at 800°C, 10 Hz, in vacuum, as compared with data from Soboyejo, Deffeyes, and Aswath [13] at 700°C in a similar alloy, 25 Hz, in air.

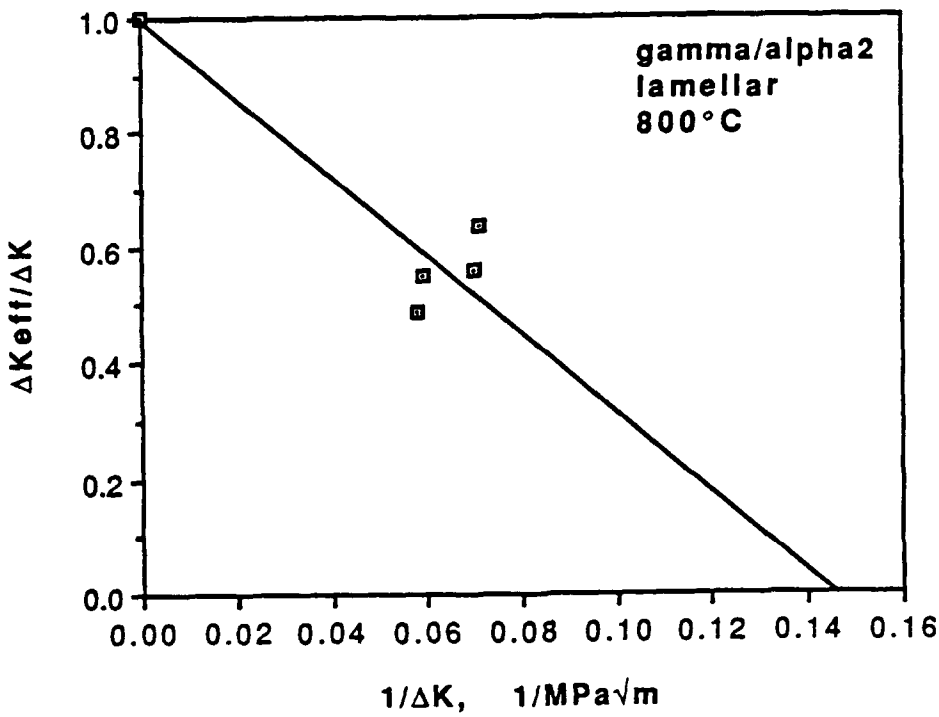

Fig. 7 Crack opening measurements at 800°C.

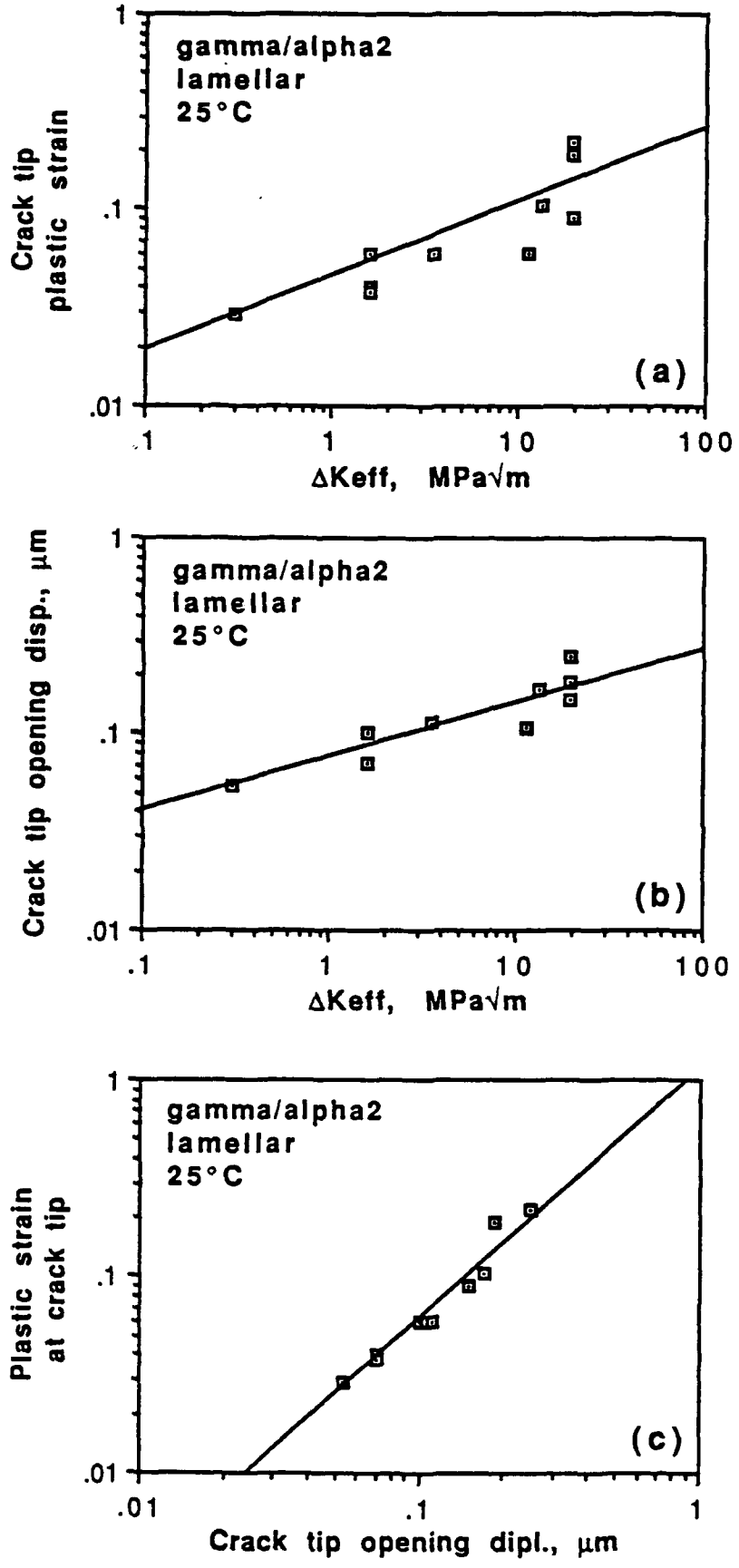

Fig. 8 Correlations of measured crack tip parameters, 25°C.

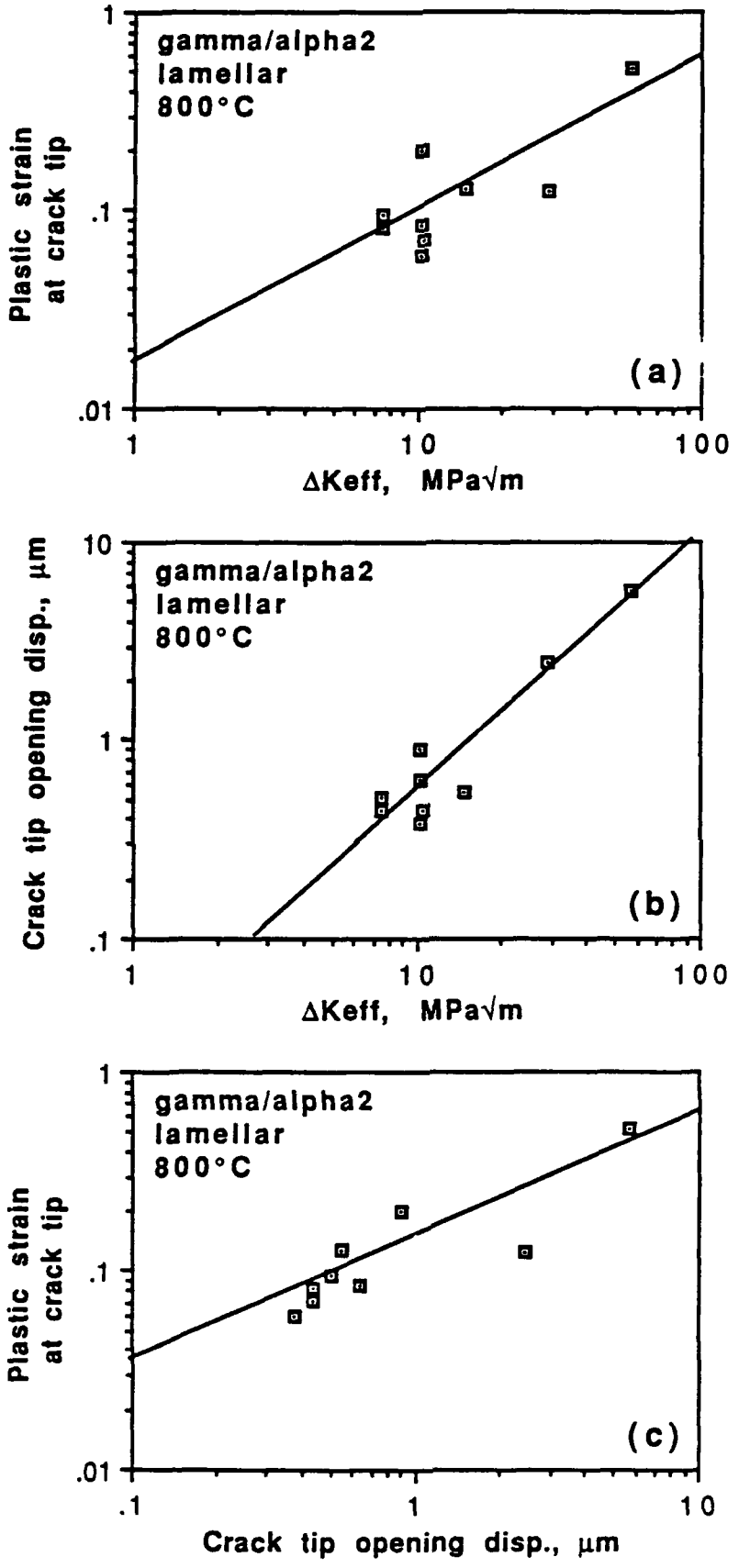

Fig. 9 Correlations of measured crack tip parameters, 800°C.

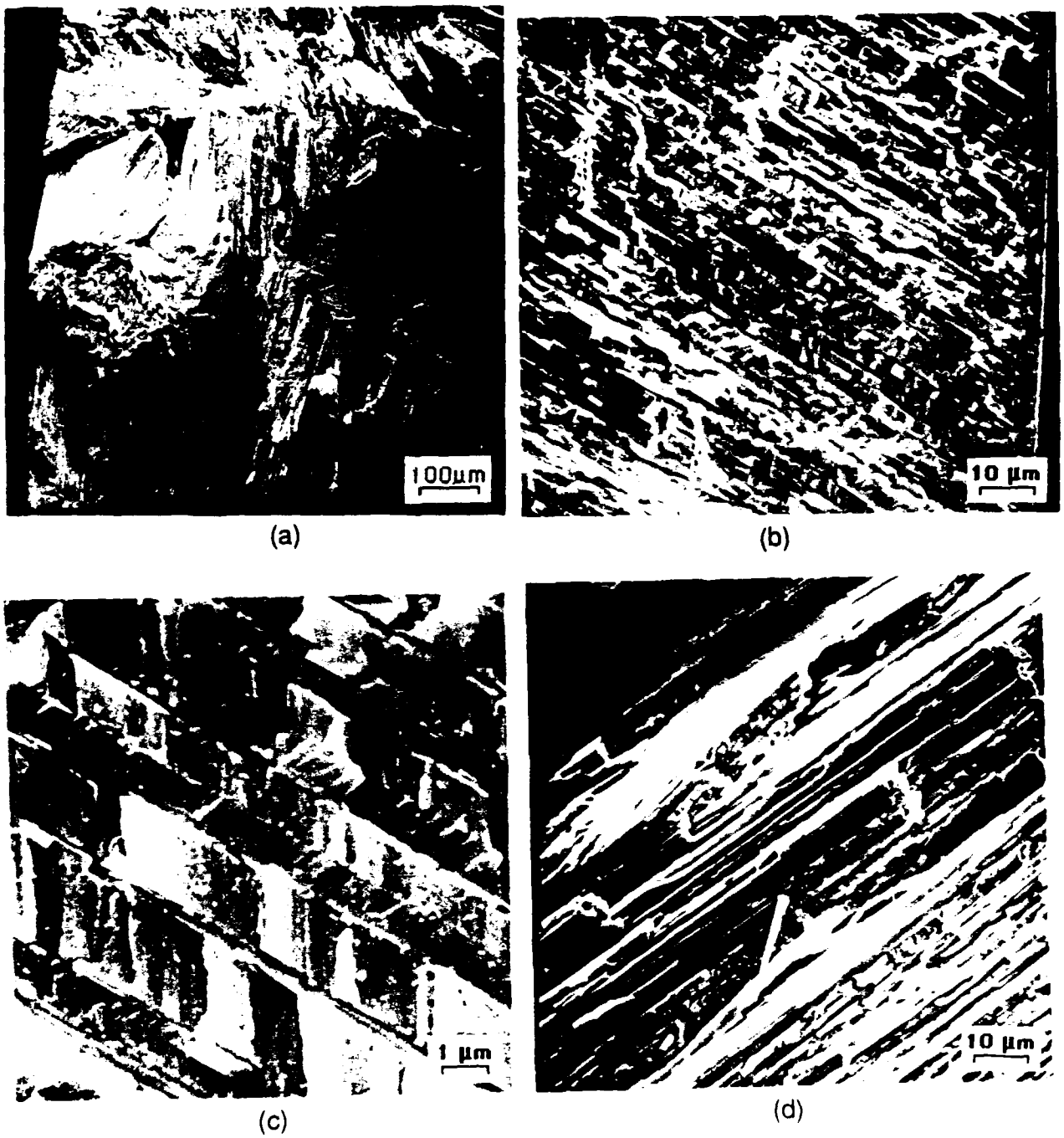

Fig. 10 Fractography of fatigue at 25°C. (a) Overall fracture surface, (b) and (c) crack growth perpendicular to lamellae, and (d) crack growth nearly parallel to lamellae.

Fracture Toughness

Introduction

Previous results obtained in this program indicated that the lamellar microstructure of the two-phase TiAl-alloy, Ti47Al-2.6Nb-2(Cr + V), exhibited a higher fracture toughness, but lower tensile ductility than the duplex microstructure [1-2]. Preliminary results also indicated that the fracture behavior of the lamellar microstructure was sensitive to the loading rate and the test environment. Efforts in the last year were therefore focused on identifying the sources of fracture toughness and the role of loading rate and test environment in the fracture process of the lamellar microstructure.

The alloy studied was the two-phase TiAl-alloy, Ti-47Al-2.6Nb-2(Cr+V), heat-treated to a microstructure consisting of lamellar colonies and about 5% equiaxed gamma grains located at colony boundaries. Designated as G1L, the alloy was supplied by Metcut-Material Research Group at Wright-Patterson AFB through Dr. Y-W. Kim.

To study toughening mechanisms, in-situ fracture tests were performed in air and in vacuum. The former was performed in a servo-hydraulic testing machine equipped with a telemicroscope and a video camera, while the latter was performed in a SEM equipped with a high-temperature loading stage. During fracture testing in air, the near-tip region of the monotonically loaded crack was videotaped at 70X magnification in order to interrogate the fracture processes ahead of the crack tip and in the crack wake. Still photographs of the near-tip region were then obtained by playing back the videotape on a monitor of a Tracor Image Analyzer. To study rate and environmental effects on fracture, conventional tensile, compression, and fracture (J_{IC}) tests were performed in air for several loading rates at 25 and 800°C. Selected tensile tests were performed in argon or vacuum environments. Fracture surfaces of selected test specimens were studied using SEM fractographic techniques. The experimental results were used in conjunction with micromechanical modeling to develop a basic understanding of the fracture and toughening mechanisms in two-phase TiAl-alloys. Key results obtained in the last year are highlighted in the following sections.

Shear Ligament Toughening

Fracture toughness in $\alpha + \beta$ Ti-alloys has generally been related to the ability of the microstructure to cause crack deflection and the tendency of the crack to meander as it zigzags between grains following planar slip bands [3-5]. As a result, the toughness in $\alpha + \beta$ Ti-alloys is frequently attributed to the tortuosity of the crack path or the

roughness of the fracture surface. Efforts in the last year revealed that the lamellar TiAl-alloy exhibited planar slip, crack deflection, and in many instances, tortuous crack paths and rough fracture surfaces. Because of these observations, toughness in this alloy could be considered to arise at least partly from crack deflection and crack-path tortuosity.

In the last year, a new toughening process, dubbed shear ligament toughening, was identified in TiAl-base titanium aluminides and used to explain roughness-induced toughness in these alloys. This toughening mechanism is based on the recognition that when a Mode I crack deflects from its original path, the angle of deflection and the plane of cracking are likely to be different among individual grains. The consequence is that the crack planes in the various grains are unconnected at either grain or phase boundaries, and are separated by ligaments, as shown in **Fig. 1**. The formation of these ligaments by mismatched crack planes might lead to an enhancement in the fracture toughness, because they must be fractured in order for total separation of the crack surfaces to occur. Since the deformation and fracture of these ligaments are likely by shear, the toughening effects of these ligaments may be referred to as shear ligament toughening. As will be shown shortly, such a fracture mechanism also leads to enhanced fracture toughness and a tortuous crack path.

The formation of shear ligaments by mismatched crack planes was observed in the lamellar TiAl-alloys, Ti-47Al-2.6Nb-2(Cr+V), at both 25 and 800°C. **Fig. 2** shows the process zone of a monotonically loaded crack in the lamellar alloy tested at 800°C in air. Five unbroken ligaments are evident within the process zone in **Fig. 2**. The manner by which shear ligament toughening occurred in the lamellar alloy at 25°C was studied in detail by in-situ fracture experiment using a telemicroscope equipped with a video camera. A complete sequence of this toughening process is presented in **Fig. 3**, which shows a series of micrographs of the near-tip fracture process zone for various K levels. As shown in **Fig. 3**, the crack started to propagate at K = 18.5 $MPa\sqrt{m}$. At K = 22.9 $MPa\sqrt{m}$, a localized shear band developed ahead of the crack tip, which eventually led to the formation of a microcrack. The microcrack crack was separated from the tip of the main crack by a ligament that was fractured by shear upon loading to K = 33.5 $MPa\sqrt{m}$. This fracture process resulted in the resistance-curve behavior shown in **Fig. 3**, and a tortuous crack path, as shown in **Fig. 4**. A key observation in **Figs. 3** and **4** is that the tortuous crack path was due to the linkage of misaligned cracks by fracture of the connecting ligaments, and not by local deflection of the tip of the main crack.

A theoretical model of shear ligament toughening was developed in this program using the J-integral approach. Details of the model development are described elsewhere [6]. The model revealed that toughness enhancement by shear ligaments increases with the area fraction, v_l, ligament size, l, and the plastic work to fracture of the ligaments, as well as the length of the process zone, L, and the angle of crack deflection, ϕ. According to this model,

$$K_c = K_m\left\{(1-v_l)\omega + v_l\Gamma_l(l/D)\left[1+\left(\frac{L}{l}\right)\tan\phi\right]\right\}^{1/2} \tag{1}$$

with

$$\omega = \frac{E(1-v_m^2)}{E_m(1-v^2)} \tag{2}$$

and

$$\Gamma_l = \frac{E\tau_l\gamma_l^* D}{(1-v^2)K_m^2} \tag{3}$$

for toughening by shear ligaments under a shear stress of, τ_l, and shear fracture strain, γ_l^*, in a material of grain size, D. In Eqs. (1) through (3), v, E, and K_c are Poisson's ratio, Young's modulus, and the critical stress intensity factor for the alloy, while the subscript m indicates quantities of the matrix. Additionally, the model was extended to treat toughening by ligaments subjected to an arbitrary stress state. For this case, Eq. (1) still applies, but Eq. (3) is replaced by

$$\Gamma_l = \frac{EW_l^* D}{(1-v^2)K_m^2} \tag{4}$$

with

$$W_l^* = \int_o^{\bar{\varepsilon}_p^*} \bar{\sigma}\, d\bar{\varepsilon}_p \tag{5}$$

where $\bar{\sigma}$ is the Mise's effective stress, and $\bar{\varepsilon}_p^*$ is effective plastic strain at fracture. For most instances, the parameter, Γ_l, can be viewed as the ratio of the toughness (work

to fracture) of the ligaments to that of the matrix. On this basis, Eq. (1) indicates that the fracture toughness (i.e., K-resistance) depends on the area fraction, size, and toughness (work to fracture) of the ligaments, as well as the process zone size and the angle of crack deflection.

It was also shown that toughening by shear or tensile ligaments was mechanically similar to ductile-phase bridging, despite the absence of bridging of crack surfaces by ductile-phase. Furthermore, the ligament toughening model was used as the basis for developing a quantitative relationship between fracture toughness, crack-path tortuosity, and the surface roughness parameter, R_s, which is the ratio of the actual surface to the projected surface. The expression obtained for the toughening ratio, K_c/K_m, due to crack path tortuosity is

$$\frac{K_c}{K_m} = \{(1 - v_l)\omega + v_l\Gamma_l(l/D)[1 + \psi(\phi, R_s)]\}^{1/2} \tag{6}$$

where

$$\psi(\theta, R_s) = \frac{\sin\phi}{\left[1 + \frac{\pi}{4}(R_s - 1)\right]\cos\phi - 1} \tag{7}$$

is a function of the surface roughness parameter, R_s, and the crack deflection angle, ϕ. **Fig. 5** shows calculated curves of the toughening ratio as a function of R_s for various values of Γ_l. The calculations reveal that fracture toughness increases with surface roughness when the toughness (or work to fracture) of the shear ligaments is larger than that of the matrix (i.e., $\Gamma_l > 1$). Under this circumstance, the shear ligaments act like a "ductile phase" reinforcement. The enhanced toughness arises from both the ductile phase (i.e., the shear ligaments) and an increase in the deformed volume as represented by the volume of the shear ligaments. On the other hand, surface roughness provides only a small toughening effect when the toughness of the ligaments is equal to or less than the matrix value. In this case, toughness is maintained primarily due to an increase in the deformed area in a rough fracture surface.

The relevance of the proposed shear ligament toughening mechanism for titanium aluminide alloys is illustrated in **Fig. 6**, which compares the K resistance curves and crack path of a two-phase TiAl-alloy, Ti-47Al-2.6Nb-2(V + Cr), in two contrasting microstructures. The microstructures of interest are: (1) the equiaxed γ microstructure, which consists of predominantly equiaxed γ grains plus a small volume fraction of

lamellar colonies and grain boundary α_2 particles, and (2) the lamellar microstructure, which is comprised mainly of lamellar $\alpha_2 + \gamma$ with a small volume fraction of equiaxed γ grains located at grain boundaries. **Fig. 6** shows that the equiaxed γ microstructure exhibits a planar crack path, a relatively low K_{IC} value, and no tearing resistance. In contrast, the lamellar microstructure manifests a higher K_{IC} value, a resistance curve behavior, a tortuous crack path, and rough fracture surfaces. The difference in the fracture behaviors of these two microstructure has been correlated with the crack-path tortuosity [6]. **Fig. 6** shows the relatively planar crack path along predominantly grain boundaries. Occasionally, mismatched crack planes with small ligaments with length on the order of 20 μm or less have been observed [6]. On the other hand, the length of the ligaments is larger in the lamellar microstructure due to a relatively large colony size ($\approx 1.6mm$). As a result, the transgranular crack path is more tortuous. There is more plastic dissipation in the lamellar microstructure, especially in the region where the crack propagation direction changes [6]. Qualitatively, the higher fracture resistance exhibited by the lamellar microstructure when compared to the equiaxed γ microstructure can be attributed to: (1) a deflected crack path, which results in shear ligaments of a relatively higher ligament length, and (2) a larger plastic dissipation contributed by fracturing of the lamellar ligaments than the equiaxed γ ligaments, i.e., a higher toughness for the lamellar ligaments.

Rate and Environmental Effects on Fracture

The tensile stress-strain curves of the lamellar alloy for ambient temperature showed no difference in behaviors between air and vacuum at the strain rate of 1×10^{-3} sec^{-1}. At this strain rate, the tensile stress-strain behavior in air and in argon at 800°C was also quite similar indicating that the test environment did not influence tensile properties of the gamma alloy at the strain rate of 1×10^{-3} sec^{-1}.

The effect of strain rate on the tensile deformation behavior at 800°C, on the other hand, was remarkable in that the tensile ductility increased significantly when the strain rate was decreased from 1×10^{-3} sec^{-1} to 1×10^{-5} sec^{-1} in air, **Fig. 7(a)**, or in argon, **Fig. 7(b)**. The results indicated that the tensile ductility of the lamellar alloy decreased with increasing strain rates at 800°C.

Tensile stress-strain curves obtained in air, argon, and vacuum at a strain rate of 1×10^{-5} sec^{-1} are compared in **Fig. 8**. The results indicated that both the strength and ductility depended on the test environment, with higher strength and ductility in vacuum than in either argon or in air. The similar tensile behaviors observed in argon and in

air could be due to the presence of small amounts of oxygen (1 wt. ppm), water vapor (3 wt. ppm), and hydrocarbons (0.5 wt. ppm) in the argon gas as impurities. The results suggested that the tensile ductility of the lamellar alloy was rate- and environment-sensitive under a relatively slow stain rate.

Fig. 9 shows comparison of the K-resistance curves at 800°C for the displacement rates of 0.0042 mm/sec and 0.042 mm/sec, which were obtained in air using standard J-testing procedures. It is apparent that the crack growth resistance of the alloy was reduced with increased displacement rate. **Fig. 9** also shows the K-resistance curve in vacuum is essentially the same as that in air under a similar displacement rate (≈ 0.0042 mm/sec). The K resistance curves of the lamellar TiAl-alloy for air and vacuum at 25°C under a displacement rate of 1×10^{-4} mm/sec were quite similar, indicating the absence of an environmental effect at ambient temperature.

The fracture surfaces of tensile specimens tested at 1×10^{-5} sec^{-1} and at 800°C in vacuum, argon, and air were studied. In vacuum, the lamellar alloy exhibited a composite-like fracture appearance with delamination along apparent alpha-two/gamma or gamma/gamma interfaces, which were manifested as low-energy fracture facets, **Fig. 9**. These fracture characteristics were also observed in specimens tested at 25°C in air or in vacuum. Energy dispersive spectroscopy (EDS) was performed on mating surfaces of individual interface facets for specimens tested in air and in vacuum at both 25 and 800°C. The EDS results indicated interface delamination occurred mostly along gamma/gamma interfaces at 25°C, but along both gamma/gamma and gamma/alpha-two interfaces at 800°C [7]. TEM studies suggested that interface delamination might be caused by impingement of dislocations and twins at gamma/gamma and gamma/alpha-two boundaries [7].

Specimens tested in argon at 800°C did not exhibit a composite-like fracture appearance, but showed low-energy facets and dimpled fracture surfaces. In contrast, the tensile tests in air at 800°C resulted in entirely dimpled surfaces, **Fig. 10**. Micrographs at higher magnifications revealed the presence of oxide particles within the dimples. These oxide particles appeared to form after the dimples were ruptured and they were not the initiation sites for dimple formation. These changes of fractographic feature with environment are not understood at the present time.

Discussions

Comparison of the fracture processes revealed that similar fracture and toughening mechanisms operated in air and in vacuum at both 25 and 800°C, with

quasi-static crack growth occurring by the formation of microcracks ahead of the main crack. The microcracks were formed either at lamellar grain boundaries or by delamination along gamma/gamma or gamma/alpha-two interfaces. The planes of the main crack and the microcracks were generally mismatched and were separated from each other by unbroken ligaments that had to be fractured prior to unstable crack propagation. Fracture of these ligaments was generally by shear across the lamellae (**Fig. 3**). Results indicated that it was more difficult for a crack to propagate across the lamellae than to fracture along the gamma/gamma or gamma/alpha-two interfaces [2]. Thus, additional plastic dissipation was needed and had to be supplied by the external load in order to cause fracture of the ligaments [6]. Therefore, the resistance curve behavior observed in the lamellar alloy was the consequence of shear ligament toughening. A characteristic feature of this fracture process was that the amount of toughening depends on the tortuosity of the crack path and the colony size, as observed. The tortuous crack path was not necessarily the result of a local deflection of the main crack, **Fig. 4**. Rather, it was due to the linkage of non-coplanar microcracks with the main crack by fracture of the shear ligaments, **Fig. 3**. According to the ligament model, a tortuous crack path and a large colony size are beneficial because they can lead to larger plastic dissipation by increasing the size and the number of the shear ligaments. Additionally, the fracture response of the material would depend critically on the shear stress-strain and fracture behaviors of the ligaments. Since these processes are expected to be rate-sensitive, it is therefore not surprising that the resulting toughening and fracture responses of the lamellar alloy are rate-dependent. Furthermore, a high strain rate can promote shear localization and fracture due to adiabatic heating and thermal softening [8], which would reduce the volume of deforming ligaments and the amount of plastic dissipation during fracture of those ligaments. A reduction of plastic dissipation would decrease the effectiveness of the toughening ligaments and lead to the inverse dependence of the K-resistance curve on strain rate, as shown in **Fig. 9**.

One of the significant differences between the $\alpha_2 + \gamma$ TiAl-alloys and conventional $\alpha + \beta$ Ti-alloys is the tendency of the two-phase TiAl-alloys to form microcracks either by interface delamination or by colony-boundary separation [1,2,7]. The consequence is that the TiAl-alloys exhibit low tensile ductility because the microcracks formed in the microstructure can be quite large due to large lamellar grain sizes [1]. Tensile ductility can be improved by refining the lamellar grain or colony size [1,2,7,9] so that the plasticity-induced microcrack size would be small and, thus, less damaging. On the other hand, the introduction of ligaments due to the formation of mismatched crack planes requires a large lamellar grain size in order to maximize the amount of materials

participated in the toughening process [2,6]. As a result, it is necessary and possible to optimize ductility and fracture toughness in these TiAl-alloys through the control of grain size and boundary morphology. The finding that interface delamination in the lamellar microstructure may be related to slip or twin impinging at interfaces [7] suggests that interface separation can be delayed by reducing the gamma/alpha-two and gamma/gamma plate spacings to submicron levels. This would reduce the buildup of dislocation pile-up stresses at the interfaces and, therefore, should make interface delamination more difficult. Another means of preventing the gamma/gamma and gamma/alpha-2 interface delamination might be to promote slip and twinning across these interfaces possibly through chemistry modification.

References

1. K. S. Chan and Y-W. Kim, "Fracture Processes in a Two-Phase Gamma Titanium Aluminide Alloy" in Microstructure/Property Relationships in Titanium Aluminides and Titanium Alloys, Y-W. Kim and R. R. Boyer, eds., *TMS*, Warrendale, PA, 1991, pp. 179-196.

2. K. S. Chan and Y-W. Kim, "Influence of Microstructure on Crack-Tip Micromechanics and Fracture Behaviors of a Two-Phase TiAl-Alloy," *Met. Trans. A*, 1992 (in press).

3. D. Eylon, J. A. Hall, C. M. Pierce, and D. L. Ruckle, *Met. Trans. A.*, vol. 7, 1976, pp. 1817-1826.

4. J. C. Chesnutt, C. G. Rhodes, and J. C. Williams, "Fractography-Microscopic Cracking Processes," ASTM STP 600, *Am. Soc. Test. Mat.*, Philadelphia, PA, 1976, pp. 99-138.

5. I. W. Hall and C. Hammon, *Mat. Sci. Eng.*, vol. 32, 1978, pp. 241-253.

6. K. S. Chan, "Micromechanics of Shear Ligament Toughening," *Met. Trans. A*, 1991, vol. 22A, 1991, pp. 2021-2029.

7. K. S. Chan and Y-W. Kim, "Rate and Environmental Effects on Fracture of a Two-Phase TiAl-Alloy," *Met Trans.*, 1992 (submitted).

8. L. S. Harbison, R. J. Bourcier, and D. A. Koss, in "Microstructure/Property Relationships in Titanium Aluminides and Alloys," eds., Y-W. Kim and R. R. Boyer, *TMS*, Warrendale, PA, 1991, pp. 437-446.

9. K. S. Chan, "Theoretical Analysis of Grain Size Effects on Tensile Ductility," *Scripta Met.*, vol. 24, 1990, pp. 1725-1730.

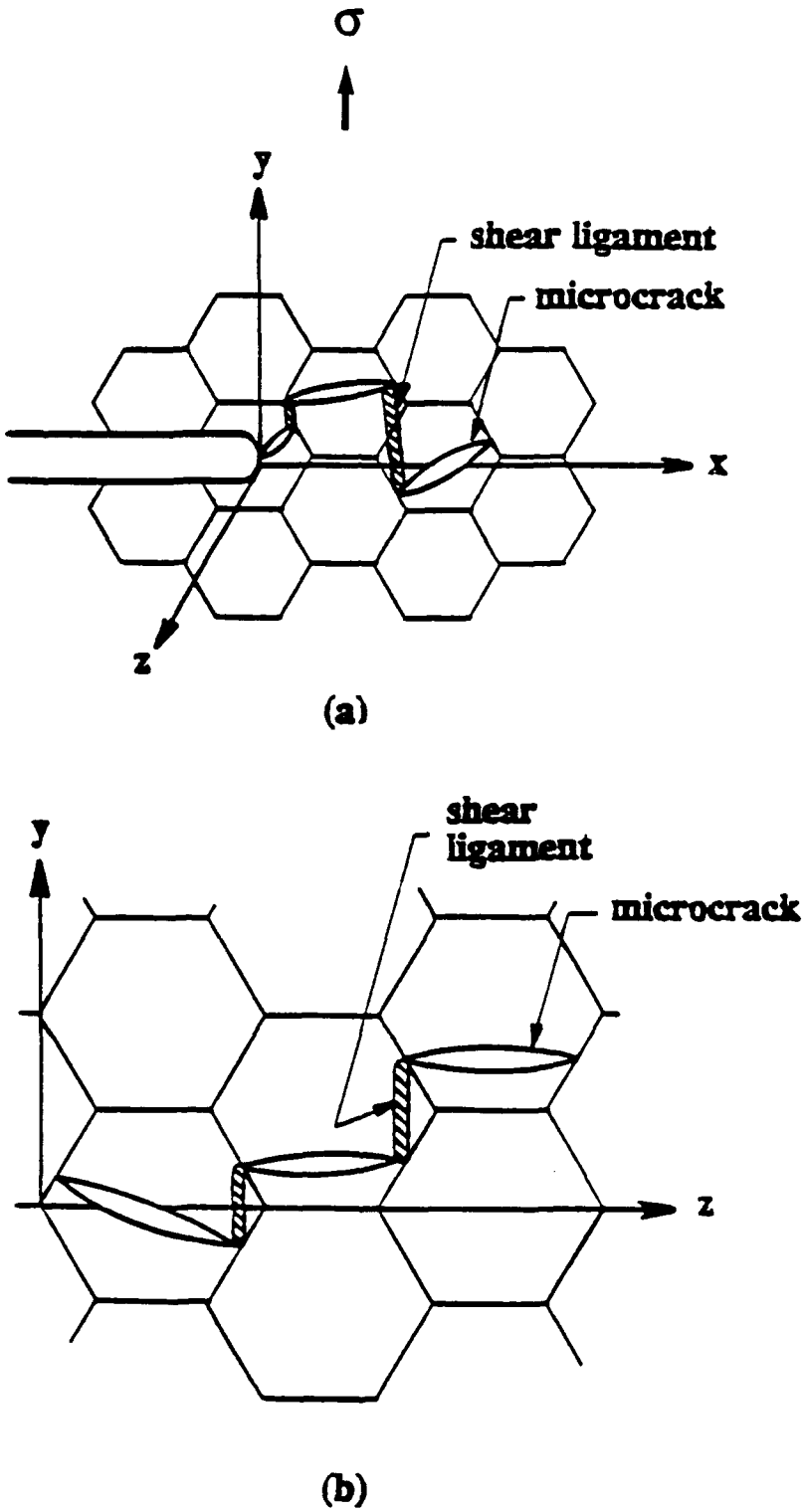

Figure 1. Schematics showing the formation of shear ligaments by mismatched crack planes: (a) ahead of the crack tip in the x-y plane on the specimen surface, and (b) along the crack front in the y-z plane in the interior of the specimen.

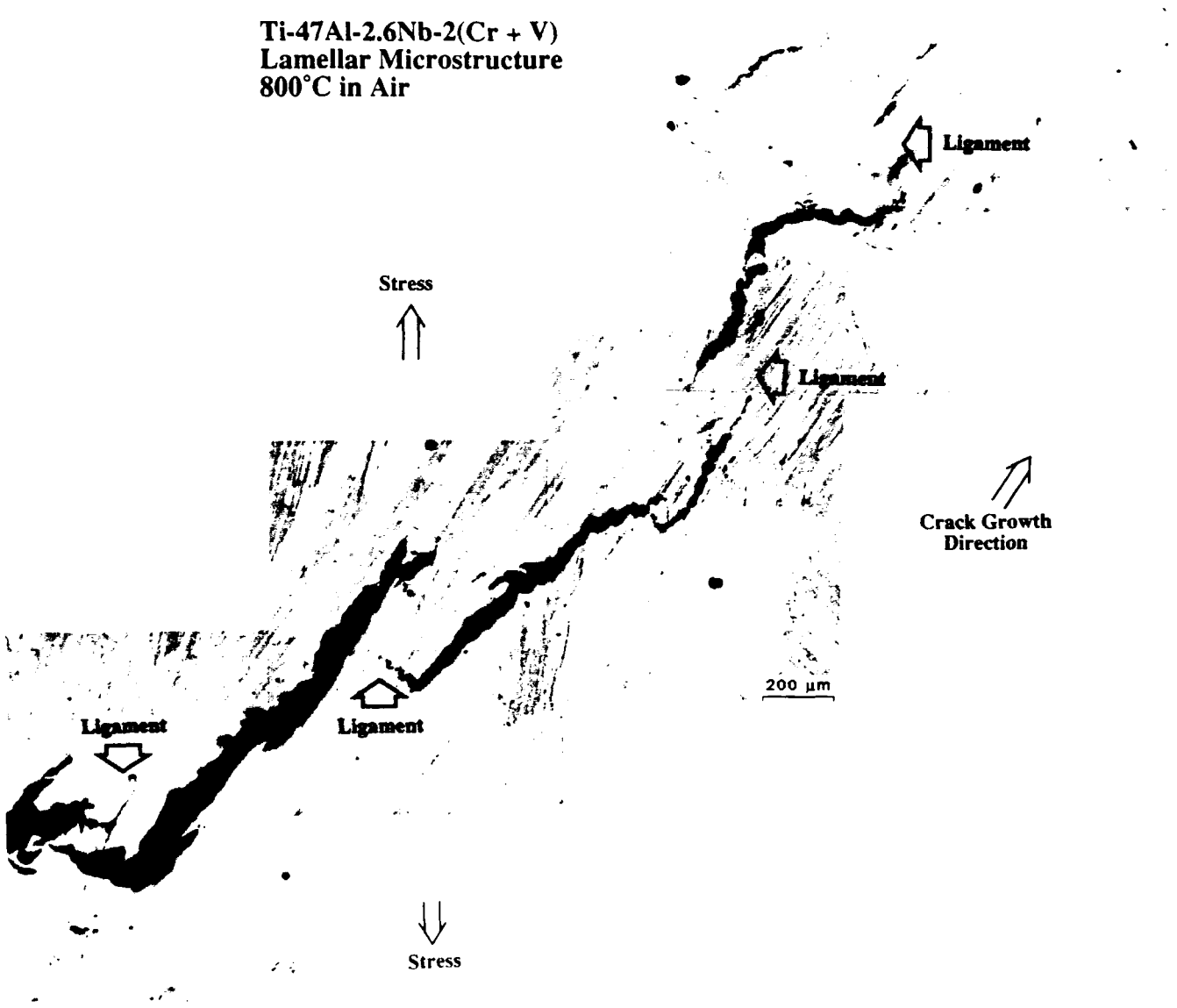

Figure 2. Process zone in the G1L alloy at 800°C showing the presence of five intact ligaments that led to the resistance-curve behavior observed in the material.

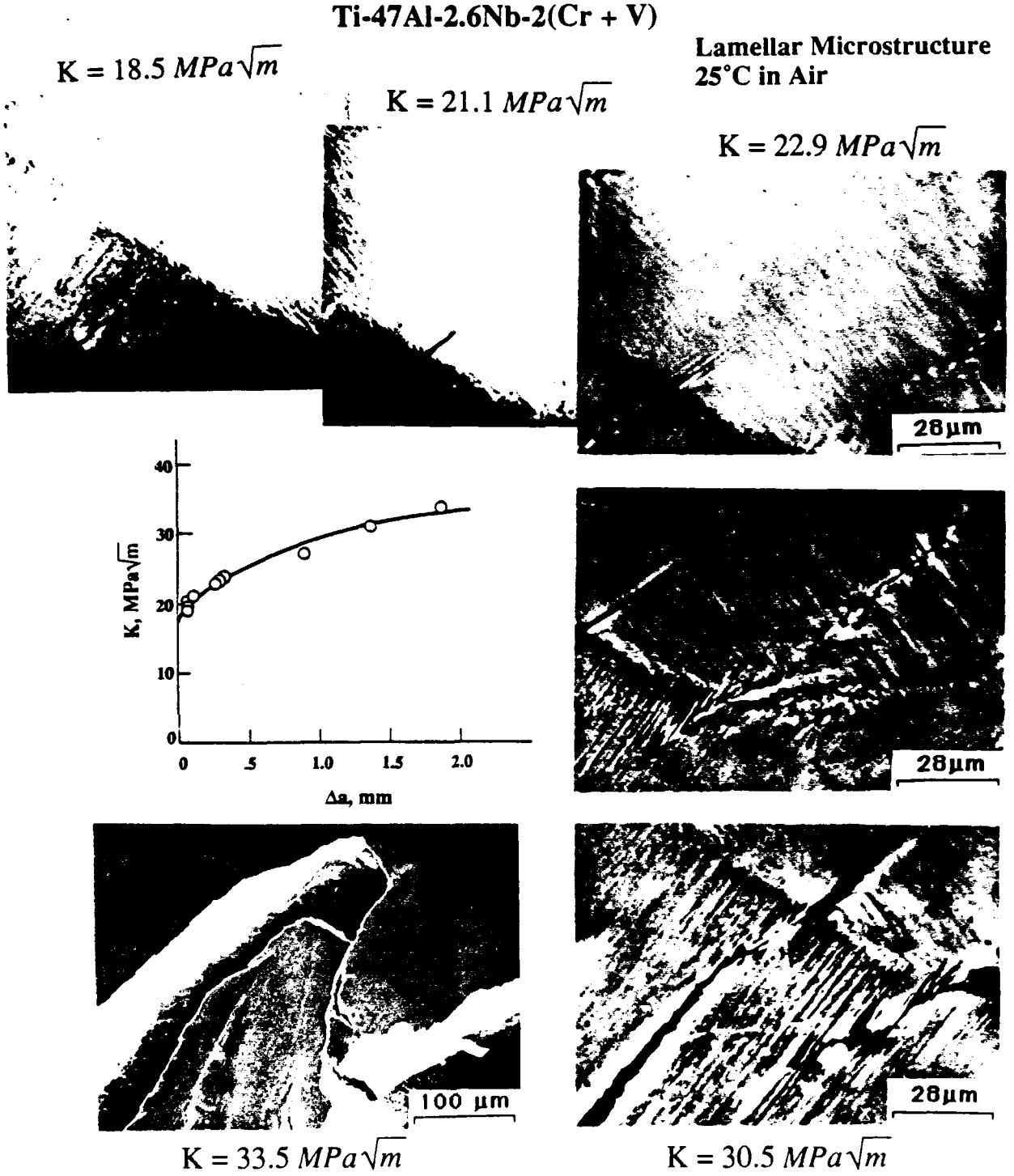

Figure 3. Composite figures showing the process by which shear ligament toughening occurs in a two-phase TiAl-alloy. The shear ligament is formed as the result of the formation of a misaligned microcrack ahead of the crack tip. Fracture of the shear ligament requires additional plastic dissipation leading to a tortuous crack path and a resistance-curve behavior.

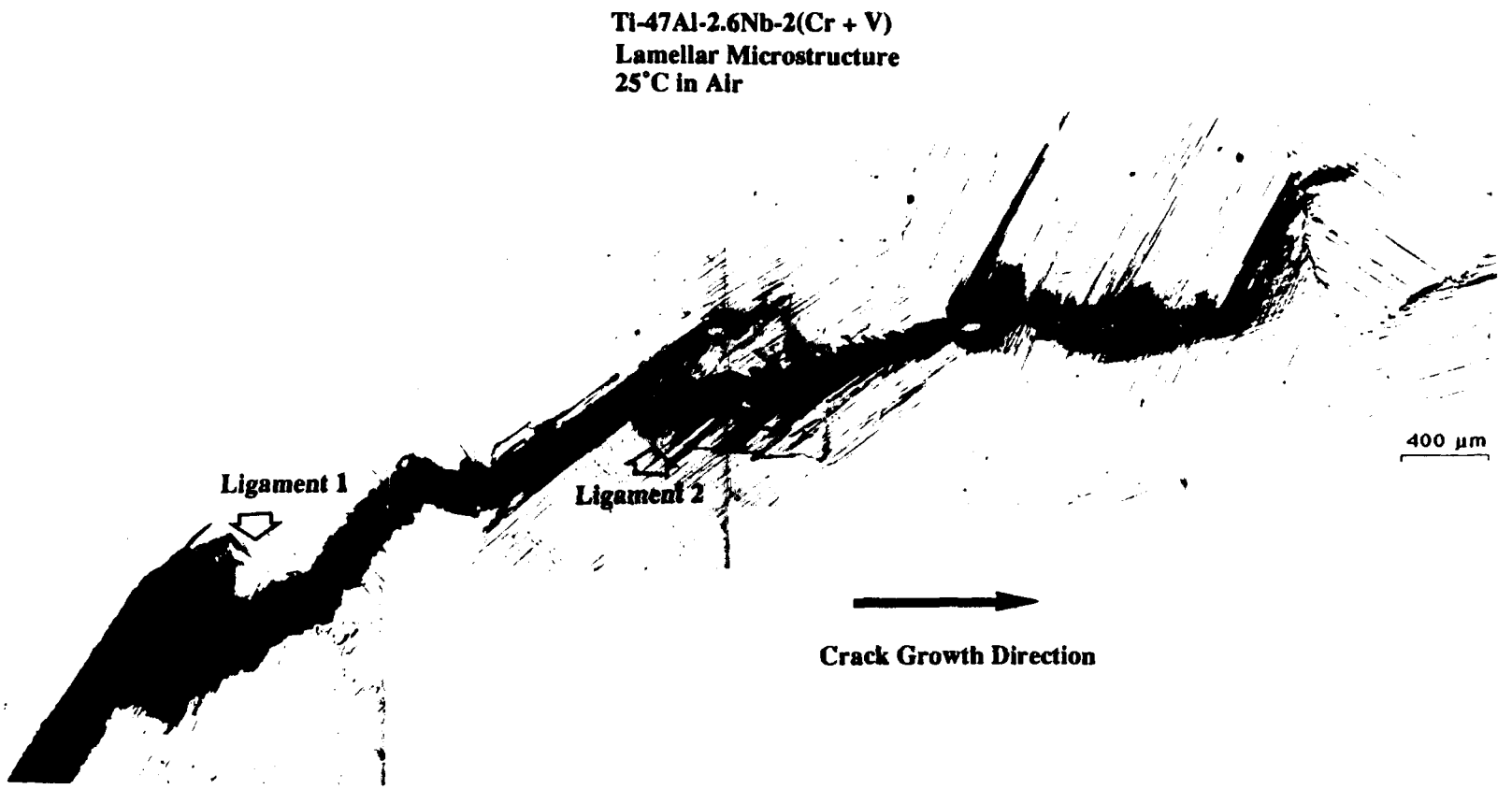

Figure 4. Crack path and process zone in the G1L alloy at 25°C showing two fractured ligaments in the crack wake.

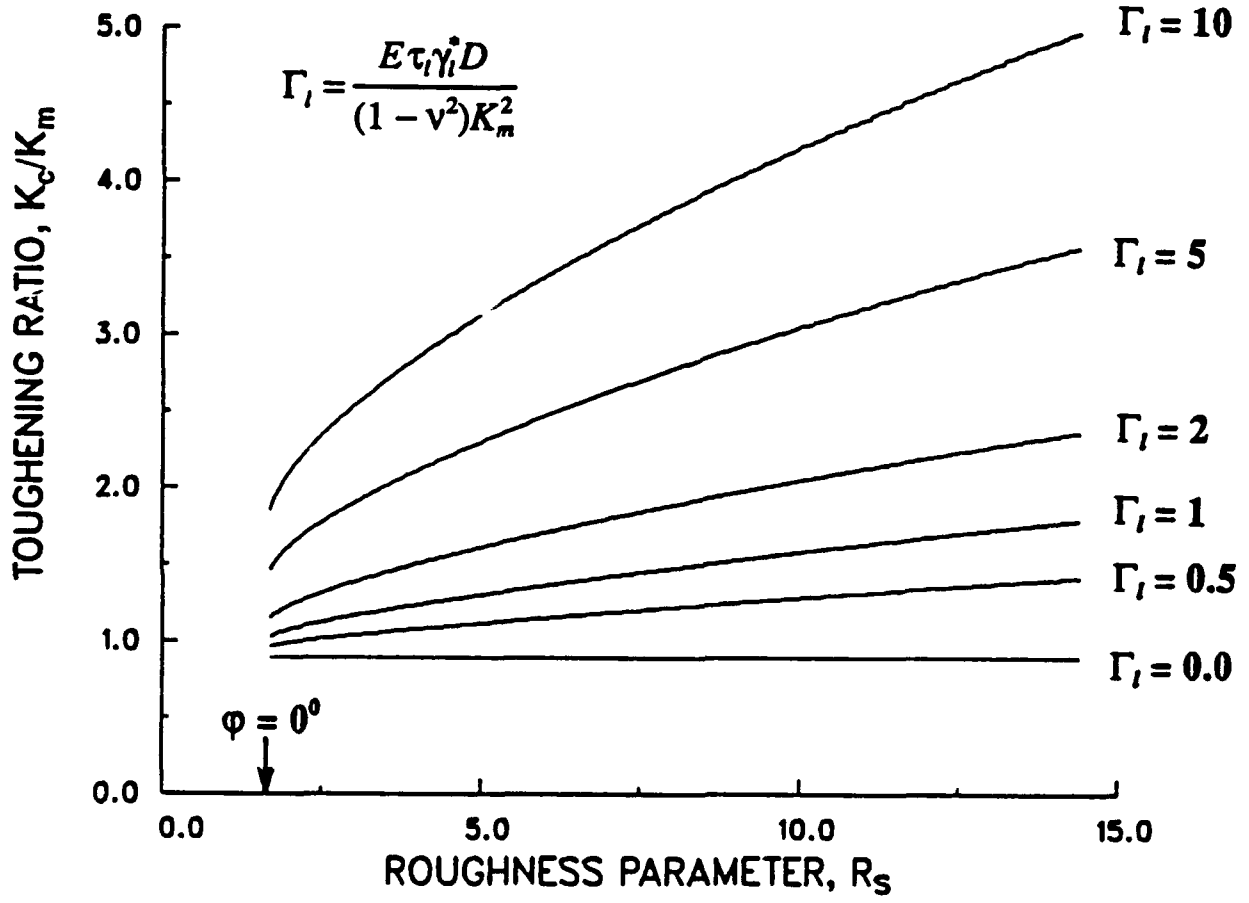

Figure 5. Toughening ratio, K_c/K_m, as a function of the surface roughness parameter, R_s, for various values of the normalized ligament toughness parameter, Γ_l.

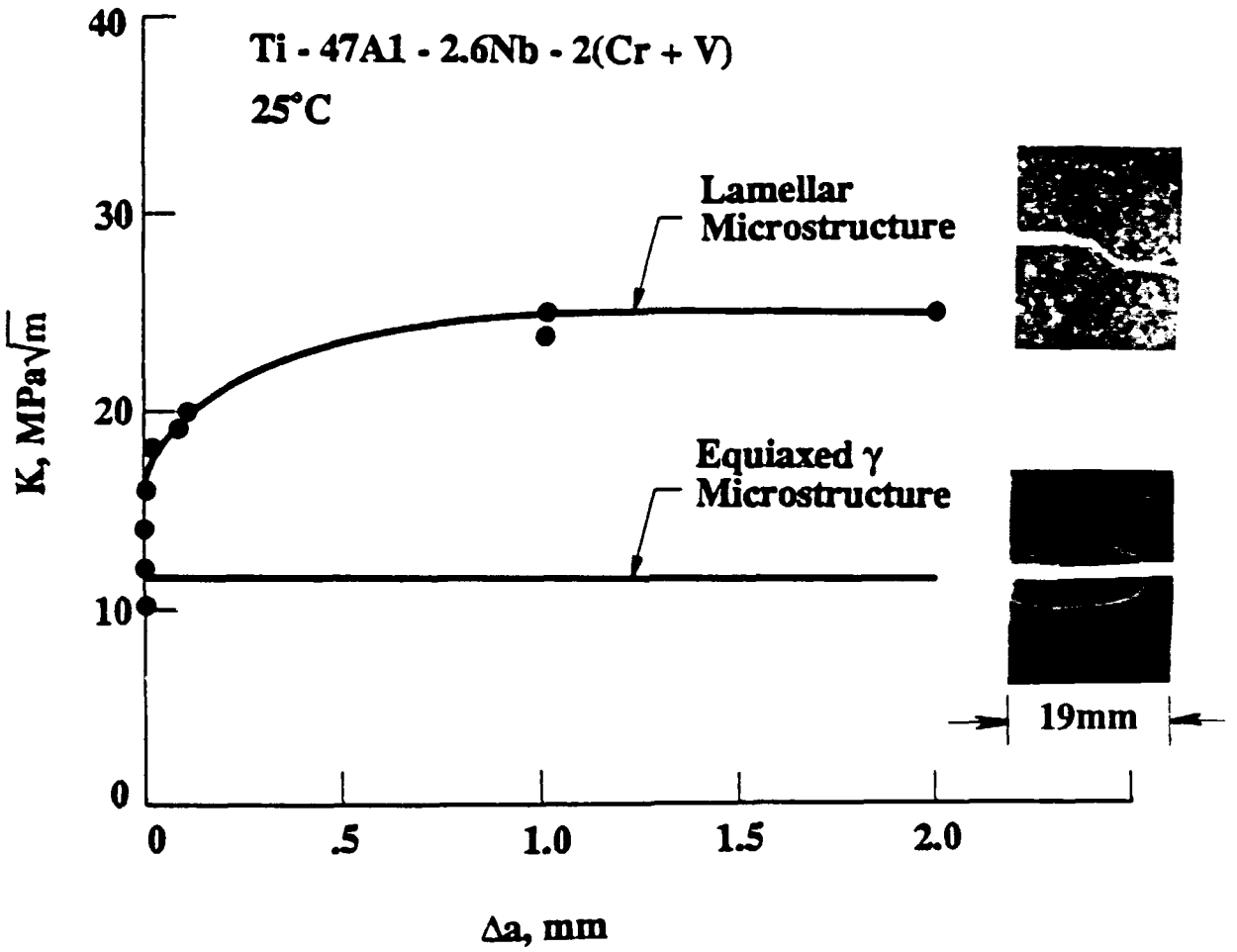

Figure 6. Comparison of K-resistance curves and crack-path tortuosity for the two-phase TiAl-alloy, Ti47Al-2.6Nb-2(Cr + V), with either a predominantly equiaxed γ grain microstructure or a predominantly lamellar microstructure.

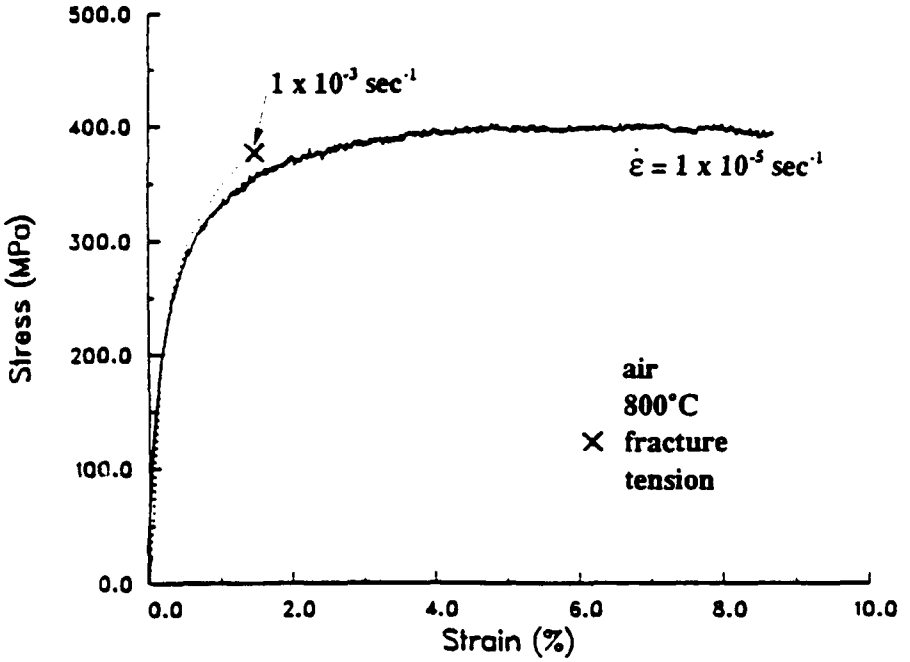

(a)

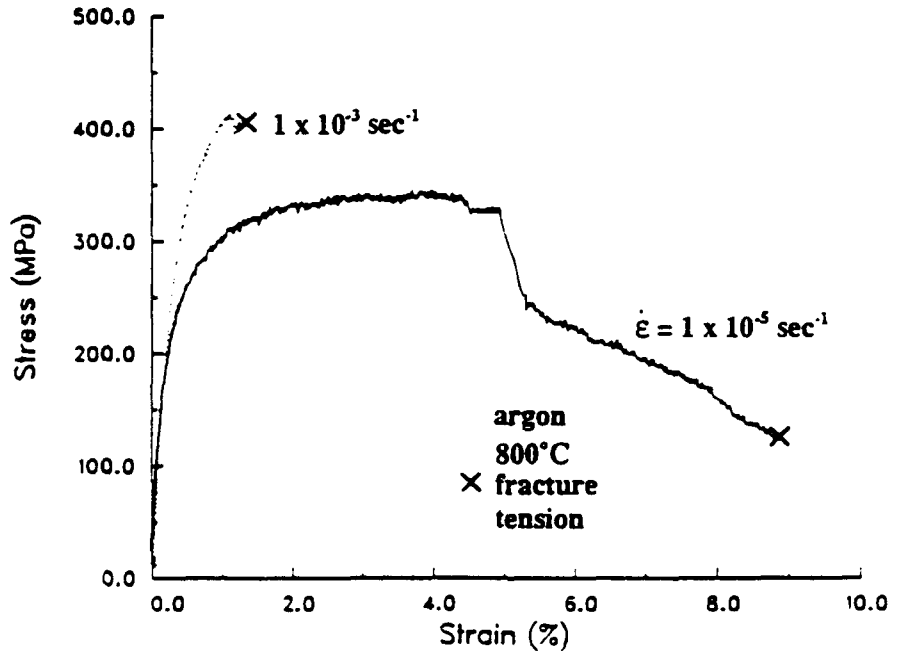

(b)

Figure 7. Comparison of the tensile stress-strain curves of the G1L alloy for two strain rates at 800°C: (a) in air, and (b) in argon.

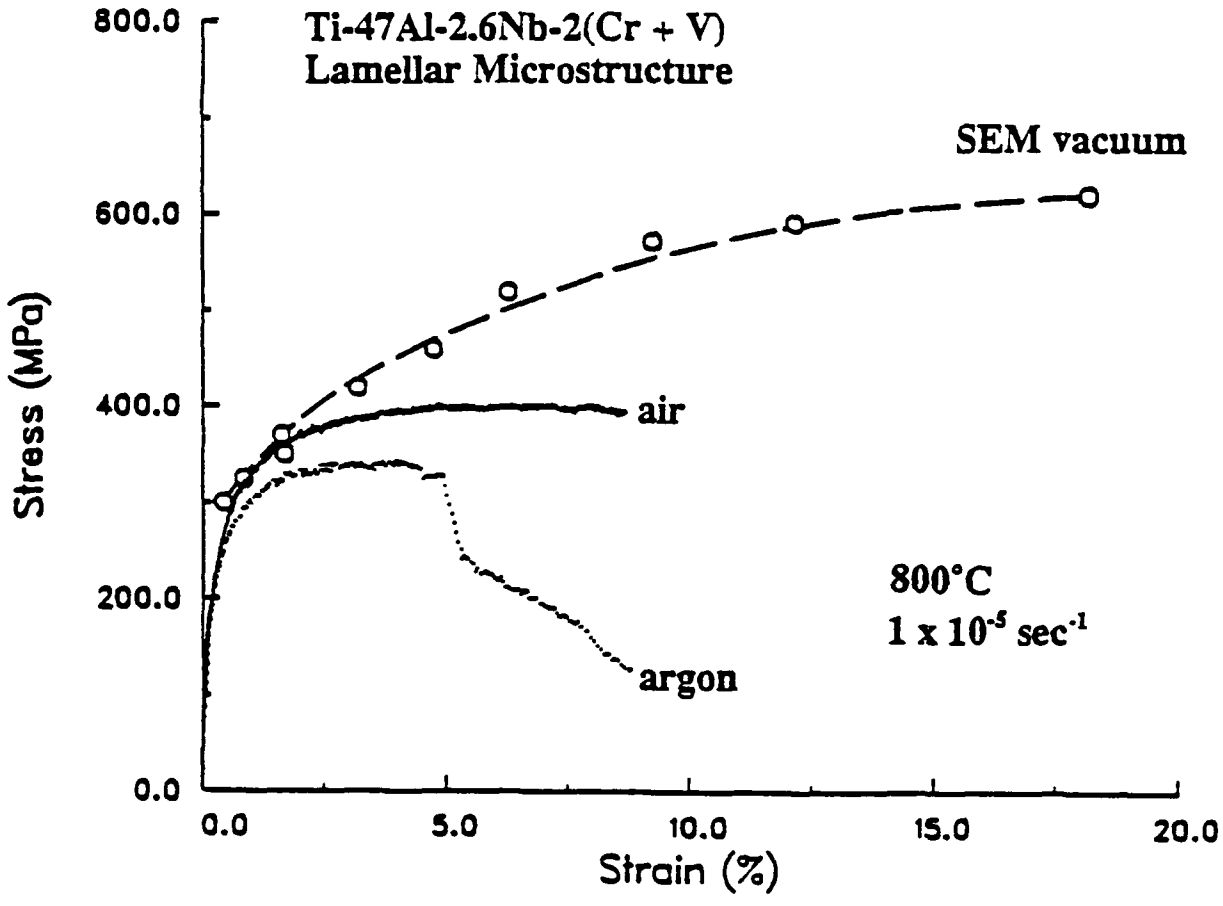

Figure 8. Comparison of tensile stress-strain curves of the G1L alloy obtained at 1×10^{-5} sec^{-1} in air, argon, and vacuum.

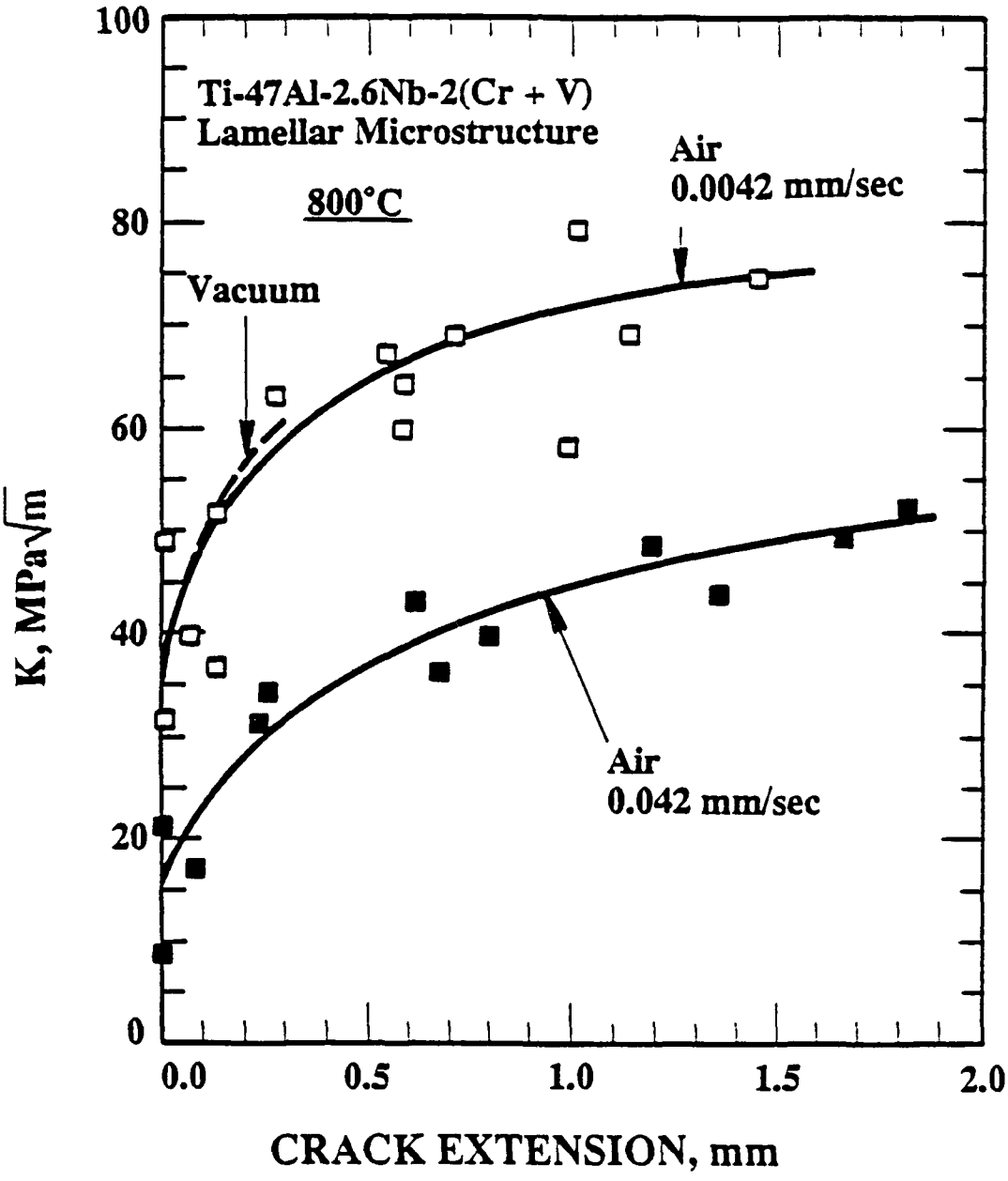

Figure 9. Effect of displacement rate on the K-resistance curves of the G1L alloy at 800°C.

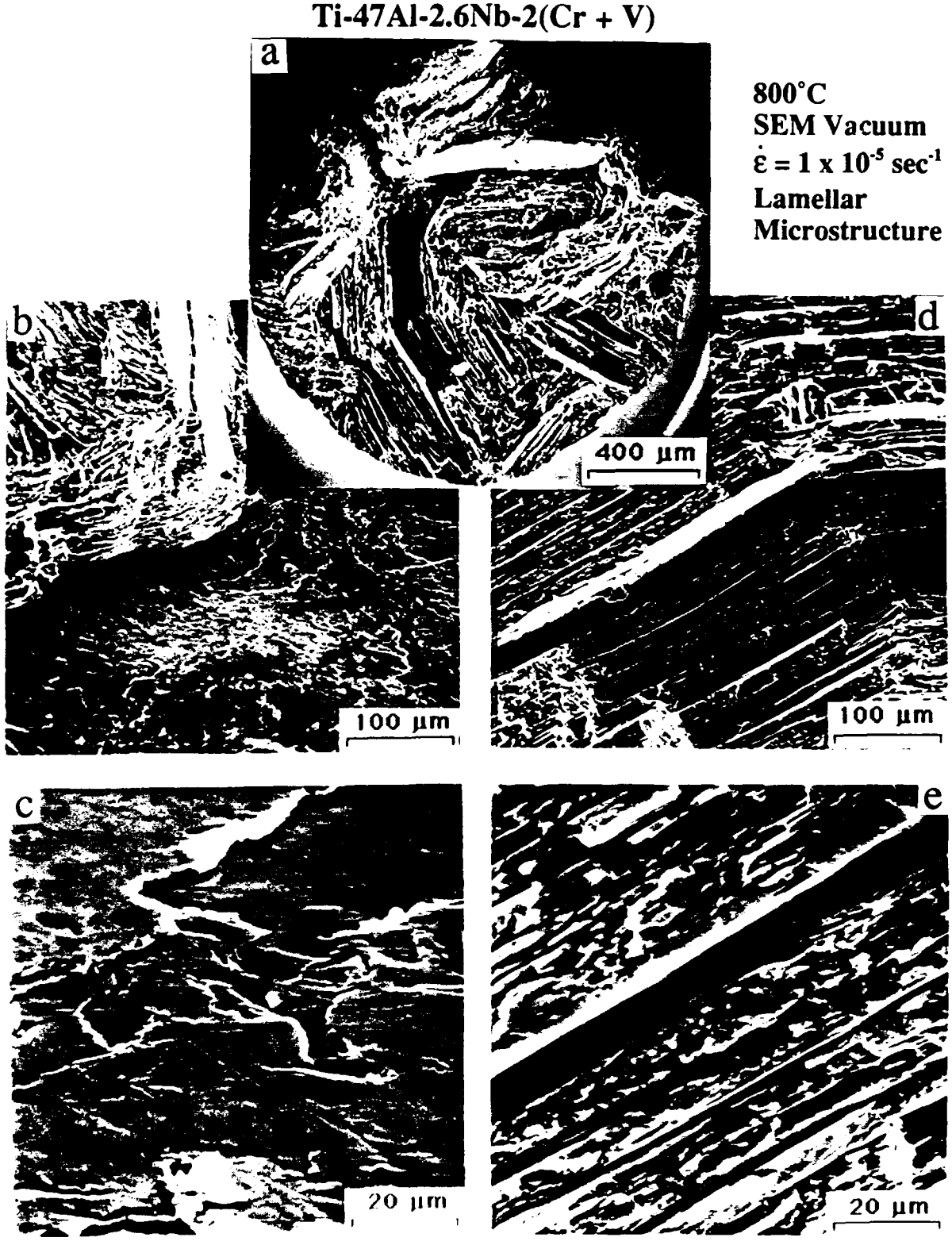

Figure 10. Composite SEM fractographs showing (a) composite-like fracture surface, (b) and (c) low-energy interface facets, and (d) and (e) delamination of lamellae observed in the G1L alloy tested under tension at 800°C in vacuum at 1 x 10^{-5} sec^{-1}.

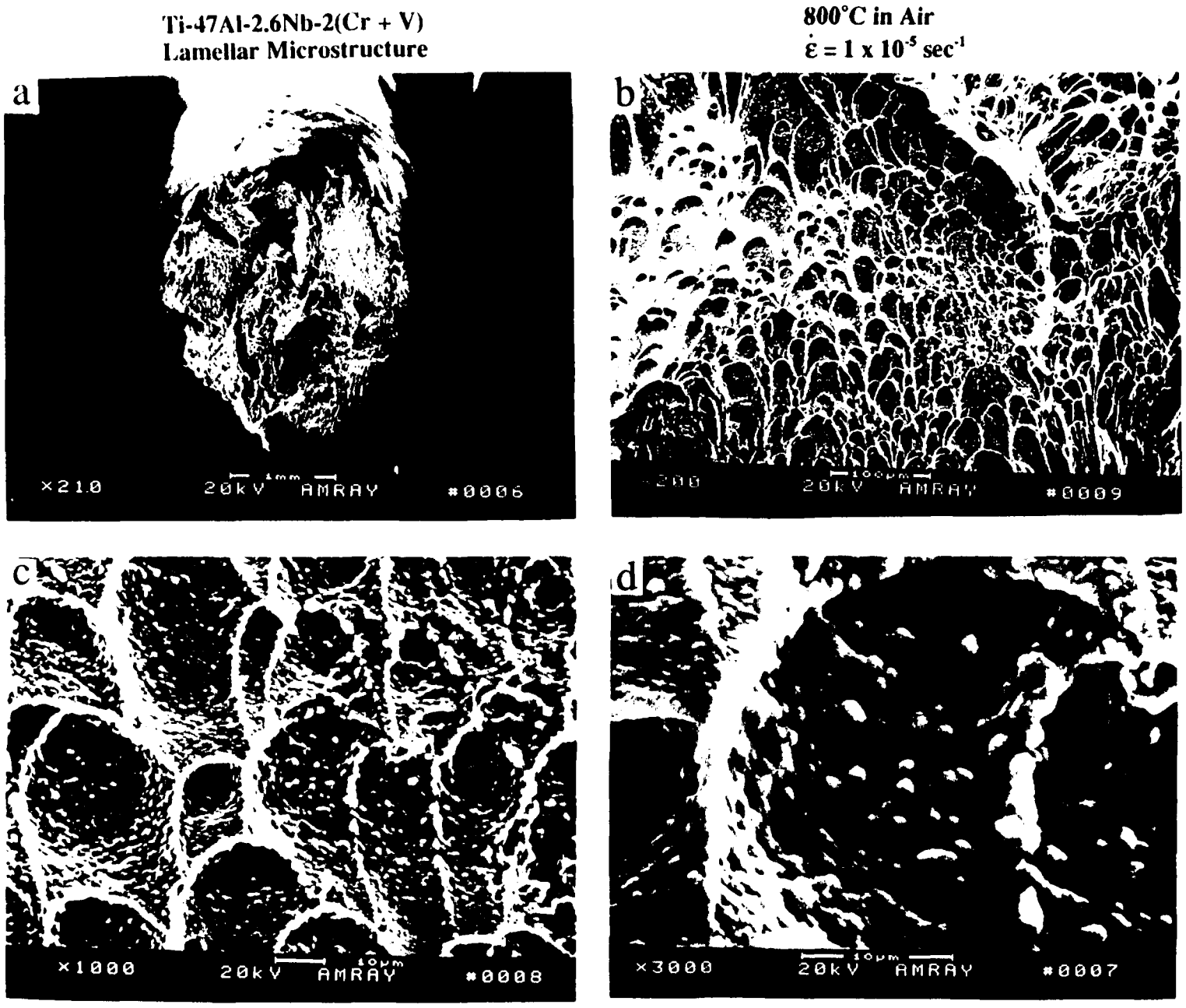

Figure 11. SEM fractographs showing dimpled fracture in the G1L tested under tension in air at 1 x 10^{-5} sec^{-1}.

Fracture of Nb_3Al-based Alloys

Several ingots of cast Nb-Al alloys were obtained from Dr. Donald Anton of United Technologies Research Center. Nominal composition of these alloys was Nb-18 at.%Al. Ingots approximately 110 mm square by 8 mm thick were cast and then aged at various times and temperatures. Upon receipt, the ingots were cut and examined for cracks and composition uniformity. Some of the ingots were found to be inhomogeneous and were not further evaluated. Small CT specimens (20 mm square, by ≈ 5 mm thick) were removed from the remaining ingots by electric discharge machining. After polishing by typical metallographic preparation techniques, specimens were notched with a diamond saw to a depth (measured from the center line of the pin holes) of about 3 mm. Compression-compression cyclic loading was used to initiate and grow a crack from the notch. Unfortunately, a several of the specimens broke during this phase of testing because it became necessary to apply unusually large loads while trying to induce fatigue crack initiation from the notch. An example of the specimen used, together with the type of fracture caused by an overload in compression, is given in **Fig. 1**.

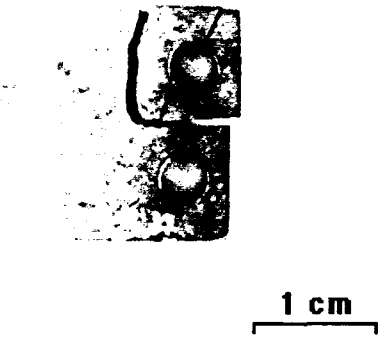

Fig. 1 Compact tension specimen used for fracture studies. Several of the specimens broke under compression-compression loading used to initiate cracks.

A total of 5 specimens were prepared, but successful tests with fatigue crack growth data were obtained from only 2 specimens, and from these, only a limited range in ΔK was covered. Information on the materials tested and a summary of the results obtained are listed in **Table 1**.

Table 1
Nb-18Al alloys

Material Designation	Heat treatment Temp.(°C)	Time (Hrs)	Hardness Rockwell C	Results
A	1000	4	37	some da/dN data pin hole failure: T-T
B3	1000 1400	4 100	47	(1) pin hole failure: C-C (2) some da/dN data
B4	1000 1200	4 100	57	(1) pin hole failure: C-C (2) K_c = 5.5 MPa$\sqrt{m}$

T-T = Tension-tension loading with R = 0.1
C-C = Compression-compression loading with R = 10

Optical micrographs of the materials tested are shown in **Fig. 2.** The two phases of materials B3 and B4 are fairly homogeneously distributed while for material A, there appear to be isolated regions of fine structure within a more uniform structure. Dark lines seen in the micrographs are cracks. The microstructure of material A was further examined prior to crack growth testing. Ion etching was used to further reveal the microstructure. The results are compared in **Fig. 3** before and after ion etching by optical and back-scattered electron microscopy (at 30 keV). These techniques revealed that the isolated regions had a very fine eutectic-like structure which formed prior to the grain boundaries (regions cross the grain boundaries). Thus, material A has a much coarser and inhomogeneous microstructure than eithe B3 or B4.

Interpretation of these micrographs, and further information about how these alloys were made, may be in the results of Anton, and Shah [1]. The composition chosen, according to the phase diagram, is on the edge of the Nb_3Al phase field. Study of this system have shown that quenching from elevated temperature produces a Nb solid solution stable to ambient temperature. Subsequent ageing results in the precipitation of Nb_3Al through a peritectic reaction. The nature of the precipitation is that of a "massive phase transformation" which "results in a highly uniform, fine

distribution of filamentary Nb within a contiguous Nb_3Al matrix."

The regions of fine structure in Fig. 2(a) and 3 are apparently "primary and secondary dendretic arms" of Nb_3Al in a matrix of Nb solid solution [1]. Further ageing results in a mixture of Nb solid solution and Nb_3Al. The ageing treatments used, Fig. 2(b) and (c) resulted in growth of the dendretic characteristic of the short aged structure (material A), yielding the relatively coarse structures of materials B3 and B4. It appears as though both materials B3 and B4 are composed of greater than 50% Nb_3Al.

The fatigue crack growth results obtained are compared to the fatigue crack growth data for the titanium aluminide alloys in Fig. 4

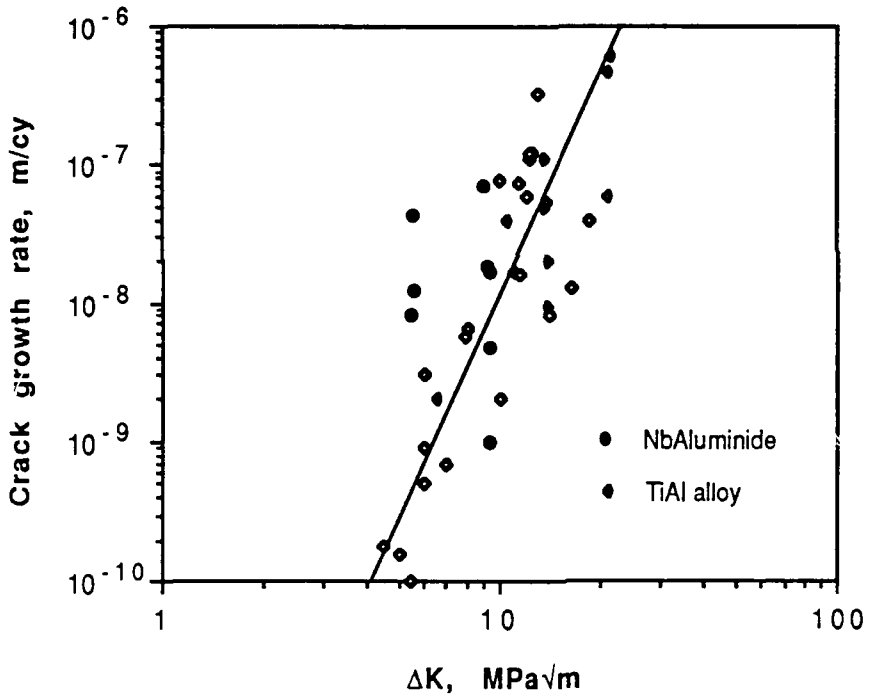

Fig. 4 Comparison of crack growth rates at 25°C for the lamellar TiAl-based alloy with that of the Nb_3Al based alloy.

These limited results indicate that crack growth rates are within the same range as for the TiAl-based alloy. Fatigue cracks grew very irratically and with great variation within that range. The most data were obtained for material A. For this alloy, a crack was initiated from the notch in C-C loading and grown until it stopped. In subsequent T-T loading, the crack would not grow at a ΔK less than 5.5 MPa$\sqrt{m}$; this value was thus

determined to be ΔK_{th}. The largest K_{max} sustained during these experiments was 10.3 MPa$\sqrt{m}$. Material B4 broke in T-T loading at K_{max} = 5.5 MPa$\sqrt{m}$ prior to any know fatigue crack growth, and a several crack growth rate values were obtained from material B3 at $\Delta K \approx 5.7$ MPa$\sqrt{m}$.

Fractography was performed on material B3 within the zone of fatigue crack growth. The results are shown in **Fig. 4**. The fine parallel lines approximately perpendicular to the direction of crack growth in some parts of the microstructure could be interpreted as periodic crack arrest lines (striations). To examine this possibility in more detail, two stage acetate carbon replicas were made from this region and examined by TEM under much higher resolution conditions; no striations could be found. Typical results of this examination are shown in Fig. 3(c). These fine lines form mainly in the Nb solid solution portion of the microstructure, as determined from the shape of the region, rather than in fractured Nb_3Al.

Anton and Shah [1] estimate the yield stress of these alloys to be something in the order of 500 MPa. Using the linear elastic fracture mechanics equation for crack tip "process zone size" (r_s)

$$r_s = (1/2\pi)\ (K_{max}/\sigma_y)^2$$

where σ_y = yield stress and K_{max} = stress intensity factor at the threshold for fatigue crack growth (6.1 MPa$\sqrt{m}$), gives $r_s \approx 20$ μm. Some microstructural features in material A might be found of this approximate size scale, but the microstructure is much finer than this for materials B3 (for which ΔK_{th} was measured) and material B4. Thus, it is not clear which microstructural feature is controlling fracture in these materials. Conversely, if the controlling microstructural feature is approximately 4μm, as estimated from Figs. 2(b) or 2(c), then the yield stress would be closer to 1100 MPa. Although the Rockwell C hardness values listed in Table 1 cannot be directly converted to strength for these alloys, the magnitudes of hardness are not incompatible with strengths of approximately 1000 MPa. It is concluded that the measured fatigue threshold is about what would be expected, at least for materials B3 and B4.

1. D.L. Anton and D.M. Shah "Ductile Phase Toughening of Brittle Intermetallics" in **Intermetallic Matrix Composites** D.L. Anton, P.L. Martin, et al., eds., Mat. Res. Soc. v. 194, Pittsburgh, PA, pp. 45-52.

(a)

(b)

(c)

Fig. 2

Microstructures of materials tested.
(a) Material A, aged 4 hrs at 1000°C,
(b) Material B3 4/1000 and 100/1400, and
(c) Material B4 4/1000 and100/1200.

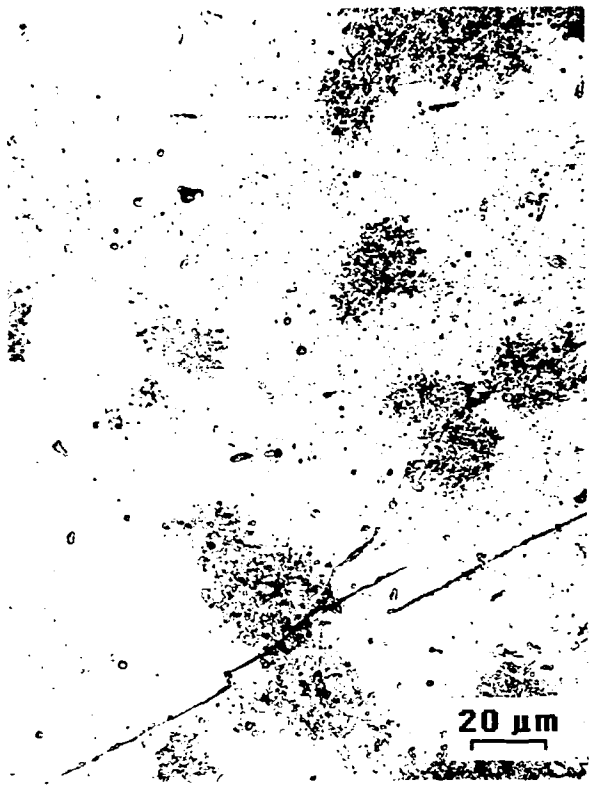

(a)

(b)

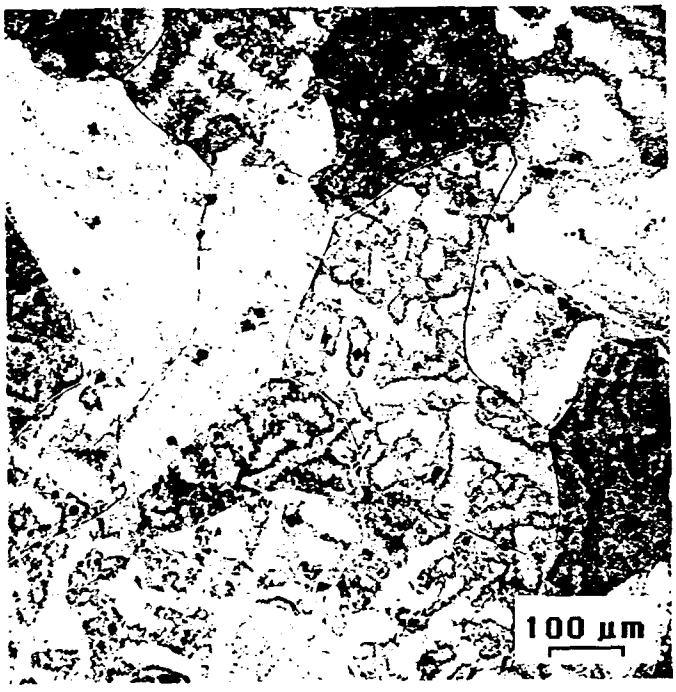

(c)

Fig. 3

Microstructure of Material A: (a) optical image, (b) nomarski (optical) image after ion etching, (c) backscattered electron image after ion etching.

(a)

(b)

(c)

Fig. 4

Fractography of Material B3 in fatigue region: (a) overall secondary electron view showing small regions with parallel lines, (b) higher magnification view, and (c) results of two stage acetate carbon replica.

STM Fractography

Introduction

Several investigators have characterized the fractography associated with fatigue crack growth in titanium aluminides. In particular, Aswath and Suresh [1] have considered a Ti-24 at% Al-11 at% Nb alloy with an $\alpha_2 + \beta$ duplex microstructure. Based on scanning electron microscope (SEM) observation, they conclude that fatigue fracture surfaces are smooth, and evidently produced by transgranular cleavage. An almost identical conclusion, again based on SEM observation, was reached by Pao, et al. [2], for the case of TiB_2-reinforced and unreinforced Ti-46 at% Al. The objective of the present work is to look into this question in greater detail, using the nanoscale resolving power of the scanning tunneling microscope (STM). For comparative purposes, a fast fracture region is included in the study.

The principals of operation of an STM are simple [3]. Basically, an extremely (usually atomically) sharp conducting tip is scanned about over the surface of a conducting specimen via an X, Y, Z piezoelectric translator. Separation between the tip and the surface of the sample is feedback controlled by the voltage applied to the Z-piezo. The feedback circuit measures and maintains the small electrical current due to electrons tunnelling across the gap under the influence of a low (millivolt-volt) bias voltage at the tip. As the tip is scanned in the X-direction across the surface, its distance above the surface is controlled so as to maintain a constant tunnelling current; a topograph of the surface in X and Z derives from the Z-piezo voltage recorded during the scanning trajectory of the tip. Repeating this scan for various Y-settings yields a three-dimensional view (known as a tunnelling or STM image) of the surface composed of multiple X-Z line scans. It is possible to operate on these data to produce computer-rendered grey-tone images, which resemble those obtained by conventional scanning electron microscopy.

Difficulties in STM work generally arise from the fact that the tunnelling current flows only when the tip is within 1 to 2 nm of the surface. This is caused by the exponential decrease in current as the tip moves away from the surface; thus, for fine-scale atomic-resolution work, vibration isolation and thermal drift are major considerations. In the present case, the rigidity of the microscope framework and, especially, the speed of its feedback system, are paramount concerns. The tip must scan rapidly enough to produce an image within a reasonable amount of time, commensurate with its ability to dodge, as it flies over the sample, the suddenly

appearing large-scale (relative to the tip-to-sample separation) obstacles characteristic of a fracture surface. This problem obviously is compounded by the inability of the operator to position accurately the tip of a stand-alone STM.

These problems probably account in large measure for the current paucity of reports in the literature of fractography via STM. To date, the technique has been used to characterize overload fracture details in polycarbonate (4), and fatigue striations in 7075-T651 Al [5] and 304 stainless steel [3]. In the latter studies, the capability of the STM was not really challenged, since the striations were visible in the SEM (although only barely, in one case [3]).

Experimental Procedures

In the present case, attention was focussed on two "zones" on the fracture surface of one of the lamellar TiAl alloy specimens whose crack growth behavior is described in other sections of this report. One of these shown in **Fig. 1** (arrow) was extremely smooth in appearance, except for a few steps, and appeared to be one of the first facets fractured when the stress intensity reached K_{IC}. It appeared likely that the facet was created by crack growth parallel to the α_2 and γ lamellae. Another area selected for study was quite rough, having been formed by fatigue, and it was evident that crack extension had occurred normal to the lamellar microstructure.

Because of the limited range (~4 μm) of the Z-piezo, it is absolutely crucial to position the STM sample in such a manner that the surface of interest is within a few degrees of normal relative to the Z-axis of the microscope. Otherwise, the already limited X-Y scan box (maximum size 125 x 125 μm) will be reduced to a strip lying within the box. In the case of interest, the "sample" consisted of specific fracture-surface facets oriented at various large angles relative to one another. It proved impossible to manipulate the entire fracture surface to correctly position and orient a single facet beneath the STM tip, while maintaining overall mechanical stability. Therefore, individual facets were cut from the surface using a slow-speed precision diamond saw, and excess material adjacent to the facets was ground away using microgrinding tools. This was a difficult and painstaking process, since great care was required not to damage the areas of interest.

In order to grip the resulting miniature specimen, it was embedded in modeling clay attached to a small conducting beam (copper-coated printed circuit board). The latter was held within the STM gripping fixture, with the specimen lying under the tip. It was possible then to rotate the specimen within the clay to a near-normal relationship,

judged by using the facet as a mirror to reflect light back along the path of a thin light beam. Once the facet was properly oriented, it was seated firmly in the clay which also served as an excellent vibration isolation medium. A conducting path finally was created by using silver paint over the clay to connect the sample with the conducting beam.

The samples were examined in air in the STM*[1] using Pt-Ir shear-fractured tips. Height contrast images were generated in the constant current scanning mode, and recorded by photographing a storage oscilloscope screen displaying the computer-generated STM tunneling image. The maximum available X-Y scan range was 135 x 135 μm. Location of the tip within each facet was random, although the nominal crack-growth direction was always known.

Complementing the STM characterization, the specimens also were examined by scanning electron microscopy. Selection of sites for SEM study was based in part on their resemblance to images obtained by the STM when the latter was operating at relatively low "magnification."†[2]

Results

It will be shown that microscale fracture surface morphologies differ significantly depending upon whether or not they derive from subcritical crack growth or fast fracture. These two cases will be considered separately in the following sections.

Fast Crack Growth Parallel to Lamellae ($K > K_{IC}$)

Shown in **Fig. 2** is an SEM view of a section of a "smooth" facet which appears to have been formed by an interlaminar mechanism during rapid fracture (In all figures, crack growth is from the bottom to the top of the picture.). At higher magnification, it can be seen (**Fig. 3**) that the "ledges" separating parallel crack planes are composed of multiple α_2 and γ layers. Increasing magnification, yields an unclear image (**Fig. 4**, 80,000X original magnification) of a generally smooth surface covered with fuzzy details.

An equivalent (X-Y magnification) STM view of a similar area shows (**Fig. 5**) that the surface consists of both elevations (E) and depressions (D), each in excess of 15 nm in height/depth, while the intervening majority of the surface consists of a bumpy,

---

1 *Nanoscope II, Digital Instruments, Santa Barbara, CA.

2 †Since the Z-axis in STM images is usually expanded relative to X and Y, it is invalid to speak of an overall magnification or scale factor.

nanoscale structure. Further magnification reveals (**Fig. 6**) the "bumps" to be virtually featureless microfacets on the order of 25 nm in width, and a few nanometers high. Thus, the crack clearly does not follow a single macroscopic cleavage plane, but instead grows by jumping out of plane from one microfacet to another.

Fatigue Crack Growth Normal to Lamellae ($\Delta K > K_{IC}$)

Scanning electron microscopy of translamellar fatigue crack growth reveals an apparently rough surface (**Fig. 7**), an impression which is preserved at successively higher magnifications (**Figs. 8 and 9**). This roughness is composed of ledges made of lamellae, which are similar in appearance (**Fig. 8**) to those created by crack plane changes during rapid fracture (**Fig. 3**).

The individual lamellae which make up the ledge structure often display a characteristic three-dimensional topography, as shown in **Fig. 10**. Lamellae typically range in thickness from nearly 10 μm (10,000 nm) (**Fig. 10**) down to a few hundred nanometers (**Fig. 11**). Here it is apparent that the fracture plane curves gently in the direction of crack growth, except at the transition from one lamella to the next. In these sections (arrows, **Fig. 10**), shallow crevices occur.

A typical crevice region, surrounded by several rounded lamellae, is shown in **Fig. 12**. Upon magnifying the bottom of the crevice, a fine substructure resembling dislocation subcells (**Fig. 13**) is revealed. The apparent subcells are elongated in the general direction of crack growth, and measure approximately 50 by 30 nm in size. Study of a lamella surface at similar magnification shows that it, too, is composed of subfeatures, in this case elongated normal to the nominal crack growth direction (**Fig. 14**). These structures appear to measure about 50 nm long by about 25 nm in the direction of crack growth. In neither case are features observed analogous to classical fatigue crack growth striations.

An appreciation of the overall variation in surface topography is achieved by using the STM as a nanoprofilometer. Surface traces (**Fig. 15**) were generated by recording line scan images for the parallel sections indicated by the numbered arrows in **Fig. 12**. In these scans, the left hand side corresponds to the upper edge of **Fig. 12**, and the right hand side to the lower edge. Based on these results, it is evident that the fatigue surface is neither microscopically smooth nor macroscopically flat.

Discussion

Fast Fracture

Chan and Kim [6] have shown that faceting produced by delamination fracture at 25°C in the present alloy occurs predominantly on γ/γ (occasionally on α_2/γ) interfaces, hence it is considered likely that the present fast fracture images were obtained from a gamma lamella. The results indicate that such fracture does not occur by pure single plane cleavage, but instead is accomplished by the linking of many parallel, but slightly out-of-plane subfacets. Since previous TEM studies [6] have revealed no such intrinsic steps in γ-γ boundaries, it would appear that the cleavage crack either oscillates back and forth across the γ-γ interface, or spends most of its time within an individual γ-lamella, near but not directly on the interface itself. Jumps from one subfacet to another appear to range in amplitude from 2 to 20 nm.

Fatigue Crack Growth

The fact that no striations were observed by STM on the translamellar fatigue fracture surface is consistent with observations of crack growth in the SEM which showed that crack growth is intermittent, and that typical crack growth increments are on the order of the lamellar spacing. Prior to these jumps, the crack tip does not extend, but gradually blunts. The latter process induces damage, typically (in other metals, at least) in the form of dislocation subcells [7], into the lamella impinged upon by the tip. Eventually, crack advance is triggered by breakdown of the subcell structure, the path of the crack presumably following the locus of highest damage density. The curved path across lammelae may reflect crack extension along the type of nonlinear slip-line field shear zone which often accommodates fatigue crack tip opening. They certainly would appear to be the product of a plastic process, as opposed to the planar features generally associated with brittle fracture.

Although no evidence of dislocation subcells has been previously reported for TiAl alloys, to the authors' knowledge there has been no effort to date to secure such information. Considerable earlier TEM work, however, has shown [7] that for a variety of materials including low carbon steel, alloy steel, Al alloys, and Ti-6Al-4V, fatigue crack tip subcells exist and range in size from 50 to 200 nm. The present "subcell" sizes are somewhat smaller, but comparable with these dimensions.

References

1 P. B. Aswath and S. Suresh, *Mats. Sci. Eng.*, **A114** (1989) L5-L10.

2 P. S. Pao, A. Pattnaik, S. J. Gill, D. J. Michel, C. R. Feng, and C. R. Crowe, *Scripta Met.*, **24** (1990) 1895-1900.

3 J. Lankford and M. Longmire, *J. Mats. Sci.*, **26** (1991) 1131-1136.

4 C. M. Agrawal, K. Hunter, G. W. Pearsall, and R. W. Henkens, *J. Mats. Sci.*, (in press).

5 A. Wahob and C. Grosskreutz, *J. Mats. Sci.*, (in press).

6 K. S. Chan and Y-W. Kim, *Met. Trans.*, (submitted).

7 D. L. Davidson and J. Lankford, *International Materials Reviews* (in press).

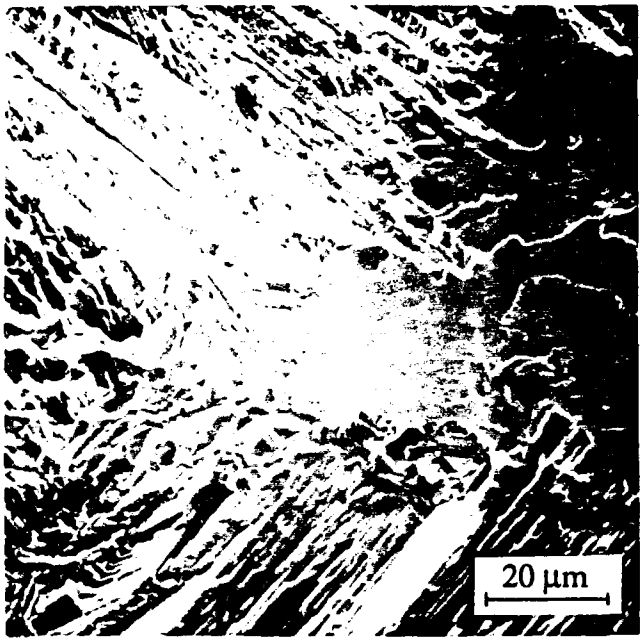

Figure 1. Fast fracture smooth facet (arrow).

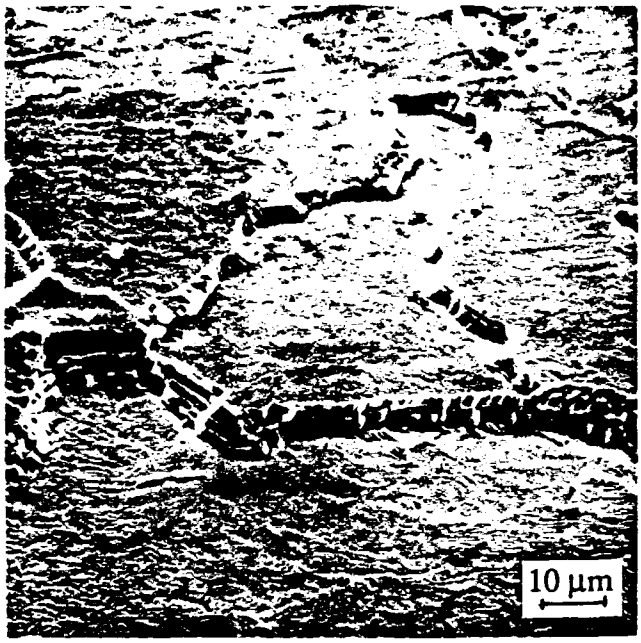

Figure 2. Delamination mode of fast fracture

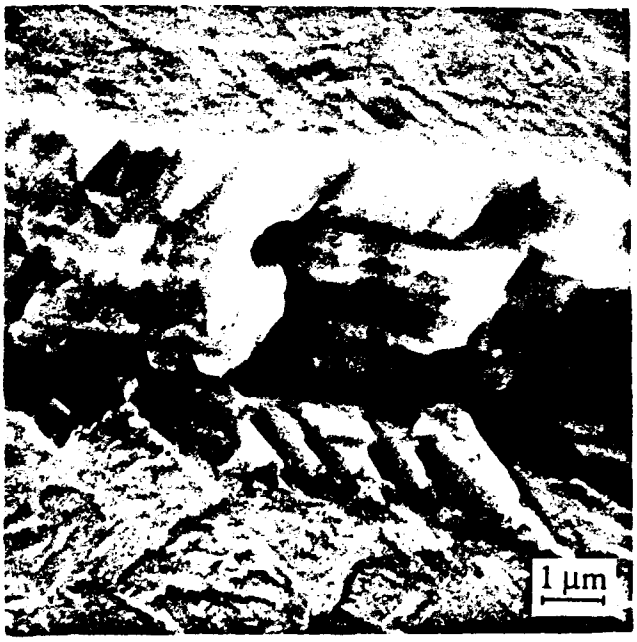

Figure 3. Fast fracture ledge composed of multiple lamellae.

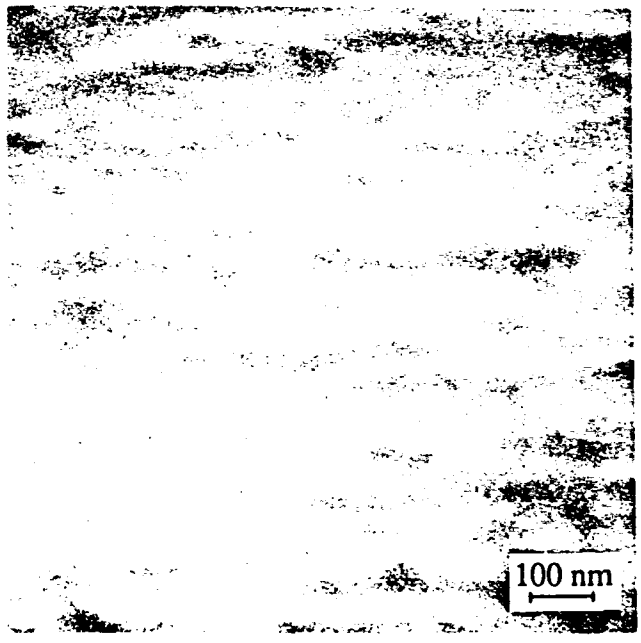

Figure 4. Delaminated fast fracture facet, composed of "fuzzy" bumps separated by apparently fractureless intervening areas.

Figure 5. Smooth facet details, showing elevations (E) and depression (D); majority of surface not truly smooth, but composed of bumpy, fine-scale structure; 60° tilt.

Figure 6. Microfacet-nature of bumps in Figure 5; 60° tilt.

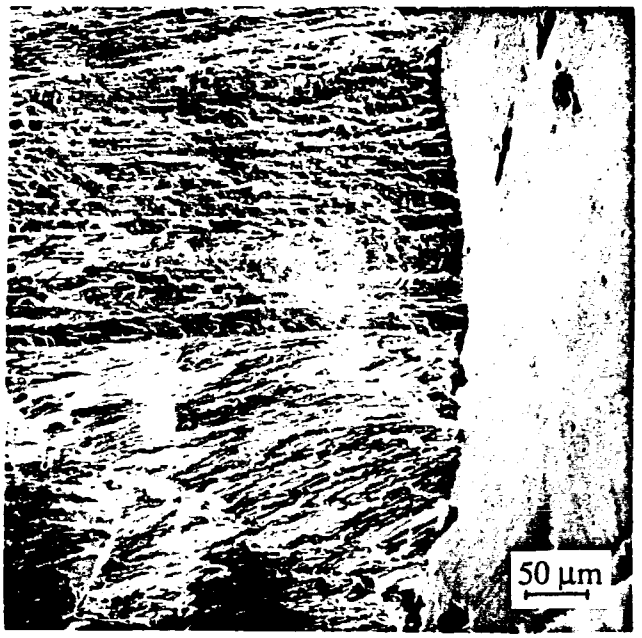

Figure 7. Translamellar fatigue crack growth.

Figure 8. Lamellar nature of crackpath; similar appearance to ledge structures observed at same magnification for fast crack growth in Figure 3.

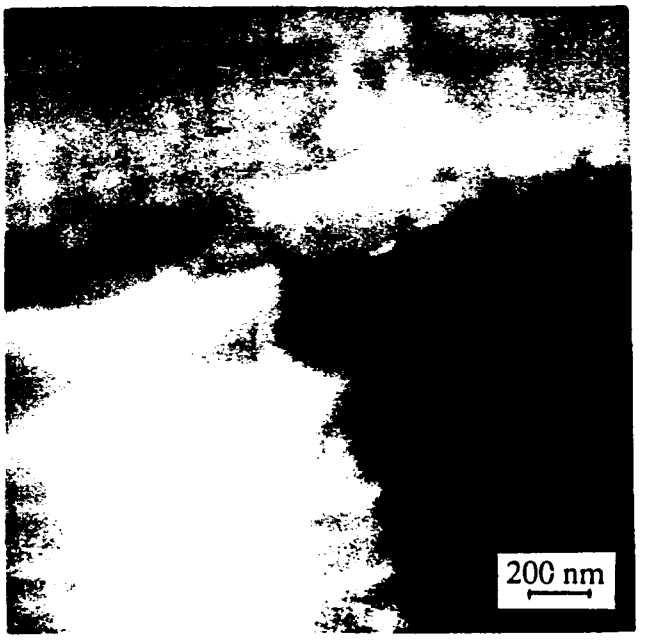

Figure 9. Poor resolution of lamellae surface details at high magnification in SEM.

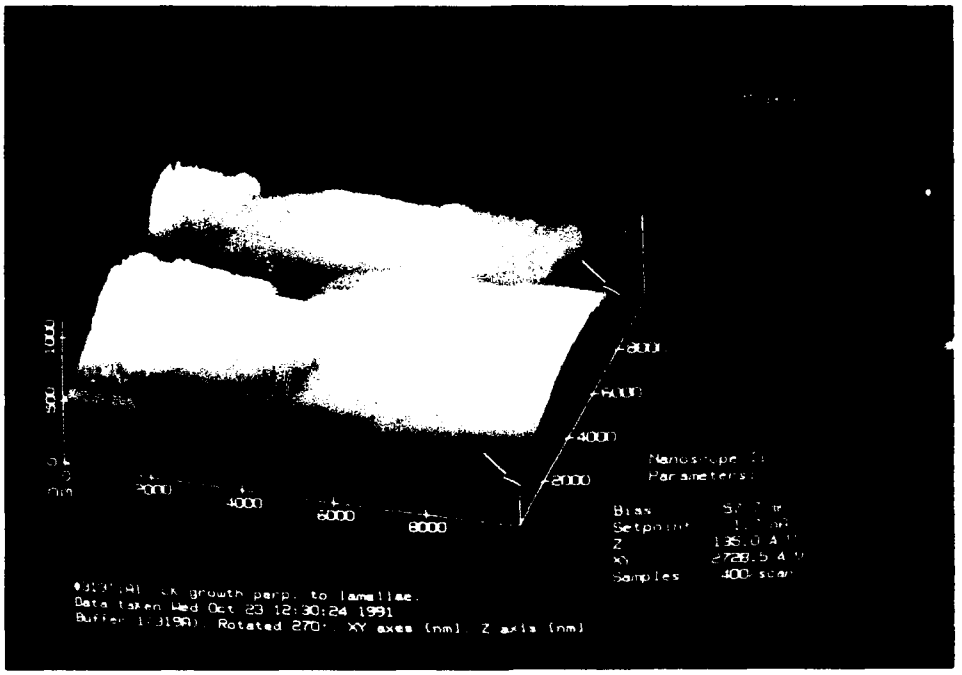

Figure 10. Translamellar fatigue crack fracture surfaces. Arrows indicate crevices which appear to constitute lamellae interfaces (r/r, etc.); 30° tilt.

Figure 11. Narrower variant of translamellar features shown in Figure 10; 30° tilt.

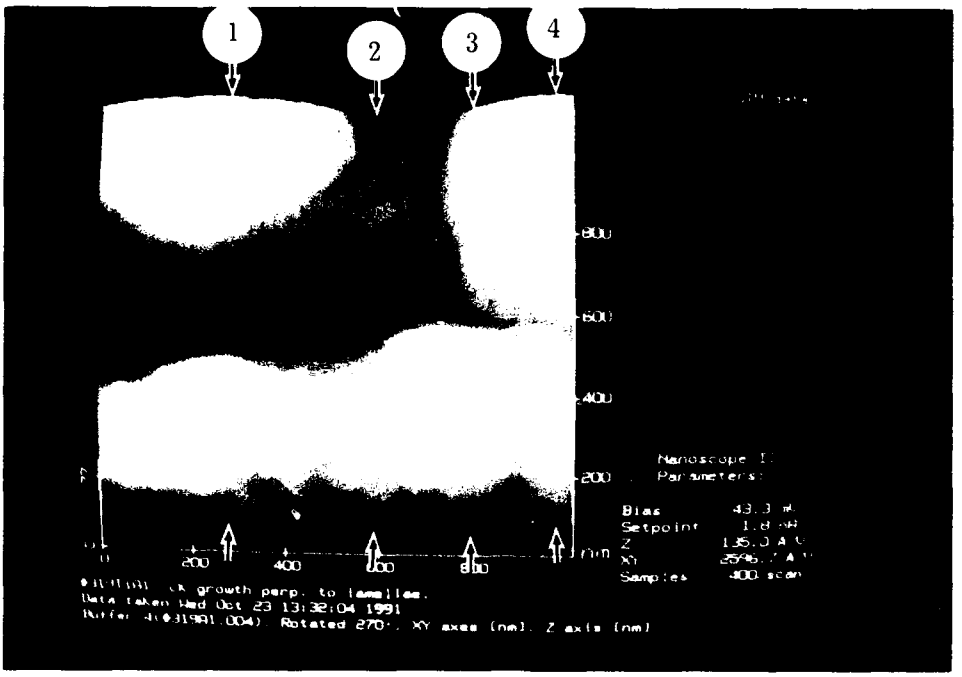

Figure 12. Crevice region (dark) surrounded by lamellae (light); 60° tilt.

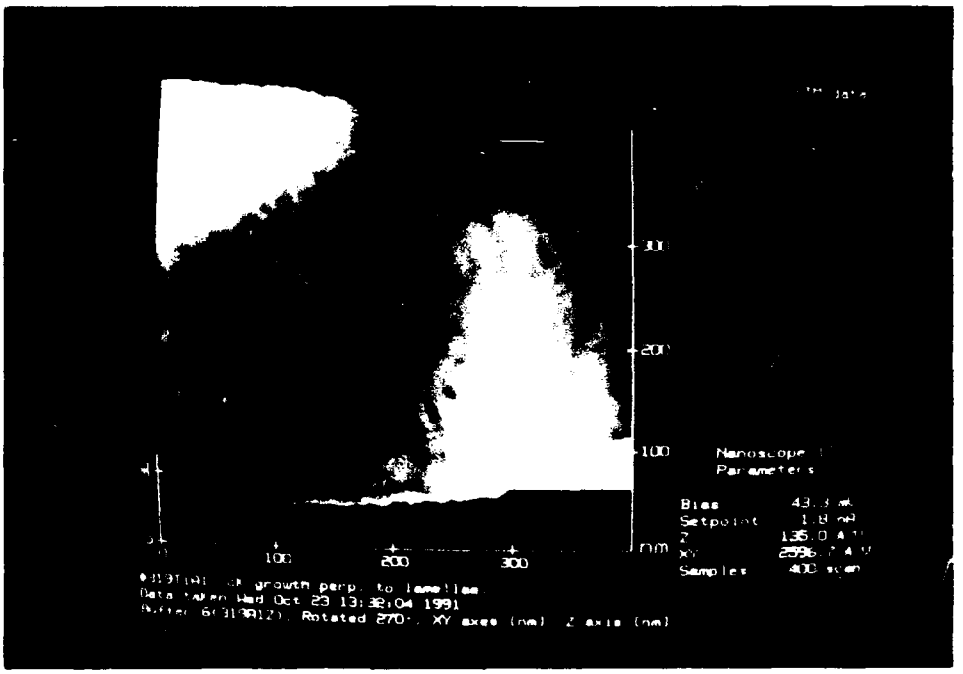

Figure 13. Apparent subgrains elongated parallel to the CG direction composing the surface of the crevice zone; 60° tilt.

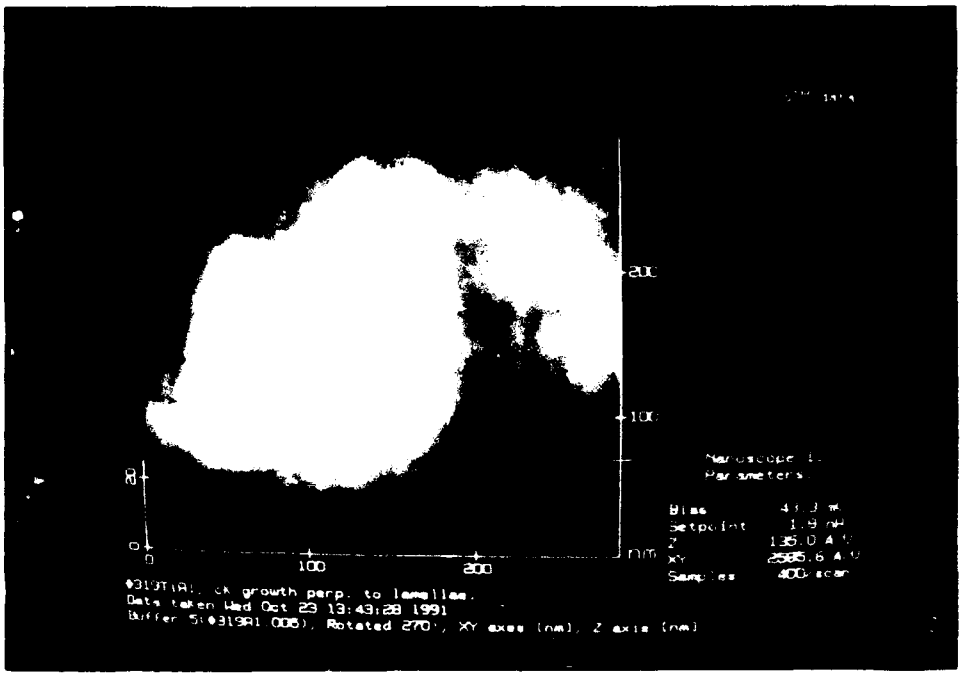

Figure 14. Lamella substructure, elongated normal to CG direction; 60° tilt.

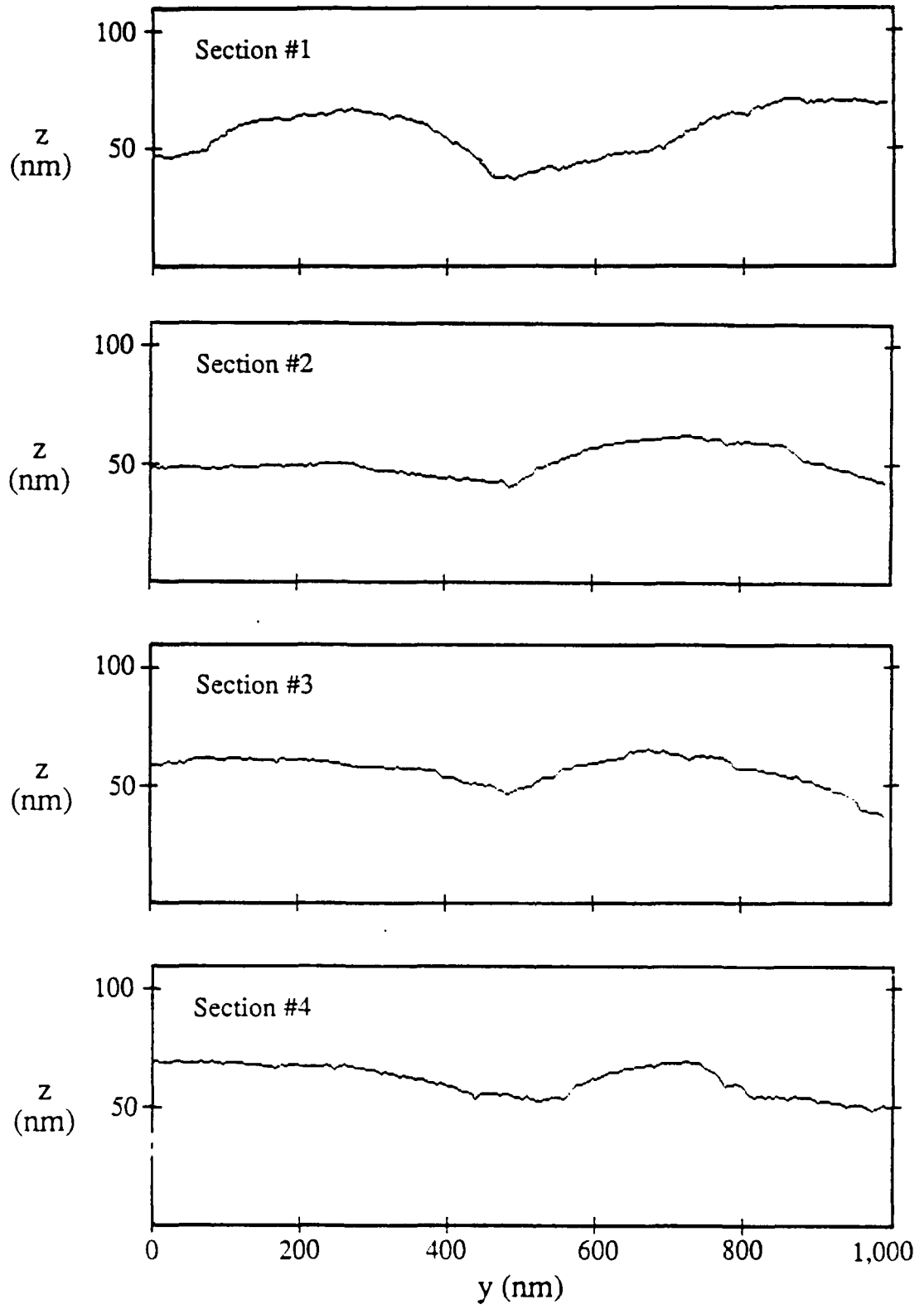

Figure 15. Crack profiles along arrowed sections in Figure 12; crack growth right-to-left.

PERSPECTIVES ON FATIGUE AND FRACTURE TOUGHNESS

This section gives an overview of the fatigue and fracture toughness work done over an extended period of time with the goal of gaining a broader perspective on these fracture processes than is available from the study of any one material. We have attempted to look for similarity in fatigue crack growth characteristics in a fairly broad range of microstructures and to use this information as a basis to model fatigue crack growth behavior; the end objective being to predict the fatigue crack growth resistance of new microstructures. Some of the links made between properties have experimental support, but should still be treated as hypotheses at this time. Although the work on fracture toughness is confined to the titanium aluminides, a range of microstructures has been examined and this has allowed a broader understanding of fracture toughness than would be available from detailed studies of any single microstructure.

Perspectives on Fatigue

Introduction

This section treats fatigue as a failure mechanism, which includes both fatigue crack initiation and growth, although most of the emphasis of our research has been on crack growth. Most, but not all, of the results from which this perspective was derived, came from funding by the Air Force. The perspective is not intended to be a review of all that is known about fatigue in many materials, but is related mainly to the materials we have studied: the aluminum and titanium alloys, and to a lesser extent a superalloy and steels.

Two approaches have been taken to describing fracture under cyclic loading:

(1) The traditional mechanical engineering approach is to produce design data - relating

$$\text{Stress } (\Delta\sigma) \text{ to cycles to failure } (\Delta N_f) \qquad (1)$$

The problem with this approach is that no information on mechanisms of fatigue are included, thus each change in conditions requires generation of another set of data.

(2) The materials science approach is to seek information on a more mechanistic level. Thus, crack initiation processes are separated from those involved in fatigue crack growth.

$$\Delta N_f = \text{cycles to initiation } (\Delta N_i) + \text{cycles of crack growth } (\Delta N_c) \qquad (2)$$

This allows the mechanisms of each of these events to be assessed separately. A fairly recent corollary to this approach recognizes that the growth of small cracks (sc) and large cracks (lc) may be different enough to require individual assessment. Thus,

$$\Delta N_c = \Delta N_{sc} + \Delta N_{lc} \qquad (3)$$

It is instructive to examine briefly what we know about each of these

aspects of fatigue.

Fatigue Crack Initiation

The discussion here is limited to metallic and intermetallic alloys and for cracks initiating from a polished surfaces without residual stresses and under conditions where environment does not have a dominant effect. Studies have shown that there are numerous sources of fatigue cracks: The most common mechanisms of fatigue crack initiation are:

1. Cracking at inclusions - many engineering alloys, especially low cost materials have numerous unwanted particles within the matrix which are introduced during extraction and manufacturing processes. These inclusions, usually ceramics or intermetallics, often debond or break, and are one of the most favorable sites for crack initiation. In some materials, a fatigue crack initiated very early in the cyclic lifetime of the material [1]. Inclusion shape and composition are important, as is the level of cyclic stress (magnitude and R-ratio).

2. When the inclusions are well bonded, or the concentration is low, or if they are very small, slip band formation within grains becomes a dominant mechanism. This process is sensitive to alloy composition and fabrication, with such factors as the grain size, number of slip systems, the propensity for single slip, and the orientation of grains on the surface becoming important. For elastic stresses, a large number of loading cycles are normally required for crack initiation when this is the mechanism. The location of cracks initiated by slip is usually at a point of stress concentration (hole, fillet, notch, etc.).

3. Fatigue cracks can initiate at grain or twin boundaries, or at a drastic change in metallurgical microstructure, such as might be found in a weld. Initiation in these locations can be especially susceptible to environment. The number of cycles to initiate a crack is dependent on the ratio between minimum and maximum load, and on the details of how the environment interacts with the alloy.

4. Other. This category can include the effects of brittle phases (as with intermetallic alloys), initiation at pores [2], which might occur during processing of powder metallurgical products, and quite a few other

factors difficult to categorize.

The finish of the surface is a very important factor for fatigue crack initiation. The degree of roughness is, perhaps, the most important factor, with residual stresses also of great importance. Surface roughness is easy to measure, but residual stresses are not. An example of recent work to relate surface finish, as measured by increasingly quantitative tools, to crack initiation is given in [3].

Two of the most common mechanisms of fatigue crack initiation listed above are illustrated in **Fig. 1**. In each case, there were many sites where cracks could have initiated, but few sites where initiation actually occurred. In one study there were 400 inclusions in a grain in the high stress region where a crack could have initiated, yet cracks developed at only 2 of these. A study in coarse grained Astroloy showed that crack initiation depended on the size of the grain and its crystallographic orientation [4].

In conclusion, there are many mechanisms of crack initiation, and numerous factors which can influence these mechanisms, many of which are difficult to measure or even assess qualitatively. Thus, our ability to predict the mechanism by which fatigue cracks will initiate is very poor, as is the ability to predict the number of cycles to crack initiation. Further research to define quantitative predictive models for crack initiation in constructional materials is badly needed.

If fatigue crack initiation is hard to predict, why not ignore it? It is, in fact, very difficult to build a structure of some complexity completely free of flaws, and these flaws are essentially cracks which are likely to grow under cyclic loading. Thus, many structural designs now incorporate the probable existence of cracks as integral to the philosophy of the design and assume that they begin growing as soon as the structure is put into service.

Damage Tolerant Design of Structures

Incorporating flaws in design has been a traditional problem in designing structures made from constructional metals and alloys, but with the development of "advanced" materials, e.g., ceramics and composites, the need to understand and predict fatigue behavior has

become even more critical. These new materials are more brittle and exhibit lower fracture toughness; therefore, the size of a crack which could transition from subcritical (fatigue) to critical (fast) crack growth is much smaller. Another application where fatigue is becoming increasingly important is in prediction of the lifetimes of microelectronic structures such as the plated through hole interconnects in printed wiring boards and solder joints in surface mounted technology. In electronics the issue of structural lifetime has become important because of the increasing density of electronics components packaging and because of the increasing severity of the environments in which electronics is being applied, e.g., engine controls for automobiles.

General Aspects of Fatigue Crack Growth

If a structure is considered to have crack-like flaws, then predicting fatigue crack growth becomes a very important issue; thus, considerable research has gone into trying to understand the factors controlling crack advance and how to design materials resistant to fatigue crack growth. The most common method used to assess fatigue crack growth is the correlation between the cyclic stress intensity factor (ΔK) and the crack growth rate (da/dN) established by experiment. This correlation is a straight line when a log-log plot is used, at least over some range of crack growth rates; at very low values of da/dN for large cracks, this correlation changes and becomes asymptotic to a value of stress intensity factor (ΔK_{th}), the threshold ΔK below which a crack will not grow. For most engineering structures, it is this lower region of crack growth which is important to the design life of the structure, and it is in this regime that an understanding of crack growth mechanisms is most required.

Research on the mechanisms of fatigue crack growth in metals and alloys has recently been examined in a review paper [5]; some parts of that review will be summarized and extended in this section. The information given below is restricted to conventional constructional materials, e.g., steels; aluminum, titanium, and intermetallic alloys. Recent studies of partially stabilized zirconia (PSZ) [6] have indicated that this "ceramic alloy" may be included with the more conventional materials. This discussion is further restricted to crack growth under constant amplitude loading and largely excludes the effects of environment. Thus, the mechanisms of fatigue crack growth that have been found are applicable generally to engineering materials. However,

the studies from which these mechanisms were identified were restricted to the materials science and mechanics of fatigue phenomena rather than to the conditions applicable in engineering use - environmental effect were largely excluded.

1. The mechanisms of fatigue crack advance are probably the same for the large variety of metals and alloys studied. This conclusion comes from observing that fatigue cracks in all of these materials at low applied stress intensity factor (ΔK) have the same characteristics: crack growth is not continuous, the crack tip undergoes a cycle of sharp to blunt to sharp crack tip opening, and periodic linear surface features (striations) are generally formed (but sometimes they are very difficult to detect; i.e., with fractography using SEM).

2. Fatigue cracks do not open to the crack tip immediately on the application of load. This phenomenon, termed "fatigue crack closure," is important because it influences the relationship between the driving force for crack growth, ΔK, and the material response, the crack growth rate (da/dN).

3. Large fatigue cracks exhibit a ΔK below which fatigue cracks will not grow, ΔK_{th}. It has been shown that ΔK_{th} is directly linked to fatigue crack closure, and in some instances, ΔK_{th} can be predicted [7].

4. As ΔK increases beyond the threshold region, the da/dN-ΔK correlation becomes linear over several decades of crack growth rate - often termed the "Paris region." This is the region over which similitude occurs at the crack tip. At the upper end of this curve, the slope of the curve increases as the instability of fracture increases, and the conditions necessary to induce fast (uncontrolled) fracture are approached. The K level at which fast fracture occurs is usually referred to as the fracture toughness, K_c.

5. Small fatigue cracks grow at values of ΔK below ΔK_{th} (for large cracks), and at rates much faster than large cracks (when ΔK values overlap). The general reasons for that behavior are (1) characterizing a crack by ΔK does not describe the same crack tip conditions for both large and small cracks, so similitude is lost, and (2) metallurgical factors such as grain structure or slip characteristics, are generally not considered by

continuum mechanics modeling but are often important. The dimensions of cracks and microstructural features and the loading conditions which cause small crack effects to occur are not, in general, established, although for many materials, small crack have been studied [8]. However, the mechanisms of crack extension have been shown to be the same for both small and large cracks [9].

6. Growing fatigue cracks in aggressive environments usually results in alterations to the levels of ΔK_{th}, and this change may persist to fairly large values of ΔK. Application of variable amplitude loading often has unpredictable effects caused mainly by disruptions in similitude at the crack tip. The effects of environment and variable amplitude loading on fatigue crack growth both need additional research.

Mechanisms of Fatigue Crack Advance

Fatigue cracks growing through metals and alloys have been observed to lengthen only intermittently; i.e., fatigue cracks grow and arrest, at least in the portion of the da/dN-ΔK curve near to ΔK_{th}. Likewise, the crack tip opening has been observed to undergo changes from cycle to cycle, in what has been termed as the sharp-blunt-sharp cycle (SBS). This behavior has also been observed in partially stabilized zirconia [6], which is a ceramic composite, but exhibits behavior similar to metals. As a sharp fatigue crack tip blunts, slip lines are observed to form at the crack tip, and with additional cycles separation often occurs along these faults, and the crack lengthens. Sharp and blunt fatigue cracks are illustrated in **Fig. 2**.

The SBS crack tip behavior and slip line formation and breakdown have been linked to the formation of periodic fracture surface features - striations - which mark the points of crack advance and arrest [10]. Striations form in nearly all materials that exhibit subcritical crack growth, and at low ΔK, the number of cycles (ΔN) required for incremental crack growth (Δa) is much greater than 1. Within the Paris region, cracks usually grow on each loading cycle. Two examples from titanium alloys of fracture surface striations are shown in **Fig. 3**; in (a) striations for the 2411 alloy appear rather rounded, while in (b) for the CORONA-5 alloy, striations appear more angular.

The description of crack advance given above is common to a large

number of metals and alloys, but assuming that cracks in "advanced" materials will exhibit the same behavior may not be justified. The following are some of the issues related to these materials:

- Ceramics: what are the mechanisms of crack growth? Is there a unique "small crack" effect?
- Composites with hard particles and whiskers: matrix properties dominate fracture properties, but the particles pay a large role in controlling material crack advance; how is the mechanism of crack advance changed? What is the effect of the K level?
- Composites with continuous fibers: interface properties predominate. Fiber bridging is the dominate mechanism in the best materials, but what are the materials science and mechanics of fracture in these materials?

Fatigue Crack Closure

This important phenomenon has been the subject of considerable investigation, but 20 years of work has not resulted in conclusive evidence about how closure is to be described. Fatigue cracks do not open immediately upon application of load, requiring some value of stress intensity to open the crack to the tip, K_{open}. If this value can be determined, the effective driving force for the crack becomes $\Delta K_{eff} = K_{max} - K_{open}$. The problem is: How can K_{open} be measured? Several methods have been used:

(1) Compliance (crack mouth or back face strain gages), and
(2) Ultrasonic methods, push rods, and other methods.

The results of all these tests has been conflicting data from which no unifying concept has emerged. The state of affairs was summarized by an ASTM round robin report [11] that concluded that the considerable data in the literature could not be used in any meaningful way.

Recently a new method for making measurements of K_{open} at crack tip has been developed using stereoimaging [12]. Experimental evidence using this technique has given (1) systematic closure results, and (2) consistent peeling open behavior. Systematic behavior has been found for the correlation between $U = K_{eff}/\Delta K$ and $1/K_{max}$ for 304SS, aluminum alloys,

CORONA-5, the titanium aluminide alloy 2411, fine grained Astroloy, and partially stabilized zirconia. This similarity in closure behavior is for a wide variation in material characteristics. Modeling closure indicates that deformation of material at and near the crack tip is the cause of closure, but that it is not possible to discriminate between plastic zone residual stresses and material deformation in the crack wake. This mechanism of fatigue crack closure is termed plasticity induced fatigue crack closure. Two examples of the experimentally derived relationship between U and $1/K_{max}$ are shown in **Fig. 4.**

Two other mechanisms have been suggested as being responsible for fatigue crack closure. Both of these mechanisms prevent a crack from fully closing on the unloading portion of the loading cycle: (1) very rough fracture surfaces are produced in some materials, and it is thought that interference between surfaces can occur. However, there is not very much actual experimental evidence for this and the models for this mechanism of closure are inadequate. (2) In contrast, there is considerable evidence for oxide induced closure. Fracture surfaces oxidize due to environmental effects, causing mating surfaces to come together at higher loads than without oxidation. Modeling of this effect is virtually not existent.

Fatigue Threshold

Extensive and careful measurements have been made of the threshold for fatigue crack growth (ΔK_{th}). It has been shown [7,13] that ΔK_{th} is a manifestation of crack closure, and that it results mainly from the cyclic plasticity needed to grow a fatigue crack, at least in the absence of environmental effects. One simple model which has been shown to have validity, at least for some alloys and composites, is

$$\Delta K_{th} = (1-R)\sigma_y\sqrt{(2\pi r_s)} \qquad (4)$$

where r_s is the slip line length found at the tips of cracks growing at rates near to ΔK_{th}. Combining the effects of plasticity induced closure with the other mechanisms for closure is still to be accomplished.

How Do All These Factors Fit Together ?

There is obviously a need to fit all these separate pieces of

information together if fatigue crack growth is to be understood and if a predictive capability is to be derived. Thus, it is necessary to model fatigue crack growth processes. A number of models have been derived, and many of them have some of the same characteristics: they couple the crack opening displacement and strain in the plastic zone of the crack tip to the cyclic stress-strain curve and use the low-cycle fatigue law as a failure criterion. These models have been reviewed as a group, indicating their similarities, differences, and the assumptions inherent in each [5]. Here, only the model derived by Davidson [14] will be used to indicate how the various fatigue parameters fit together, but this model has many similarities to other models [5]. The physics incorporated in this model is based on considering the geometry of the crack tip. The approach is empirical, as it must be until adequate continuum models for parameters such as crack tip opening or crack tip strain and the cyclic stress strain curve exist.

The following parameters are measured and used in the analysis:

Cyclic stress-strain:	$\Delta\sigma = K_1(\Delta\varepsilon_p)^{n'}$	(5)
Low cycle fatigue:	$\Delta\varepsilon_p \Delta N^{\beta} = \varepsilon_c$	(6)
Crack tip strain:	$\Delta\varepsilon_p(0) = K_o \Delta K_{eff}^{r}$	(7)
Crack growth rate:	$da/dN = B' \Delta K_{eff}^{s'}$	(8)
Striation spacing:	$\Delta a = A_o \Delta K_{eff}^{n}$	(9)

Where applicable, ΔK_{eff} is used as the correlating parameter in order to include the effect of ΔK_{th}. In this model, crack opening displacement occurs because dislocations are generated at the crack tip as ΔK exceeds ΔK_{th}. The high levels of stress and strain at the crack tip are sufficient to require other dislocations to form at sources other than at the crack tip and move within the outer parts of the plastic zone, but these secondary events are not considered to directly effect the crack extension process.

The relationships between macroscopic crack growth rate, crack tip strain variation, and number of loading cycles is shown schematically in **Fig. 5**. This variations in crack tip strain shows what has been observed - there are variations in the crack tip events leading to the macroscopic

growth observed. These detailed events leading to crack advance have not been described by modeling. Striation spacing, crack tip strain, and crack growth rates are averaged for modeling purposes.

Unfortunately, microstructure is not explicitly incorporated into these expressions, but microstructural effects are included indirectly through the empirical correlations used. At this time there is no direct method of including a metallurgical description of the material in models.

The model allows the parameters describing crack growth (B' and s') to be directly related to the crack tip parameters describing material failure (β and ε_c). The following relationships may be derived [12]:

$$s' = (n'+1/\beta)/r \approx 1/\beta r \quad (10)$$

$$\varepsilon_c = K_0(A_0/B')^{\beta} \quad (11)$$

$$n = n'r \quad (12)$$

Thus, slope of the da/dN-ΔK_{eff} curve is related to the slope of the low-cycle fatigue curve, the rate of increase in strain at the crack tip with increasing ΔK_{eff}, and to minor extent, the cyclic work hardening rate. Likewise, the slope of the relation between striation spacing and ΔK_{eff} is related to the cyclic work hardening rate and the rate of increase in strain at the crack tip with increasing ΔK_{eff}. These correlations indicate that the parameter **r** is an important variable, but one for which there is presently no continuum mechanics model. These equations have been used with measured values of **r** to derive parameters describing material failure at the crack tip (β and ε_c). Derived values of these parameters are given in Table 1.

Some trends may be seen in these variables even though there is scatter. The general relationships between the slope of the da/dN-ΔK_{eff} curve and that of the low cycle fatigue correlation are shown in **Fig. 6.** The trends shown are observed for separate determinations of crack growth rates and LCF.

Table 1
Fatigue Crack Modeling Parameters

Material	r	β	ε_c	s'
2411	0.73	0.55	0.18	2
Super α2	1.6	0.57	0.28	1.8
Ti-6Al-4V	1.9	0.77	0.47	3.1
CORONA-5	1.1	0.64	0.66	1.8
7091(dry)	0.32	0.17	0.34	2.1
304SS	1.2	0.68	0.34	3.1
PSZ	0.29	0.029	0.04	10
$\gamma+\alpha_2$ lamellar	0.36	0.16	0.15	2.26

The problem with most continuum analyses of fatigue crack growth is that the slope of the da/dN-ΔK_{eff} curve must be either 2 or 4 (depending on the analysis) [5], while many materials exhibit curves which are not integer values. The empirical analysis presented here, together with several other, similar analyses found in the literature [5], allow the slope **s'** to vary according to the material and its characteristics. The reasons for this limitation to continuum modeling of fatigue crack growth have not been identified, but further work should be done so that the limitations inherent to the empirical models can be overcome.

What Can We Predict ?

Our knowledge of fatigue crack growth mechanisms and mechanics is ultimately put to the test by asking this question. Unfortunately, the answer at this time is "nothing with certainty." Thus, the fatigue properties of a newly synthesized material cannot be predicted. However, it is possible to estimate some factors and trends with current knowledge.

Microstructural effects may be incorporated into the growth of large fatigue cracks through an estimate of ΔK_{th}. Accounting for the effects of microstructure on the growth of small cracks is more difficult. Evidence of microstructural effects on small cracks has been reviewed [8], and

some ideas were given on how to assess these effects, but there is still considerable research to be done on this subject. For large cracks, microstructure can be incorporated as follows:

- Estimate the slip distance (r_s) from a knowledge of the microstructure, or from slip lines observed on compression test specimens,
- Measure the tensile yield stress (σ_y), and use the estimate to calculate
- $\Delta K_{th} = (1\text{-}R)\ \sigma_y\ \sqrt{(2\pi r_s)}$.

An example of this procedure was shown in the section on fatigue of the Nb_3Al alloys. It must be recognized that there are a number of microstructural features that can influence this estimate in some alloys, e.g., colony boundary effects in some titanium alloys. Thus, this equation provides only an estimate of the value of ΔK_{th} measured from actual crack growth experiments. The crack growth rate at ΔK_{th} may be taken as 10^{-10} meters/cycle; therefore, one point on the crack growth rate curve is established when this estimate is used.

To determine the remainder of the da/dN-ΔK_{eff} curve, it is necessary to establish the slope of the line. The slope for many metallic alloys is approximately s' = 2, as may be seen from Table 1, or slope may be estimated using eq. (10)

- $s' \approx 1/\beta r$

but β and r must be known, implying that the low-cycle fatigue and cyclic stress-strain curves must be known to make this estimate. It may be more difficult to determine these parameters than to measure s'. Thus, it might be more feasible to measure the da/dN-ΔK curve, estimate ΔK_{th} and derive s'; then, assuming r=1, derive the value of β using the above equation, thereby establishing the *slope* of the low-cycle fatigue crack initiation relationship. To determine the *magnitude* requires determination of ε_c, which may be estimated from eq. (11)

- $\varepsilon_c = K_0(A_0/B')^{\beta}$

but this requires measurement of crack tip strains (K_o), striation spacing (A_o) and B' from the crack growth rate equation. These parameters are not easily measured.

In summary, prediction of the fatigue crack growth rate curve from material characteristics without extensive measurements is still difficult, but estimates may be made based on empirical correlations. Further development of continuum models and estimating techniques are needed.

Design of Fatigue Resistant Microstructures

Whether or not a material may be considered more "fatigue resistant" may depend as much on the initiation characteristics as on the rate of crack growth. Fatigue crack initiation resistance is best enhanced by decreasing the level of defects in the material, specifically inclusions and pores, and decreasing grain size.

If fatigue crack growth alone is considered, one of the main beneficial effect of changes in alloy composition and microstructure would be to increase the level of ΔK_{th}. As may be seen from eq. (4), this can only occur if slip length (r_s) is not much reduced when flow stress is increased. The slope of the crack growth rate curve can be decreased by increasing the value of the LCF constant ε_c and decreasing β. One way to consider ε_c is that it represents the magnitude of damage accumulation which must be accrued from crack tip strain before the crack grows. The larger ε_c, the more cycles needed to obtain a growth increment. The slope of the LCF equation β is a measure of how much damage is done to the material by crack tip strain; thus, the smaller β, the less damaging to the microstructure is the crack tip strain. The most desirable microstructure is one with a large ε_c and a small β. For a given alloy system, it is not known how to design the microstructure to achieve this result. From Table 1, there is remarkable similarity in values of the LCF constants for the conventional alloys, which indicates that there is not much effect of compositional or microstructural manipulation. Apparently, there is little that can be done by microstructural manipulation to alter the mechanism of damage accumulate at the tip of a fatigue crack, or the level of damage

required for crack advance. The final reason to consider altering microstructure concerns increasing the fracture toughness, K_c, the stress intensity factor at which fast fracture begins. It would be desirable to create a microstructure that prevents fast fracture until large crack growth rates are achieved ($\approx 10^{-5}$ m/cycle).

The reason metal matrix composites offer attractive alternatives to conventional alloys is that the mechanisms of damage accumulation may be changed, usually by adding new mechanisms for controlling the concentration of stress at the crack tip, such as crack bridging. Continuous fiber composites may greatly alter the kinetics of crack growth, depending on the interface characteristics of the material [15]. This effect is shown schematically in **Fig. 7**.

If interface strength is too high, then the fibers act mainly to increase the modulus, which does not affect crack growth mechanism, but alters the driving force ΔK, shifting the curve to the right on the da/dN-ΔK curve. There is no effect if the modulus-normalized value ($\Delta K/E$) is used. If the interface is sufficiently weak, then the crack is bridged by unbroken fibers and the magnitude of ΔK driving the crack is strongly reduced, together with growth rates through the composite. The mechanism of crack growth through the matrix is not changed. When interfaces are very weak, then crack growth occurs along the matrix/fiber interfaces and the composite is not very useful; again the mechanism of crack advance is not affected.

Particulate reinforced metal matrix composites do not offer opportunities for changes crack growth rate available for continuous fiber composites. High modulus particulates my increase ΔK_{th}, but the mechanisms of crack advance through the matrix are not changed, at least not at low ΔK where the plastic zone is very small. The onset of static modes of fracture may occur a lower values of ΔK than for unreinforced matrix due to the constraint of plastcity by the nondeforming reinforcement particles. The net effect is to increase the apparent value of ΔK_{th} but also increase the slope of the crack growth rate curve. The overall fatigue resistance of these composites, especially crack initiation, is highly dependent on the processing techniques and the level of quality control used in manufacture.

Lifetime Prediction

The lifetime prediction of structures is a practical matter very much related to the fatigue characteristics of materials. The starting point for these analyses is deciding whether or not a crack is considered as being present. Large structures, e.g., aircraft and gas turbines, are very likely to contain cracks, while small structures, e.g., microelectronic components, probably do not have actual cracks after fabrication.

If **no cracks** are assumed to be inherent in the structure, then **initiation** is the greatest uncertainty in predicting structural lifetime under constant amplitude loading conditions. If **cracks** are considered as being present, then a knowledge of how to account for the growth of **small fatigue cracks** is the likely to be greatest uncertainty.

The importance of the "small crack effect" appears to be less of an issue for brittle materials than for ductile alloys because the critical crack size for fracture is still quite small for brittle materials, causing fracture toughness to be the design limiting factor rather than the growth of small cracks by cyclic loading. Research has shown [16] that a simple method for including the small crack effects (at least as a first approximation) is to use the growth rate curve for large cracks, and assume that there is no threshold for fatigue crack growth. For fatigue cracks grown in the copper plated into holes in printed wiring boards, which has a very small columnar grain morphology, this assumption was also found to be valid.

Summary and Conclusions

Having reliable fatigue properties for a material is a major limitation to its use in engineering structures. This brief review has extracted some general conclusions about fatigue crack growth from more extensive work and considered, in addition, crack initiation and the growth of small fatigue cracks. Adequate knowledge of fatigue characteristics is limited by the following factors:

(1) Prediction of the number of cycles to cause crack initiation is very difficult because there are several mechanisms, and most of those

are not well enough understood to have been modeled mathematically.

(2) The mechanism of fatigue crack growth is reasonably well understood for metals and alloys, but there are problems with predicting crack growth rates with out extensive measurements. Empiricism is used mainly for crack growth rate predictions due to inadequate crack tip continuum models. For crack growth under variable amplitude loading, there remains much to be learned about how remotely applied loads are transmitted to the crack tip.

(3) Plasticity induced fatigue crack closure can be systematically determined, and linked to ΔK_{th}, which may be estimated from using the relation $\Delta K_{th} = (1-R)\sigma_y\sqrt{2\pi r_s}$, where r_s is derived from microstructural characteristics. Experimental techniques generally in use for measurement of crack closure are not adequate, and neither are continuum models for closure. Other mechanisms, particularly the formation of oxides within the crack, may further alter ΔK_{th}.

(4) The da/dN-ΔK_{eff} and low-cycle fatigue curves are linked: it is likely that one can be determined from the other, but extensive measurements are now required due to the lack of adequate crack tip continuum models. The low-cycle fatigue curve represents both the rate of damage accumulation caused by strain at the crack tip and the cumulative damage which can be endured by the crack tip prior to fracture. Microstructural manipulation in conventional materials does not alter these processes very much.

(5) The "small crack effect," characterized by fatigue crack growth rates in excess of those expected from the growth of large cracks, is a decreasing issue as the ductility of the material decreases. For lifetime predictions where small crack effects are to be considered, assuming there is no fatigue crack threshold is a reasonably good way to include small crack effects.

(6) The onset of fast fracture in metals is usually controlled by the work dissipated in the plastic zone. Other mechanisms can add to the fracture toughness, but the principal determinant is deformation within the crack tip plastic zone. Continuum mechanics has provided much better models for this aspect of fracture than for fatigue, but prediction is still

difficult from first principles.

The Appendix gives a short list of research needs based on linking fundamental materials characteristics and crack mechanics to engineering fatigue problems. The importance of better understanding for each of these items is indicated.

Appendix A
Research Needs
(Fatigue and Fracture Resistance)

- Better mathematical models for predicting fatigue crack initiation are badly needed. New experimental tools and analytical methods appear to be needed to enhance the fundamental understanding and predictability of these phenomena. (Importance: This is the limiting factor in predicting the lifetime of uncracked structures).

- Fatigue crack Initiation often occurs at multiple sites. Several of these small cracks coalesce and a large crack results. How should these events be included in life prediction? (Importance: Life prediction for uncracked structures).

- When and how should microstructure enter into the continuum mechanics modeling of fatigue? (Importance: Connects continuum mechanics modeling to non-continuum effects.)

- Continuum mechanics modeling with reverse loading is too complex to use in an engineering sense. How can this modeling be simplified (Analytical vs. Finite Element)? (Importance: Fundamental understanding of cyclic loading and accurate life prediction under variable amplitude loading).

- Fatigue crack growth in ceramics and composites is not very well understood. What are the mechanisms of crack growth? What factors are important to model? What is the correct description of interface effects in composites? (Importance: Fundamental understanding is needed for better materials to be developed and for confidence when composites or ceramics are used in structures.)

- Experimental and analytical micromechanics need to be more

effectively coupled. New developments are needed in each.

- The importance of fracture research on actual materials should be emphasized; e.g., model materials should be used only when they must be to test concepts, and then these should be used with caution. The reason for this is that fracture modes in model materials are not necessarily the same as those found for actual constructional materials.

References

1. J. Lankford "The growth of small fatigue cracks in 7075-T6 aluminum" Fatigue of Eng. Mater. Struct., 1985, v. 5, pp. 233-248.

2. D.A. Gerard and D.A. Koss "The influence of porosity on short fatigue crack growth at large strain amplitudes" *Int. J. Fatigue*, 1991, v. 13, pp. 345-352.

3. C. Wiesner, H-U. Kunzl and B. Ilschner "Characterization of the topography of turned surfaces and its influence on the fatigue life of Al-7075" *Mat. Sci. and Eng..*, 1991, v. A145, pp.151-158.

4. D.L. Davidson and K.S. Chan "The crystallography of fatigue crack initiation in coarse grained Astroloy at 20°C" *Acta Metallurgica*, 1989, v. 37, pp. 1089-1097.

5. D.L. Davidson and J. Lankford "Fatigue crack growth in metals and alloys: mechanisms and micromechanics" *Int. Mat. Reviews*, 1992 (in press).

6. D.L. Davidson, J.B. Campbell and J. Lankford "Fatigue crack growth through partially stabilized zirconia at ambient and elevated temperatures" *Acta Metallurgica*, 1991, v. 39, pp. 1319-1330.

7. D.L. Davidson "Fatigue crack closure" *Eng. Fracture. Mech.*,1991, v. 38, pp. 393-402.

8. J. Lankford and D.L. Davidson "The role of metallurgical factors in controlling the growth of small fatigue cracks" in **Small Fatigue Cracks**, R.O. Ritchie and J. Lankford, eds, TMS-AIME, 1986, pp. 51-71.

9. D.L. Davidson and J. Lankford "High resolution techniques for the study of small cracks" in **Small Fatigue Cracks**, R.O. Ritchie and J. Lankford, eds, TMS-AIME, 1986, pp. 455-470.

10. D.L. Davidson and J. Lankford "The breakdown of crack tip microstructure during fatigue crack extension aluminum alloys" **High Strength Powder Metallurgy Aluminum Alloys - II**, TMS, Warrendale, PA, pp. 47-57.

11. E.P. Phillips "Results of the round robin on opening load measurement" NASA Technical Memorandum 101601, Langley Research Center, Hampton, Virginia, May 1989.

12. D.L. Davidson "Plasticity induced fatigue crack closure" **Mechanics of Fatigue Crack Closure** ASTM STP 982, J.C. Newman and W. Elber, eds., ASTM, Philadelphia, PA, 1988, pp. 44-61.

13. D.L. Davidson "Small and large fatigue cracks in aluminum alloys" *Acta Metallurgica*, 1988, v. 36, pp. 2275-2282.

14. D.L. Davidson "A model for fatigue crack advance based on crack tip metallurgical and mechanics parameters" *Acta Metallurgica*, 1984, v. 32, pp. 707-714.

15. K.S. Chan and D.L. Davidson "Fatigue crack growth in fiber reinforced metal matrix composites" **Fatigue of Advanced Materials**, R.O. Ritchie, R.H. Dauskardt and B.N. Cox, eds., Mater. and Component Eng. Publ., P.O. Box 1550, Birmingham, UK, 1991, pp. 325-342.

16. S.J. Hudak, D.L. Davidson, K.S. Chan, A.C. Howland, and M.J. Walsch "Growth of small cracks in aeroengine disc material" AFWAL-TR-88-4090, Materials Lab., Wright Patterson AFB, OH, June 1988, Sect. 9, p. 4.

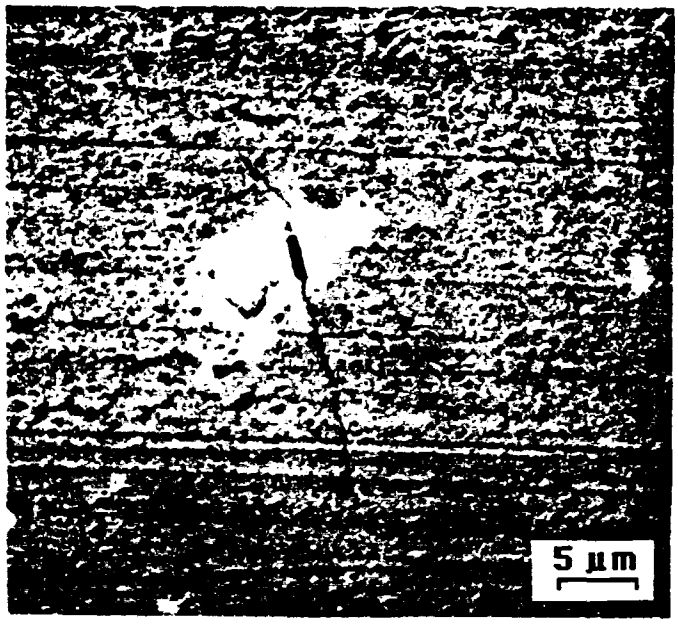

(a)

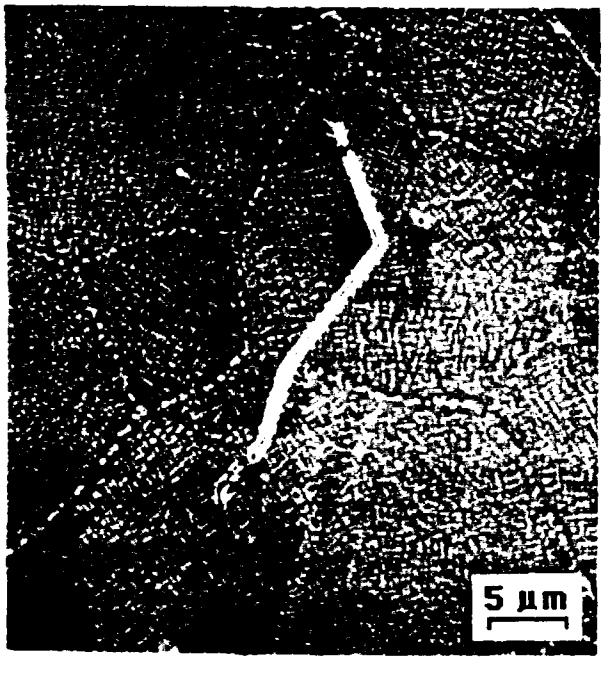

(b)

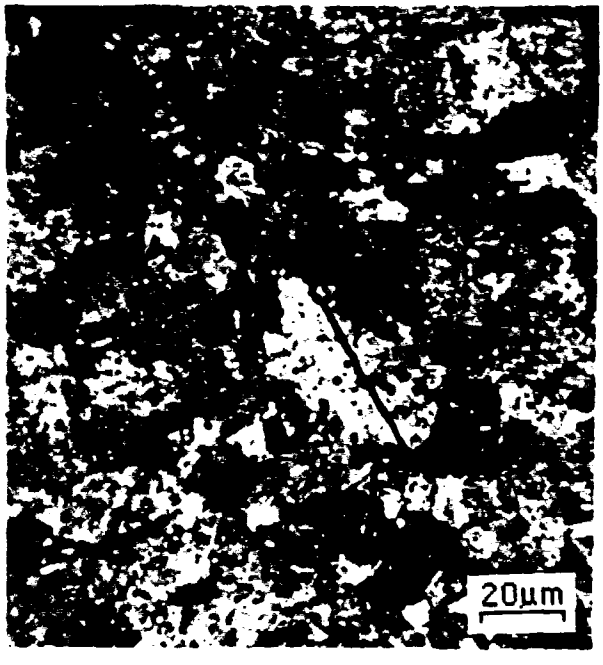

(c)

Fig. 1 Fatigue cracks just after initiation. (a) Crack in 2024-T6 aluminum alloy initiated from the inclusion seen. (b) Crack in the nickel based superalloy Astroloy initiated by slip within the large grain. (c) Crack in fine grained Astroloy initiated by slip.

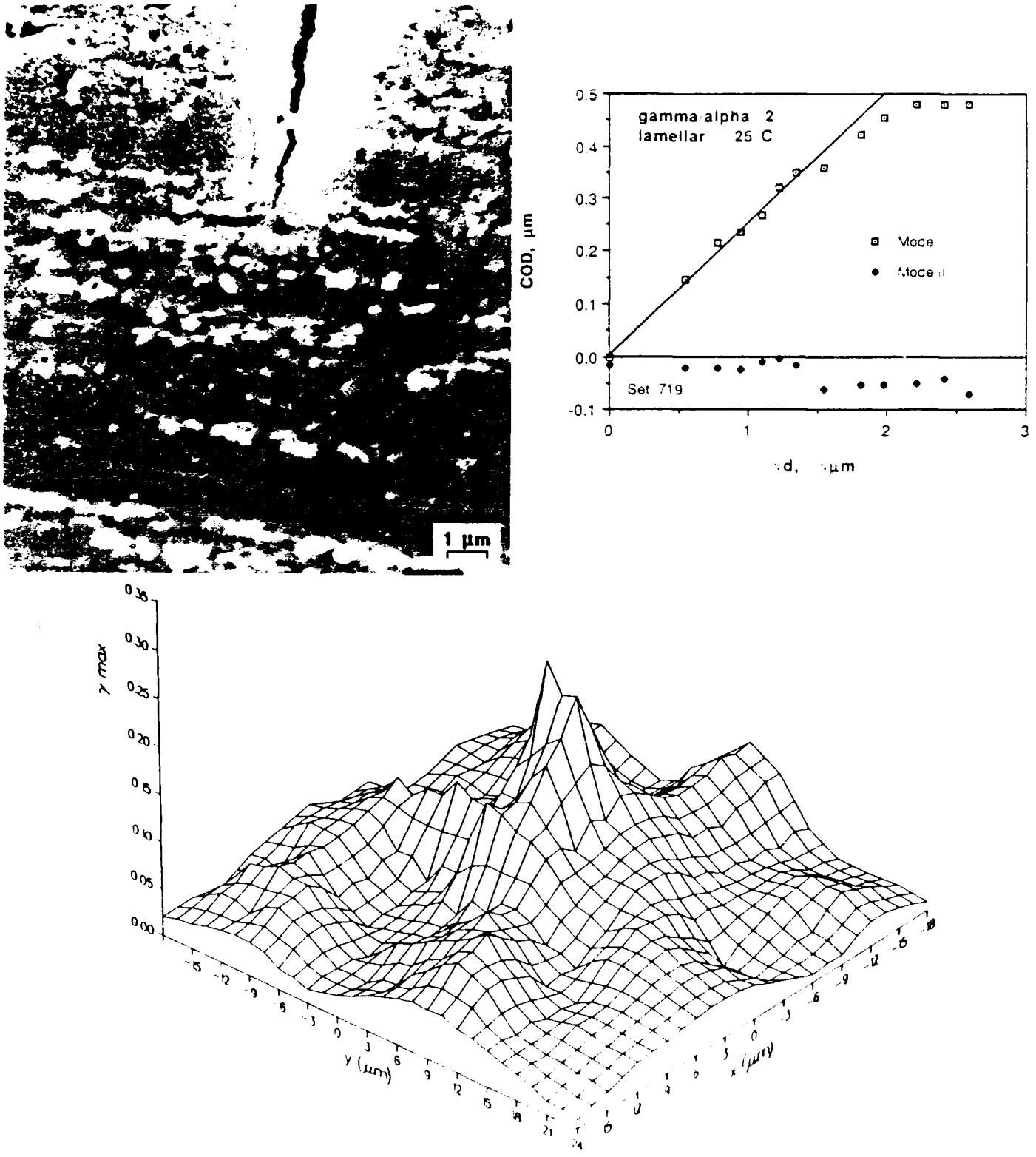

Fig. 2(a) A sharp fatigue crack tip, as indicated by both the photograph and measurement of the crack opening displacement (COD). Tip of the crack is beneath the maximum strain.

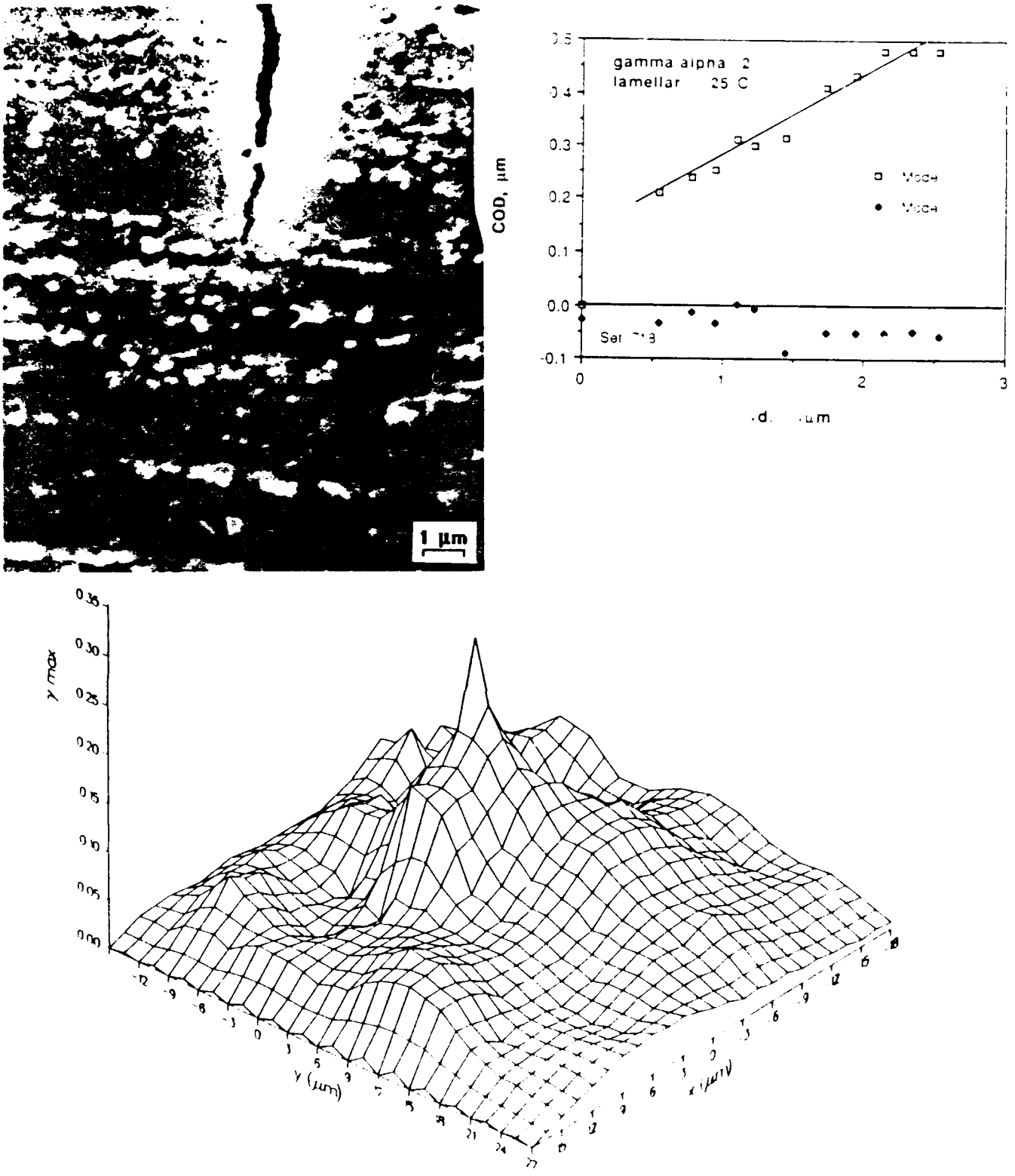

Fig. 2(b) The same crack tip as in (a) a few cycles later after it has blunted without growth. Comparison of the strain plots shows that the blunt crack tip has the largest strain at the crack tip.

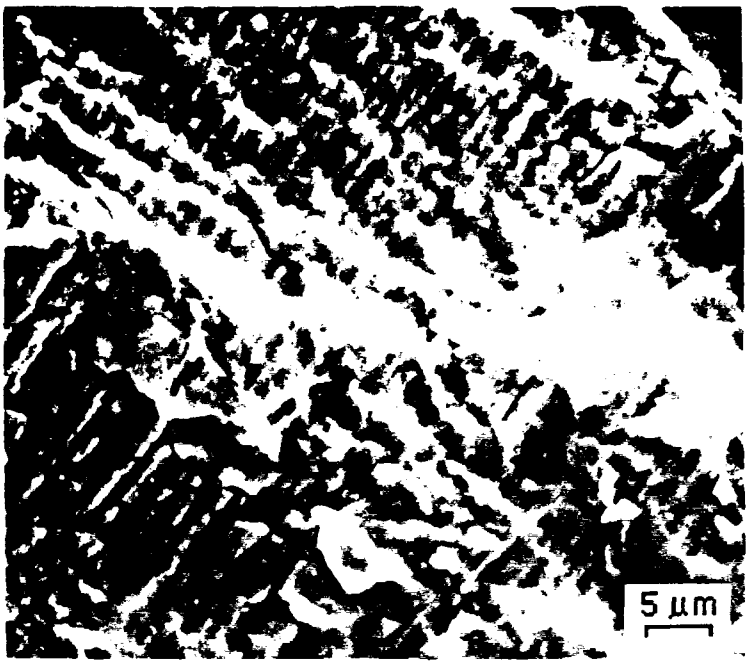

(a)

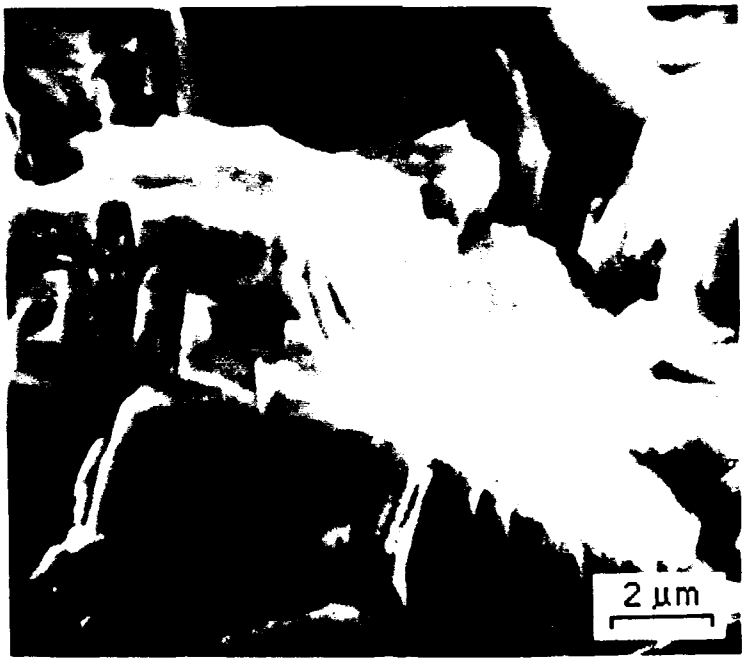

(b)

Fig. 3 Fracture surfaces of two titanium alloys showing the periodic nature of crack advance and arrest. These parallel lines are often called fatigue striations. (a) CORONA-5, and (b) Ti-14Al-24Nb.

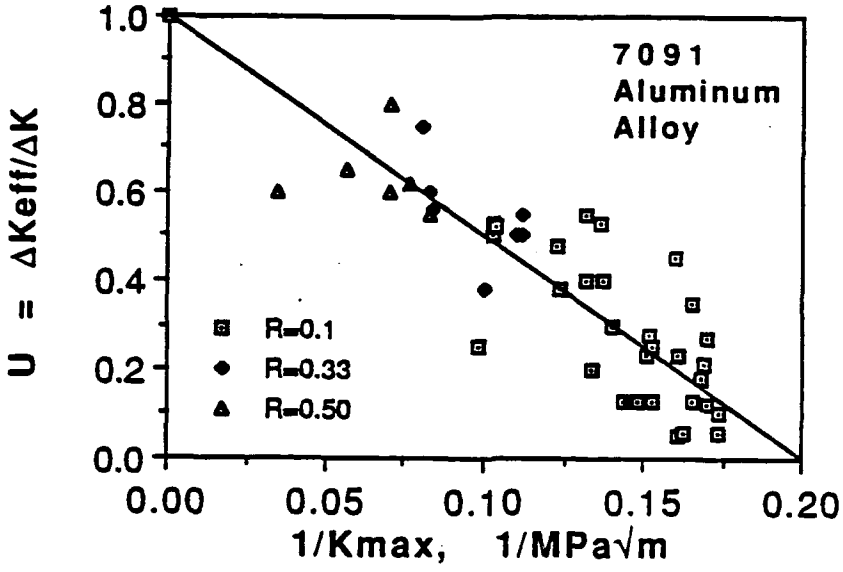

(a)

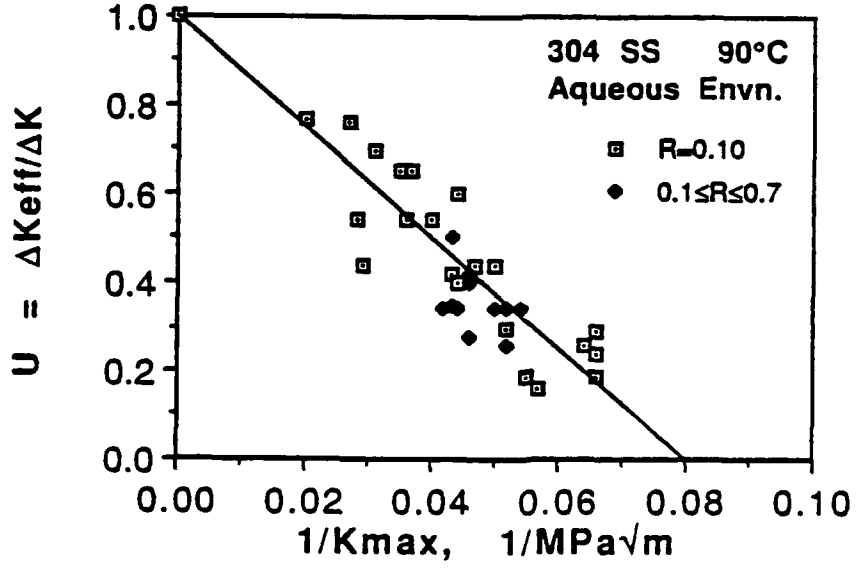

(b)

Fig. 4 Fatigue crack closure, as expressed through ΔK_{eff}, for (a) the powder metallurgy aluminum alloy 7091, and (b) 304 stainless steel. Data taken at various values of R (= min. load/max. load) have the same behavior when correlated in this way.

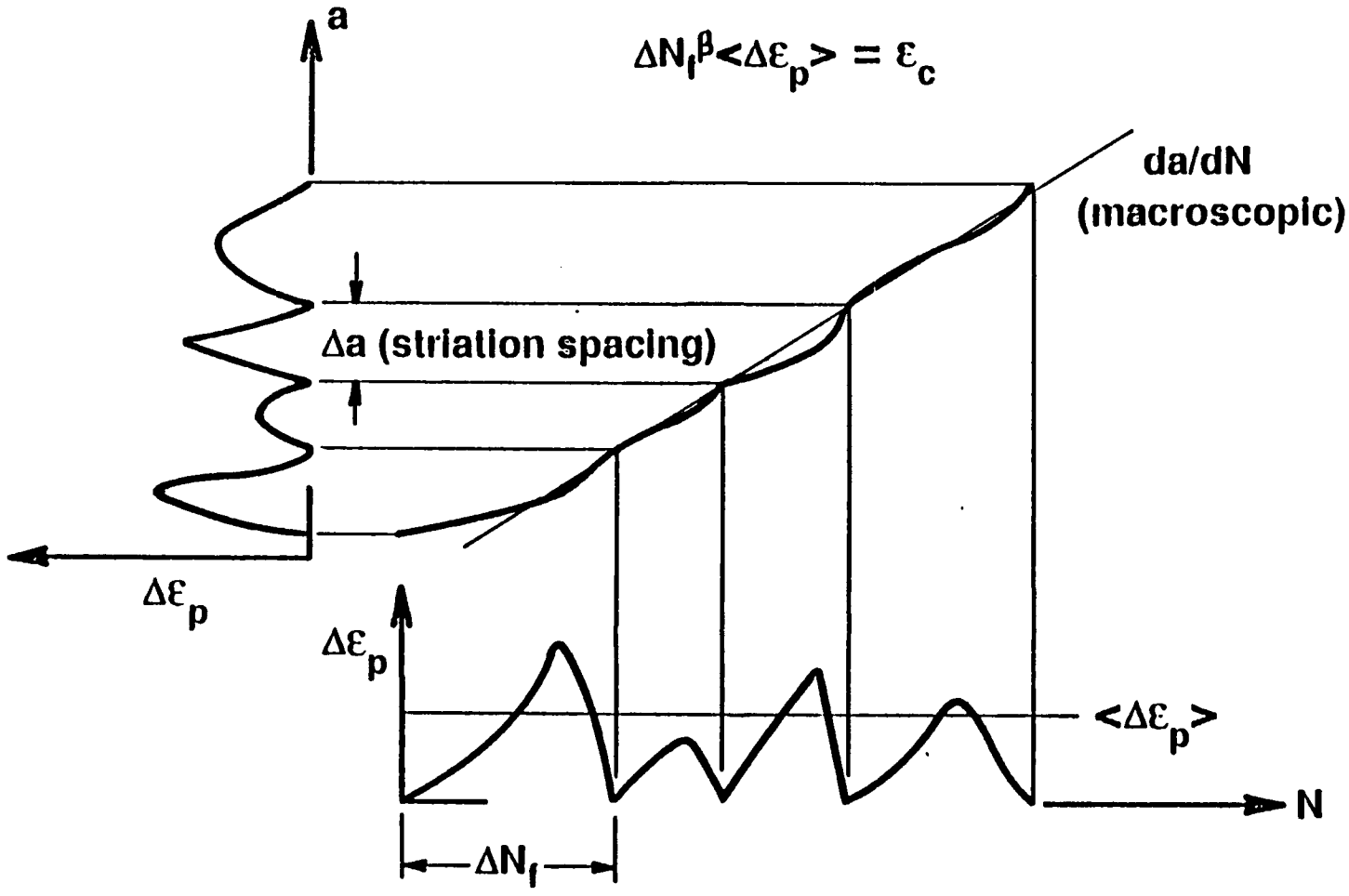

Fig. 5 A schematic of how crack tip strain changes with crack length and number of cycles to give the crack growth rate. This schematic is the result of direct observation of the crack growth process and measurement of crack tip strain.

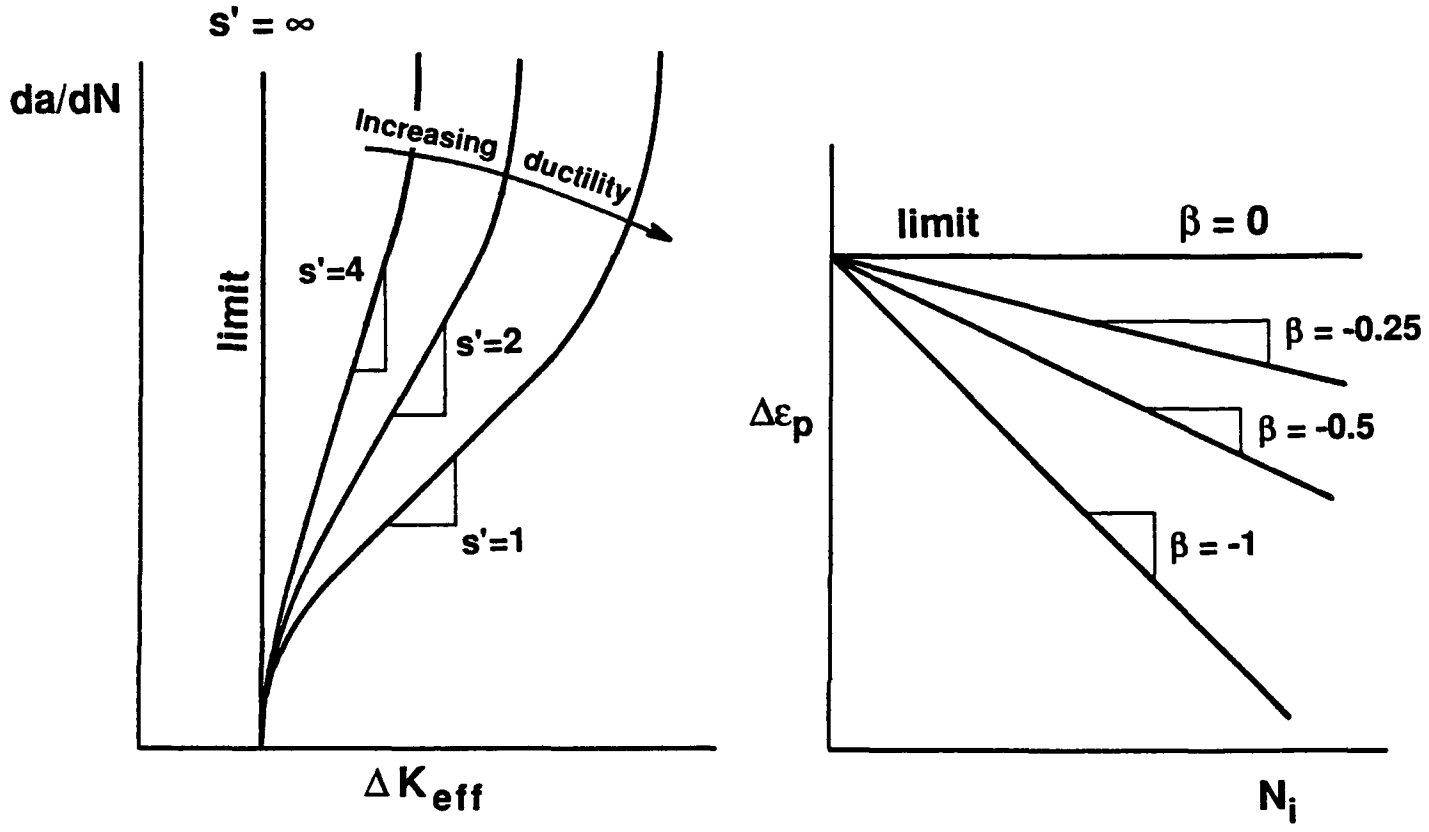

$$da/dN = B'\Delta K_{eff}^{s'}$$

$$\Delta\varepsilon_p \Delta N^{\beta} = \varepsilon_c$$

$$s' = (n' + 1/\beta)^r$$

If r = 1 and n' = 0, then $s' = 1/\beta$

Fig. 6 The relationship between crack growth rate and low-cycle fatigue behavior. The slopes of the curves on each diagram are related through the equations shown.

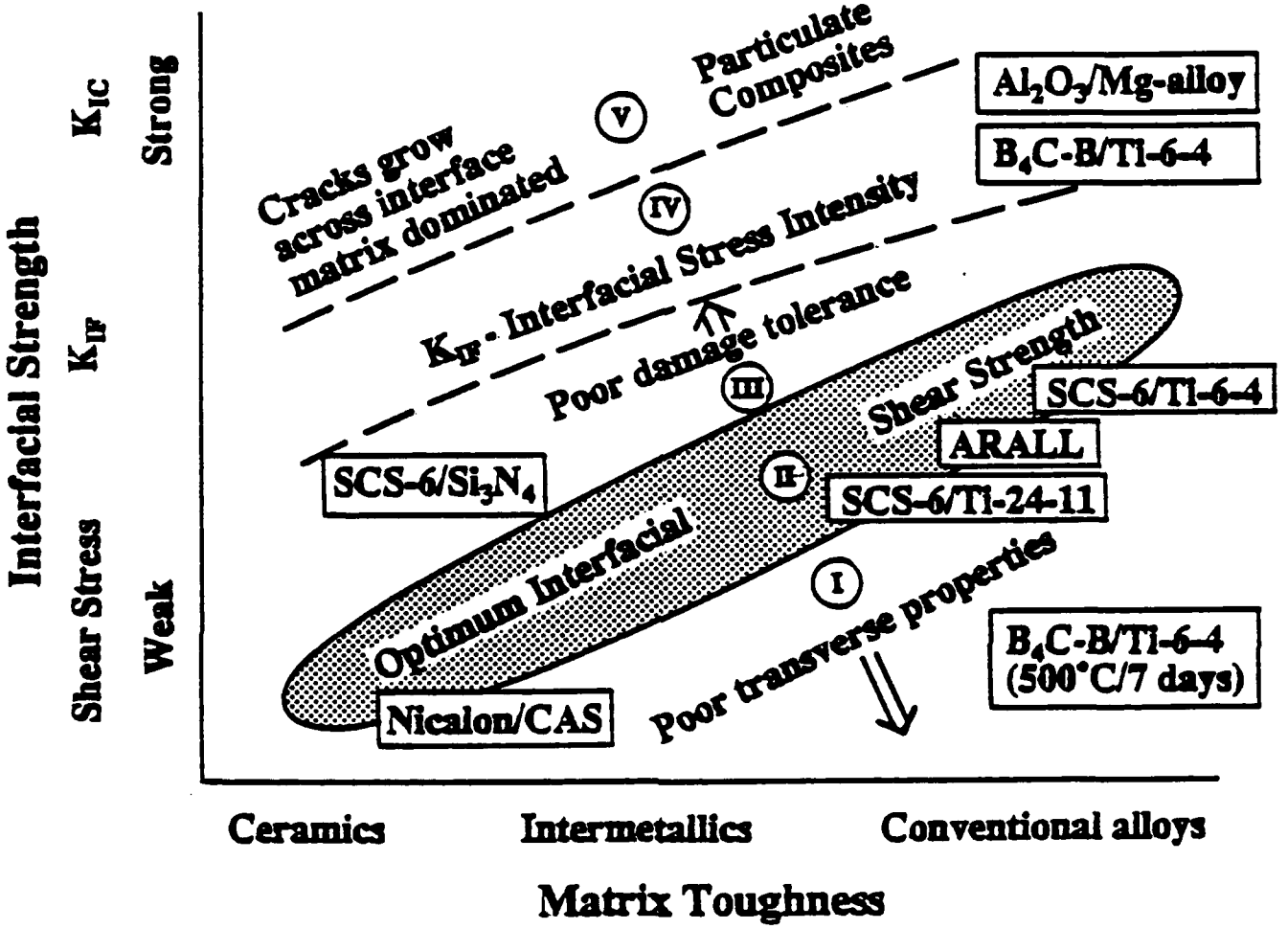

Fig. 7 How the damage tolerance of inorganic matrix composites is linked to the desirable strength of the interface and toughness of the matrix. Interfacial strength may be characterized in several ways, depending on how strong it is.

Fracture Toughness

Introduction

Titanium aluminides that are of engineering significance include Ti_3Al- and TiAl-base intermetallic alloys [1,2]. Single-phase Ti_3Al and TiAl compounds are of limited potential for structural applications because they exhibit low tensile ductility and fracture toughness at ambient temperature [3,4]. By macro-alloying, ductility and fracture toughness can be imparted in both Ti_3Al- and TiAl-base systems by increasing dislocation and twinning activities [5-12]. More importantly, macro-alloying in many instances lead to two-phase microstructures containing an intermetallic matrix (Ti_3Al or TiAl) with one or more second phase(s) [6-10,13-15]. The second phase might be a ductile, metallic phase (e.g., body-centered-cubic Ti in Ti-24Al-11Nb) or another intermetallic phase that might or might not be ductile (e.g., Ti_3Al in lamellar TiAl-alloys).

Ti_3Al-base (α_2) alloys developed to date are two-phase systems with compositions based on Ti-(23-25)Al-(11-18)Nb-X(V, Mo, Cr, or V), where X ranges from nil to a few percent [7]. Typical compositions of selected Ti_3Al-base alloys are Ti-24Al-11Nb, Ti-25Al-10Nb-3V-1Mo (Super α_2), and Ti-25Al-17Nb-1Mo. In comparison, current TiAl-alloys have typical compositions based on Ti-(46-52)Al-(1-10)M [8-10], where M represents at least one element from V, Cr, Mn, Nb, Ta, W, and Mo. Both single and two-phase alloys are possible in this range of compositions [8-10]. Ti_3Al-base alloys studied in this program were Ti-24Al-11Nb and Ti-25Al-10Nb-3V-1Mo, while Ti-47Al-2.6Nb-2(Cr + V) was the TiAl-base alloy studied. These alloys are representatives of the current two-phase titanium aluminide alloys.

Like conventional $\alpha + \beta$ Ti-alloys, two-phase titanium aluminides can be heat-treated to a variety of microstructures [1,7-10,16-20]. Microstructures in α_2-alloys studied in this program included equiaxed $\alpha_2 + \beta$, coarse basketweave, and fine basketweave microstructures. Three types of microstructures can be obtained in TiAl-alloys [7-10]: (1) equiaxed gamma, (2) fully lamellar, and (3) duplex microstructures. The equiaxed gamma microstructure consists entirely of γ grains in single-phase alloys or predominantly γ grains with small amounts of grain boundary alpha-two particles in two-phase alloys. The fully lamellar microstructure consists entirely of lamellar colonies (i.e., grains) which are comprised of alternating layers of α_2 and γ platelets aligned according to the $\{111\}_\gamma // (0002)_{\alpha_2}$ and $<110>_\gamma // <1120]_{\alpha_2}$

crystallographic relations [21]. The duplex microstructure contains a mixture of both gamma grains and lamellar colonies. The duplex and the nearly fully lamellar microstructures were studied in this program.

Extensive efforts in this program [22-25], as well as others [26-28], have demonstrated that microstructure exerts significant effects on the fracture processes and toughening mechanisms in two-phase titanium aluminides [22-28]. The results to date indicates that two-phase titanium aluminides derive a significant part of their fracture toughness from the ductile, second phase in the microstructure through a variety of toughening mechanisms. The presence of a ductile phase in a brittle matrix can enhance the overall fracture toughness of the two-phase material by: (1) accommodating plastic incompatibility at grain or phase boundaries [22-24], (2) blunting of pre-existing flaws or deformation-induced microcracks [22-24], and (3) bridging of the crack surfaces in the crack wake [22,29]. All three toughening mechanisms exist in Ti_3Al- and TiAl-base alloys, but the details and the effectiveness of these mechanisms vary in individual alloys. Other toughening mechanisms observed in two-phase titanium aluminides involve the formation and fracture of shear ligaments [29-31], deformation by mechanical twinning [31,32], matrix plasticity [23], and the formation of a diffuse zone of microcracks within the crack-tip process zone [23].

The unique combination of in-situ fracture experiment and micromechancial modeling in this program had allowed detailed studies of individual toughening mechanisms and microstructure/fracture toughness realtionships. The knoweledge gained from these studies are generic and are applicable to other two-phase microstructures containing a ductile phase in a brittle matrix. The importance of these various toughening mechanisms in two-phase Ti_3Al- and TiAl-base alloys will be highlighted in order to elucidate microstructure/fracture toughness relationships.

Ductile-Phase Accommodation and Blunting

The concept of ductile-phase toughening through accommodation of plastic incompatibility and crack-tip blunting is based on the recognition that a common mode of fracture in Ti_3Al and TiAl is slip-induced cracking either by grain boundary decohesion or cracking along planar slipbands. Both of these processes are directly related to having an insufficient number of independent slip systems to relieve plastic incompatibility strains that develop at grain boundaries when incipient yielding commences within individual grains, and they result in a relatively low near-tip strain distribution. Both types of slip-induced fracture can be alleviated if a ductile phase is

present at the grain or phase boundaries to serve as a source for providing the geometrically necessary dislocations required to accommodate plastic incompatibility developed at those locations. One possible consequence of ductile-phase accommodation is that the matrix phase can be deformed to a greater extent without leading to the formation of microcracks at the adjoining grain or phase boundaries. This will lead to a higher attainable strain distribution near the crack tip and thus a higher K_{Ic} value than that can be achieved in the matrix alone.

A particular example of the ductile-phase toughening process is shown in **Fig. 1** for Ti-47Al-2.6Nb-2(Cr + V), which is a TiAl-based alloy that can be heat-treated to exhibit a wide range of microstructures, ranging from a nearly fully gamma grain microstructure to a fully lamellar microstructure consisting of alternating $\alpha_2 + \gamma$ platelets. **Fig. 1** compares the near-tip strain distributions for the duplex microstructure of equiaxed gamma and lamellar grains and the nearly fully lamellar microstructure which consists of mostly lamellar colonies and about 5% equiaxed gamma grains at colony boundaries. The duplex microstructure is prone to slip-induced grain boundary decohesion. The maximum strain attained near the crack tip prior to the onset of crack growth is on the order of the yield strain (yield stress/Young's modulus), as shown in **Fig. 1**. In contrast, the thin alpha-two plates in the lamellar microstructure appears to be relatively ductile and can better accommodate plastic incompatibility at the $\alpha_2 + \gamma$ interface. As a result, the near-tip strain that can be attained prior to the onset crack growth is higher in the lamellar material, leading to a higher observed K_{Ic} value (measured at the onset of crack extension).

Another common feature of ductile-phase toughening is that the crack tends to terminate and blunt at the ductile phase, as shown in **Fig. 2** for Ti-24Al-11Nb with a coarse basketweave microstructure. In this case, the crack tip is arrested and blunted by the more ductile β (body-centered cubic) phase. By virtue of this crack-tip interaction, both ductile-phase accommodation and crack-tip blunting are more effective in microstructures with a continuous ductile-phase network than in those with a discontinuous one. This point is best illustrated in **Fig. 3** which compares the K-resistance curves for Ti-24Al-11Nb heat-treated to exhibit either an equiaxed $\alpha_2 + \beta$, a coarse or a fine basketweave microstructure. The former two microstructures exhibit a higher toughness value because of a larger volume fraction (26-39%) of a continuous ductile β phase, while the fine basketweave microstructure contains a smaller volume fraction (25%) of discontinuous β phase. The lack of continuity in the β phase makes

it possible for the crack tip to propagate predominantly in the matrix and around the beta phase in the fine basketweave microstructure, rendering the beta phase an ineffective toughening agent.

Toughness enhancement resulting from crack-tip blunting by a ductile phase has been modeled [23] using a critical strain criterion [33] and the Hutchinson, Rice, and Rosengran (HRR) crack-tip field [34,35]. **Fig. 4** shows a comparison of the crack-tip blunting model with experimental K_{IC} results obtained in this program as well as those from the literature [36-38]. The calculated curve was obtained via the blunting model using $K_m = 12.5\ MPa\sqrt{m}$, which is the toughness value of Ti-24Al-7.5Al [38], a single phase alpha-two alloy, as the appropriate toughness value for the alpha-two matrix in Ti-24Al-11Nb. The agreement between model calculation and experimental results suggests that the initiation toughness in the Ti-24-11 alloy arises partly form the toughness of the alpha-two matrix and partly from crack-tip blunting by the ductile phase. Furthermore, both the model calculation and experimental result indicate that the initiation fracture toughness (K_{IC}) of the Ti_3Al-base alloys increases with increasing volume fraction of the ductile phase.

Ductile-Phase Bridging

Beside ductile-phase blunting, another means of imparting fracture toughness is by dispersing ductile phase in a brittle material to form a particulate or a laminated composite [39-47]. The basic concept of the toughening process is that the dominant crack in the brittle matrix would be bridged by the ductile phase particles or plates [48-51]. The bridging forces exerted by the particles would tend to close the crack surface opening and lower the near-tip stress intensity factor of the dominant crack. As a result, the remotely applied stress intensity factor must be increased when the crack and the bridged zone increase in length, thereby leading to a higher crack growth toughness in the form of a resistance curve behavior.

The presence of the ductile, body-centered cubic (b.c.c.) β phase in Ti-24Al-11Nb and Ti-25Al-10Nb-3Mo-1V makes it logical for one to think that ductile-phase bridging might be present in these Ti_3Al-base intermetallic systems. Indeed, in-situ fracture toughness tests have revealed the occurrence of ductile-phase bridging in the Ti-24-11 alloy [22,29]. However, the length of the bridging zone observed was quite small. Application of the ductile-phase bridging theory to alpha-two titanium aluminides indicated the ductile-phase bridging contributed no more than 12% of the observed

fracture toughness [23,28]. Thus, ductile-phase bridging by β is not an important toughening mechanism in the heat-treated, uncomposited microstructures of alpha-two titanium aluminides.

Ductile-phase bridging was not observed in the two-phase TiAl-alloy studied in this program, but a similar toughening mechanism based on unbroken ligaments located in the crack wake was observed [29,30]. The importance of these ligaments on toughness enhancement in titanium aluminides is discussed in a later section. While absent in monolithic materials, ductile-phase bridging and toughening can be imparted in either single- or two-phase TiAl-alloys by compositing with Nb or Ti-Nb particles or plates [42,45,46]. The use of Nb particles for improving the fracture toughness of niobium silicides has also been demonstrated [47]. Large toughness increases in the form a resistance curve behavior were obtained for particle-reinforced gamma composites [42]. The toughness enhancement in these materials was primarily the result of the formation of a bridging zone in the crack wake. On the other hand, less toughening was obtained by compositing TiAl with Ti-6Al-4V particles due to the absence of a large bridging zone [42]. These two contrasting behaviors of Nb and Ti-6Al-4V particles on the K-resistance curves of TiAl-composites are illustrated in **Fig. 5** by comparing with the K-resistance curve of the single-phase TiAl-alloy, Ti-51Al-2Ta [32].

Important microstructural features necessary for instigating ductile-phase bridging in a brittle material have been studied by others via model composites in several investigations [43-45]. These studies demonstrated that the work to fracture the crack-wake particles depends on the debonded length, the state of stress and plastic constraints associated with particle deformation [43-44], and with the debonded length [45]. For maximizing fracture toughness, it is necessary to increase the work to fracture the bridging particles or ligaments by relaxing the constraints associated with the plastic flow process or by increasing the size of the deforming volume [43]. The former can be accomplished by inducing interface debonding through the use of weakly bonded ductile particles or plates, while the latter can be achieved by using particles with a high work-hardening capacity [43,45]. Whether interface debonding is beneficial also depends on the deformation characteristics of the ductile ligaments [45]. The size and concentration of ductile phase are expected to be important factors in instigating bridging-induced fracture toughness, with fracture toughness increasing with particle size and bridging length [50]. Quantitative understanding of the relationships

between the particle size and length of the bridging zone has not been established, however. There is essentially no information about the dependence of the bridging zone length on the characteristics of the ductile phase.

Shear Ligament Toughening

Fracture toughness in titanium alloys has generally been related to the ability of the microstructure to cause crack deflection and the tendency of the crack to meander as it zigzags between grains following planar slip bands [52-54]. As a result, the toughness in Ti-alloys is frequently attributed to the tortuosity of the crack path or the roughness of the fracture surface. Efforts in this program [22-25,29,30] have revealed that titanium aluminide alloys based on either the alpha-two or gamma phases exhibit planar slip, crack deflection, and in many instances, tortuous crack paths and rough fracture surfaces. Because of these observations, toughness in both types of titanium aluminide alloys has been considered to arise at least partly from crack deflection and crack-path tortuosity.

During the course of this program, a new toughening process, dubbed shear ligament toughening, was identified in both Ti_3Al- and TiAl-base titanium aluminides and used to explain roughness-induced toughness in these alloys. This toughening mechanism is based on the recognition that when a Mode I crack deflects from its original path, the angle of deflection and the plane of cracking are likely to be different among individual grains. The consequence is that the crack planes in the various grains are unconnected at either grain or phase boundaries [55], and are separated by ligaments, as shown in **Fig. 6**. The formation of these ligaments by mismatched crack planes might lead to an enhancement in the fracture toughness, because they must be fractured in order for total separation of the crack surfaces to occur. Since the deformation and fracture of these ligaments are likely by shear, the toughening effects of these ligaments may be referred as shear ligament toughening [29]. As will be shown shortly, such a fracture mechanism also leads to an enhanced fracture toughness and a tortuous crack path.

The formation of shear ligaments by mismatched crack planes were observed in the alpha-two alloy, Ti-24Al-11Nb [22,23,29], and in the lamellar TiAl-alloys, Ti-47Al-2.6Nb-2(Cr + V) [29,30]. **Fig. 7** shows the process zone of a monotonically loaded crack in the lamellar Ti-47Al-2.6Nb-2(Cr + V) alloy tested at 800°C in air. Five unbroken ligaments are evident within the process zone in **Fig. 7**. The manner by which shear ligament toughening occurred in the lamellar alloy was studied in detail

by in-situ fracture experiment using a telemicroscope equipped with a video-camera. A complete sequence of this toughening process is presented in **Fig. 8**, which shows a series of micrographs of the near-tip fracture process zone for various K levels. As shown in **Fig. 8**, the crack started to propagate at $K = 18.5\ MPa\sqrt{m}$. At $K = 22.9\ MPa\sqrt{m}$, a localized shear band developed ahead of the crack tip, which eventually led to the formation of a microcrack. The microcrack crack was separated from the tip of the main crack by a ligament that was fractured by shear upon loading to $K = 33.5\ MPa\sqrt{m}$. This fracture process resulted in the tortuous crack path and the resistance-curve behavior shown in **Fig. 8**.

A theoretical model of shear ligament toughening was developed in this program [29] using the J-integral approach [56]. The model revealed that toughness enhancement by shear ligaments increases with the area fraction, the length, and the plastic work to fracture of the ligaments, as well as the size of the process zone and the angle of crack deflection. Additionally, the model was extended to treat toughening by ligaments subjected to an arbitrary stress state. It was shown that ligament toughening by shear or tensile fracture is mechanically similar to ductile-phase bridging, despite the absence of bridging of crack surfaces by a ductile-phase in a crack wake. Furthermore, the shear ligament toughening was also used as the basis for developing a quantitative relationship between fracture toughness, crack path tortuosity, and the surface roughness parameter, R_s, which is the ratio of the actual surface to the projected surface [57,58]. Model calculations have revealed that fracture toughness increases with surface roughness when the toughness (or work to fracture) of the shear ligaments is larger than that of the matrix. Under this circumstance, the shear ligaments act like a "ductile phase" reinforcement. The enhanced toughness arises from both the ductile phase (i.e., the shear ligaments) and an increase in the deformed volume as represented by the volume of the shear ligaments. On the other hand, surface roughness provides only a small toughening effect when the toughness of the ligaments is equal to or less than the matrix value. In this case, toughness is maintained primarily due to an increase in the deformed area in a rough fracture surface.

The relevance of the proposed shear ligament toughening mechanism for titanium aluminide alloys is best illustrated in **Fig. 9**, which compares the K-resistance curves and crack paths of the two-phase TiAl-alloy, Ti-47Al-2.6Nb-2(V + Cr), in two contrasting microstructures. The microstructures of interest are [29]: (1) the equiaxed γ microstructure that consists of predominantly equiaxed γ grains plus a small volume fraction of lamellar colonies and grain boundary α_2 particles, and (2) the lamellar microstructure, which is comprised mainly of lamellar $\alpha_2 + \gamma$ with a small volume fraction

of equiaxed γ grains located at grain boundaries. **Fig. 9** shows that the equiaxed γ microstructure exhibits a planar crack path, a relatively low K_{IC} value, and no tearing resistance. In contrast, the lamellar microstructure manifests a higher K_{IC} value, a resistance curve behavior, a tortuous crack path, and rough fracture surfaces. The difference in the fracture behaviors of these two microstructure has been correlated with the crack paths. The equiaxed γ microstructure exhibited a relatively planar crack path along predominantly grain boundaries and cleavage plans [24,29]. Occasionally, mismatched crack planes with small ligaments with length on the order of 20 μm or less have been observed [29]. On the other hand, the length of the ligaments is larger in the lamellar microstructure due to a relatively large colony size ($\approx 1.6mm$). As a result, the transgranular crack path is more tortuous, **Fig. 9**. There is more plastic dissipation in the lamellar microstructure, especially in the region where the crack propagation direction changes [29]. Qualitatively, the higher fracture resistance exhibited by the lamellar microstructure when compared to the equiaxed γ microstructure can be attributed to: (1) a deflected crack path which results in shear ligaments of a relatively higher ligament length, and (2) a larger plastic dissipation contributed by fracturing of the lamellar ligaments than the equiaxed γ ligaments, i.e., a higher toughness for the lamellar ligaments.

Twin Toughening

In additional to slip, many TiAl-alloys exhibit mechanical twinning as a mode of plastic deformation [7-10]. In two-phase TiAl-alloys, the deformation modes in both gamma grains and lamellar colonies include (1) slip by 1/2[110] type dislocations, and (2) twinning with <112] twin dislocations. The activities of twinning appear to be limited at ambient temperature but increase with increasing temperatures [30]. The importance of the twinning process in affecting the deformation behavior of single and two-phase TiAl-alloys are well recognized, and it has studied extensively [12,59-61].

The use of mechanical twinning for toughening TiAl-alloys have been reported by Deve and Evans, who measured the K-resistance curves for Ti-50Al and Ti-51Al-2Ta [32]. The Ti-50Al alloy was found to exhibit twinning and a crack growth toughness of 16 $MPa\sqrt{m}$. In contrast, the Ti-51Al-2Ta alloy that did not exhibit twinning manifested a fracture toughness of 8.5 $MPa\sqrt{m}$ without any resistance against crack growth [32]. As shown in **Fig. 10**, the result suggests that twinning might be a viable mechanism for imparting fracture toughness in TiAl-base alloys. In the Ti-50Al alloy, the enhanced toughness was associated with the formation of twins within the fracture process zone. Most of the twins were observed in the crack-wake, with the toughening

process reminiscent of that observed in transformation toughening of partially stabilized zirconia [32]. In a recent study, Deve et al., reported that twin toughening and ligament bridging both occurred in Ti-48Al-2Cr-2Nb, with each mechanism contributing approximately equal toughness increments [31].

Growing Crack Singularity

Alpha-two alloys such as Ti-24Al-11Nb and Ti-25Al-10Nb-3V-1Mo (Super Alpha-two) exhibit high fracture toughness at elevated temperatures [1,62]. The fracture toughness values reported in the literature are generally based on the conventional K tests using the maximum fracture load. These values include contributions both from initiation toughness (K_{Ic} or J_{Ic} measured at the onset of crack growth) and crack growth toughness (the difference between K at fracture and K_{Ic}). Results in this program have demonstrated that a significant portion of high-temperature fracture toughness in Ti-24Al-11Nb is crack growth toughness [22,23]. The J-resistance curve for Ti-24Al-11Nb with an equiaxed microstructure for 25 and 600°C is shown in **Fig. 11**. It illustrates that the initiation toughness of this alloy at 600°C is relatively low, as crack extension occurred at a K level of only 12 $MPa\sqrt{m}$. The fracture resistance of the alloy, however, increases rapidly with increasing crack extension. Thus, most of the toughness of this alloy arises from crack growth toughness. Similar behaviors have also been observed in this alloy with either a coarse and a fine basketweave microstructure [23] and in the Super Alpha-two alloy [62].

One of the possible origins of the crack growth toughness is the change in the crack-tip singularity from one of stationary crack, which is the HRR [34,35] (power-law type) in Ti-24-11, to that of the growing crack, which is of the logarithmic type (Rice, Drugan, and Sham) [63]. Such a change in the crack-tip singularity was not observed in any of the three microstructures of the Ti-24-11 alloy tested at 25°C, which is consistent with the low tearing resistance in these materials. In contrast, stable crack growth in the equiaxed microstructures at 600°C was accompanied by a change in the crack tip singularity from the HRR to the logarithmic one. This occurrence of transition is presented in **Fig. 12**, which shows the crack surface opening displacement as a function of distance behind the crack tip for an initially stationary crack in the equiaxed microstructure subjected to various K levels at 600°C. Also shown in **Fig. 12** are the calculated crack surface profiles for the stationary crack. The results indicate that the measured crack profile was well described by the HRR field for the plane stress condition. The agreement between the measured and calculated crack profiles started to deviate when crack extension occurred at K levels above 12 $MPa\sqrt{m}$, with the amount

of deviation increasing with increasing K levels. At K = 30 MPa$\sqrt{m}$, the crack had grown well into the plastic zone. **Fig. 12(b)** shows that the tip of the growing crack field was sharp, and the near-tip crack profile was described well by the logarithmic singularity for growing cracks in a perfectly plastic material. Further behind the crack tip, the crack surface profile was well-described by the HRR singularity, indicating that the HRR singularity was prominent prior to crack extension. The results provide solid evidence that at least part, if not all, of the high crack growth resistance at 600°C arise from crack tip plasticity due to deformation both in the matrix and in the ductile phase. Similar to those observed previously in Al-Fe-X alloys and other metallic systems [64], this type of resistance-curve behavior is associated with the nonproportional loading and the change in the crack tip singularity when a stationary crack extends into a plastic zone.

Previous work has demonstrated that the transition of the HRR singularity to the logarithmic one occurs when the normalized ductility parameter, $\Omega = E\varepsilon_{1f}/\sigma_o$, where ε_{1f} is the true fracture strain and σ_o is the flow stress, exceeds a critical value ($\Omega \geq 34.5$) [64]. This criterion is generally not met by either the Ti_3Al- or TiAl-alloys except at elevated temperatrues where ε_{1f} is increased and σ_o is reduced [22,23] with increasing temperature. The resistance-curve behavior observed in most monolithic titanium aluminides at ambient temperature arises from extrinsic mechanisms such as ligament toughening or twin toughening, while ductile-phase bridging is the mechanism responsible for the resistance-curve behavior in TiAl-alloy composites.

Microcrack Toughening

The fracture process in Ti_3Al- and TiAl-alloys generally involves the formation of microcracks ahead of the tip of the main crack [22-24,29,30]. For alpha-two alloys such as Ti-24Al-11Nb, microcracks can initiate at planar slip bands within the α_2 grains, at the α_2/β interface, and possibly at the β phase [22,23]. In two-phase TiAl-alloys, microcrack formation occurs either by cleavage of gamma grains, decohesion of γ grain boundaries, decohesion of lamellar colony boundaries, and delamination of lamellar interfaces or gamma/gamma twin boundaries [24,25,30]. In most cases, microcracks formed are few in number, located directly in front of the main crack tip, and lead to increase in the local stress intensity factor and embrittlement, rather than toughness enhancement [23,65]. On the other hand, the Ti-24-11 alloy with the coarse basketweave microstructure exhibits a diffuse zone of microcracks ahead of the main crack tip during fracture toughness testing at 600°C [23]. As the main crack propagated into this diffuse zone of microcracks, the crack growth toughness was increased when compared to the equiaxed microstructure which did not manifest microcracking [23].

The toughness enhancement observed in the basketweave microstructure is consistent with microcrack toughening analyses [66-68] that indicate that a diffuse zone of microcracks at the crack wake lead to crack-tip shielding and an increase in the apparent fracture resistance.

Trade-Offs in Mechanical Properties

Several trade-offs in the mechanical properties of titanium aluminides have been observed [24,25,30,69]. These include trade-offs between fracture toughness and hydrogen tolerance, tensile ductility, and fatigue crack growth resistance. Incorporating a large volume fraction of ductile, metallic phase in the microstructure might also lead to a reduction of creep resistance, but this subject will not be discussed here.

The trade-off in hydrogen tolerance and fracture toughness is best illustrated using Ti-24Al-11Nb as an example. For this alloy, a large volume fraction of the ductile beta phase in the form of a continuous network is required to promote crack-tip blunting and to achieve a high fracture toughness. As a result, the coarse basketweave microstructure that contains a continuous beta phase is preferred over the fine basketweave microstructure with a discontinuous beta phase based on fracture toughness consideration, **Fig. 3**. On the other hand, recent work at SwRI has shown that of the coarse basketweave microstructure and the equiaxed microstructure are more susceptible to hydrogen embrittlement than the fine basketweave microstructure [70]. This is illustrated in **Fig. 13** which shows the fine basketweave microstructure is able to maintain a 2% total elongation for hydrogen contents up to 1500 wt. ppm, while the tensile ductility of the other two microstructures decreases rapidly with increasing hydrogen content. Hydrogen tolerance in the fine basketweave microstructure has been attributed to the fact that hydride formation in this material occurs at α_2/β interfaces [70]. A discontinuous beta phase (fine basketweave) would limit hydride formation to the interfacial regions, while a continuous beta network would allow the formation of a continuous hydride network and an easy path for crack propagation, once a hydride crack is nucleated. Since hydrogen transport is more rapid in beta than in alpha-two, a continuous beta network would also favor hydride formation by providing an easy path for hydrogen diffusion [70].

Another potential trade-off in mechanical properties in titanium aluminides is in tensile ductility and fracture toughness. **Fig. 14** shows that the tensile ductility is inversely related to the fracture toughness for a number of TiAl-alloys. This lack of correlation between fracture toughness and tensile ductility has also been observed

previously in alpha-two alloys [1,22]. This inverse correlation can be understood on the basis that the fracture toughness of the TiAl-alloys originates from shear ligament toughening, whose magnitude increases with the area fraction and fracture toughness of the shear ligaments on the crack plane, as well as the size of the lamellar colony [29]. On the other hand, tensile ductility of the TiAl-alloys is dictated by the nucleation of a microcrack, whose length at initiation is greater than that required to attain the K_{IC} or J_{IC} [22,24,71]. Under this circumstance, the tensile ductility is dictated by the J_{IC} or K_{IC} value and the length of the microcrack, which is the gamma grain size in the microstructure, but is the colony size in the lamellar microstructure. Thus, trade-offs between tensile ductility and fracture toughness arise because of their opposite dependence on colony or grain size.

While a ductile phase can enhance fracture toughness through crack surface bridging, there is evidence that it might not increase the fatigue resistance of titanium aluminides reinforced with ductile particles [28,72]. For TiNb-reinforced TiAl, the fatigue crack growth resistance of the composite is actually lower than monolithic TiAl [72]. The lack of improvement in fatigue crack growth resistance has been attributed to the absence of crack surface bridging in the composite under cyclic loads due to fatigue failure of the ductile particles. Thus, the fracture and fatigue characteristics of the ductile phase particles play an important role in those properties of the composite.

Overall Assessment of Individual Toughening Mechanisms

A summary of the important microstructural factors for improving the fracture toughness of two-phase titanium aluminides through individual toughening mechanisms is presented in **Table 1**. Because of potential trade-offs between fracture toughness and other mechanical properties, microstructural conditions that are advantageous for fracture toughness might not be beneficial for other mechanical properties.

The change of near-tip strain distribution from the HRR to the logarithmic type requires a minimum value of the normalized ductility parameter be exceeded [64]. For most of the titanium aluminide alloys examined, there is insufficient matrix deformation to exceed that requirement except at elevated temperatures [22,23]. As a result, toughening mechanisms such as ductile-phase blunting, bridging, ligament toughening, and twin toughening are required for improving ambient temperature fracture toughness. Although microcrack toughening occurs in some alloys under certain

loading conditions and temperatures, the presence of a large diffuse zone of microcracks in the materials make this particular process unattractive and it is not considered a viable toughening mechanism for monolithic structural materials.

From the studies of alpha-two alloys [22-23,28], it is apparent that crack-tip blunting by the ductile phase is an important mechanism in imparting initiation toughness. For this mechanism to be effective, a relatively large volume fraction of the continuous ductile phase is preferred over a discontinuous one for the same volume fraction [23]. The ductile phase must also exhibit thermal stability, relatively high strength, ductility, and toughness. The Ti-24-11 result, shown in **Fig. 4**, indicates that the matrix properties cannot be overlooked.

Both ductile-phase blunting and bridging models indicate that fracture toughness is enhanced with increasing volume fraction, strength, and fracture strains of the ductile phase. For effective bridging, the ductile phase must be continuous or the crack must be attracted to the ductile phase particles in the case of particulate composites. The limited experimental data available suggest that the size of the ductile phase might also be important in both ductile-phase blunting and bridging, but the extent and nature of its impact remain unresolved. At the present time, it remains unexplained why a large bridging zone does not occur in monolithic titanium aluminide alloys.

The lamellar microstructure of the TiAl-alloys appears to provide many of the attributes that are lacking in the $\alpha_2 + \beta$ microstructure in the Ti-24Al-11Nb alloy. The aligned $\alpha_2 + \gamma$ morphology in the coarse-grained lamellar microstructure provides a naturally "continuous" ductile phase in the α_2 platelets, which the crack tip cannot avoid without a substantial deviation of the crack path from its original Mode I direction. The observation that the α_2 might be ductile when it exists in the form of sub-micron-sized thin plates in the gamma alloy, but is relatively brittle when it exists in grain or matrix form in the alpha-two alloy is amazing, which indicates that besides alloy composition, the fine microstructural scale in the lamellar microstructure is a desirable and an important feature for imparting toughness in the intermetallic alloy at both ambient and elevated temperatures. The sources of ductility and fracture toughness exhibited by individual colonies of α_2 and γ platelets, however, remain unknown and the effects of size scale on these properties have yet to be studied.

The lamellar microstructure is conducive to ligament toughening and roughness-induced fracture toughness. A potentially important means for instigating these toughening mechanisms in TiAl-alloys is to introduce secondary colonies within

primary ones by heat-treatment procedures [31]. Such a process can potentially improve both the tensile ductility and fracture toughness. The former is achieved through a reduction of the size of microcracks nucleated during tensile deformation, while the latter is obtained through increases in the number of ligaments and the length of the process zone. Another possible advantage of ligament toughening is that unlike ductile-phase bridging, the in-situ ligaments would not introduce adverse effects on creep and fatigue properties.

The prospect of twin toughening in titanium aluminides appears to be promising. Alloy addition appears to be the only effective means for instigating mechanical twinning. Thus, efforts to identify alloy compositions with twinning as one of the deformation modes are required. One area that has not be examined in detail is whether or not synergistic toughening effects can be obtained through a combination of toughening mechanisms, which might include ductile-phase blunting, ductile-phase bridging, ligament toughening, and twin toughening. In this regard, the alloy system of interest is one that exhibits twinning and can be heat-treated to produce a microstructure of primary and secondary lamellar colonies.

References

1. J. M. Larsen, K. A. Williams, S. J. Balsone, and M. A. Stucke: "High Temperature Aluminides and Intermetallics," S. H. Whang, C. T. Liu, and D. Pope, eds., *TMS*, Warrendale, PA, 1990, pp. 521-556.

2. H. A. Lipsitt: "Processing and Properties of Advanced High-Temperature Alloys," S. M. Allen, R. M. Pelloux, and R. Widmer, eds., *ASM*, Metal Park, OH, 1985, pp. 157-164.

3. H. A. Lipsitt, D. Shechtman, and R. e. Schafrik: *Met. Trans.*, vol. 6A, 1975, pp. 1975-1991.

4. H. A. Lipsitt, D. Schechtman, and R. E. Schafrik: *Met. Trans.*, vol. 11A, 1980, pp. 1369-1375.

5. M. J. Blackburn: *Trans-AIME*, vol. 239, 1967, pp. 1200-1208.

6. J. C. Williams and M. J. Blackburn: "Ordered Alloys: Structural Applications and Physical Metallurgy," B. H. Kear, et al., eds., Claitor's Publishing Division, Baton Rouge, LA, 1970, pp. 425-445.

7. Y-W. Kim and F. H. Froes: "High-Temperature Aluminides and Intermetallics," S. H. Whang, C. T. Liu, D. Pope, and J.O. Stiegler, eds., *TMS*, Warrendale, PA, 1990, pp. 465-492.

8. Y-W. Kim: *JOM*, vol. 41, no. 7, 1989, pp. 24-30.

9. Y-W. Kim: "High Temperature Ordered Intermetallic Alloys IV," J. O. Stiegler, L. A. Johnson, and D. P. Pope, eds., *MRS*, Pittsburgh, PA, 1991, pp. 777-794.

10. Y-W. Kim and D. M. Dimiduk: *JOM*, August, 1991, pp. 40-47.

11. E. L. Hall and S-C. Huang: "Microstructure/Property Relationships in Titanium Aluminides and Alloys," Y-W. Kim and R. R. Boyer, eds., *TMS*, Warrendale, PA, 1990, pp. 47-64.

12. S.-C. Huang and E. L. Hall: "High-Temperature Ordered Intermetallic Alloys III," vol. 133, C. T. Liu, A. J. Taub, N. S. Stoloff, and C. C. Koch, eds., *MRS*, 1989, pp. 373-383.

13. M. J. Blackburn, D. L. Ruckle, and C. E. Bevan: Technical Report AFML-TR-78-18, Air Force Materials Laboratory, Dayton, OH, 1978.

14. M. J. Blackburn and M. P. Smith: Technical Report AFWAL-TR-81-4046, Air Force Wright Aeronautical Laboratories, Dayton, OH, 1981.

15. M. J. Blackburn and M. P. Smith: Technical Report AFWAL-TR-82-4086, Air Force Wright Aeronautical Laboratories, Dayton, OH, 1982.

16. C. H. Ward: Int. Materials Reviews, 1991 (in press).

17. D. A. Koss, D. Banerjee, and D. A. Luksasak: "High Temperature Aluminides and Intermetallics," S-H. Whang, C. T. Liu, D. Pope, and J. O. Stiegler, eds., *TMS*, Warrendale, PA, 1989, pp. 175-196.

18. H. T. Kestner-Weykamp, C. H. Ward, T. F. Broderick, and M. J. Kaufman: *Scripta Metall.*, vol. 23, 1989, pp. 1697-1702.

19. D. Banerjee, A. K. Gogia, T. K. Nandi, and V. A. Joshi: *Acta Met.*, vol. 36, 1988, pp. 871-882.

20. R. Strychor, J. C. Williams, and W. A. Soffa: *Met. Trans. A.*, vol. 19A, pp. 225-234.

21. D. S. Shong and Y-W. Kim: *Scripta Met.*, vol. 23, 1989, pp. 257-261.

22. K. S. Chan: *Met. Trans. A*, 1991, vol. 21A, 1990, pp. 2687-2699.

23. K. S. Chan: *Met. Trans. A*, vol. 23A, 1992, pp. 183-200.

24. K. S. Chan and Y-W. Kim: "Microstructure/Property Relationships in Titanium Aluminides and Titanium Alloys," Y-W. Kim and R. R. Boyer, eds., *TMS*, Warrendale, PA, 1991, pp. 179-196.

25. K. S. Chan and Y-W. Kim: *Met. Trans. A*, 1992 (in press).

26. *D. S. Shih, S-C. Huang, G. K. Scarr, H. Jang, and J. C.* Chesnutt: "Microstructure/Property Relationships in Titanium Aluminides and Alloys," *TMS*, Warrendale, PA, 1991, pp. 135-148.

27. S. L. Kampe, P. Sadler, D. E. Larsen, and L. Christodoulou: "Microstructure/Property Relationships in Titanium Alloys and Titanium Aluminides," Y.-W. Kim, R. R. Boyer, and J. A. Hall, eds., *TMS*, Warrendale, PA, 1990 (in press).

28. W. O. Soboyejo: *Met. Trans. A*, 1992 (in press).

29. K. S. Chan: *Met. Trans. A*, 1991, vol. 22A, 1991, pp. 2021-2029.

30. K. S. Chan and Y-W. Kim: *Met Trans.*, 1992 (submitted).

31. H. E. Deve, A. G. Evans, and D. S. Shih: *Acta Met.*, 1992 (submitted).

32. H. E. Deve and A. G. Evans: *Acta Met.*, vol. 39, 1991, pp. 1171-1176.

33. R. O. Ritchie and A. W. Thompson: *Met. Trans. A*, vol. 16A, 1985, pp. 233-248.

34. J. W. Hutchinson: *J. Mech. Phys. Solids*, vol. 16, 1968, pp. 13-31.

35. J. R. Rice and G. R. Rosengren: *J. Mech. Phys. Solids*, vol. 16, 1968, pp. 1-13.

36. D. P. DeLuca, B. A. Cowles, F. K. Haake, and K. P. Holland: *Fatigue and Fracture of Titanium Aluminides*, WRDC-TR-89, 1989, pp. 4136.

37. W. O. Soboyejo, B. A. Abbott, S. Midea, and D. S. Schwartz: unpublished research, McDonald Douglas Research Laboratories, St. Louis, MO (1990).

38. R. G. Rowe, J. A. Sutliff, and E. F. Koch: *MRS Symposia Proceedings*, B. G. Girssen, D. E. Polk, and A. I. Taub, eds., vol. 58, *MRS*, Pittsburgh, PA, 1986, pp. 359-64.

39. V. D. Kristic: *Phil. Mag.*, vol. 48A, 1983, pp. 695-708.

40. B. D. Flinn, M. Rühle, and A. G. Evans: *Acta Met.*, vol. 37, 1989, pp. 3001-3006.

41. L. S. Sigh, P. A. Mataga, B. J. Dalgleish, R. M. McMeeking, and A. G. Evans: *Acta Met.*, vol. 36, 1988, pp. 945-953.

42. C. K. Elliott, G. R. Odette, G. E. Lucas, and J. W. Sheckard: MRS Proceeding, vol. 120, 1988, pp. 95-101.

43. M. F. Ashby, F. J. Blunt, and M. Bannister: *Acta Met.*, vol. 37, 1989, pp. 1847-1857.

44. H. C. Cao, B. J. Dalgleish, H. E. Deve, C. Elliott, A. G. Evans, R. Mebrabian, and G. R. Odette: *Acta Met.*, vol. 37, 1989, pp. 2969-2977.

45. H. E. Deve, A. G. Evans, G. R. Odette, R. Mehrabian, M. L. Emiliani, and R. J. Hecht: *Acta Met.*, vol. 38, 1990, pp. 1491-1502.

46. W. O. Soboyejo, K. T. Venkateswara Rao, S.M.L. Sastry, and R. O. Ritchie: *Met. Trans. A*, 1992 (submitted).

47. R. M. Nekkanti and D. M. Dimiduk: MRS Symposium Proc., vol. 194, *MRS*, Pittsburgh, PA, 1990, pp. 175-182.

48. B. Budiansky, J. C. Amazigo, and A. G. Evans: *J. Mech. Phys. Solids*, vol. 36, pp. 167-187.

49. L.R.F. Rose: *J. Mech. Phys. Solids*, vol. 35, 1987, pp. 383-405.

50. A. G. Evans and R. M. McMeeking: *Acta Met.*, vol. 34, 1986, pp. 2435-2441.

51. P. A. Mataga: *Acta Met.*, vol. 37, 1989, pp. 3349-3359.

52. D. Eylon, J. A. Hall, C. M. Pierce, and D. L. Ruckle: *Met. Trans. A.*, vol. 7, 1976, pp. 1817-1826.

53. J. C. Chesnutt, C. G. Rhodes, and J. C. Williams: "Fractography-Microscopic Cracking Processes," ASTM STP 600, *Am. Soc. Test. Mat.*, Philadelphia, PA, 1976, pp. 99-138.

54. I. W. Hall and C. Hammond: *Mat. Sci. Eng.*, vol. 32, 1978, pp. 241-253.

55. D. A. Koss: Pennsylvania State University, Dept. of Mat. Sci. and Eng., Private Communication, 1990.

56. J. R. Rice: *J. Appl. Mech.*, vol. 35, 1968, pp. 379-386.

57. D. L. Davidson: *J. Mat. Sci.*, vol. 24, 1989, pp. 681-687.

58. E. E. Underwood and K. Banergi: *Mat. Sci. Eng.*, vol. 80, 1986, pp. 1-14.

59. D. Shechtman, M. J. Blackburn, and H. A. Lipsitt: *Met. Trans.*, vol. 5, 1974, pp. 1373-1381.

60. W. T. Donlon, W.E. Dowling, Jr., and J. E. Allison: "Microstructure/Property Relationships in Titanium Aluminides and Alloys," Y-W. Kim and R. R. Boyer, eds., *TMS*, Warrendale, 1990, pp. 75-88.

61. D. S. Schwartz and W. O. Soboyejo: "Microstructure/Property Relationships in Titanium Aluminides and Alloys," Y-W. Kim and R. R. Boyer, eds., *TMS*, Warrendale, PA, 1991, pp. 65-74.

62. K. S. Chan: Southwest Research Institute, San Antonio, Texas, unpublished research, 1992.

63. J. R. Rice, W. J. Drugan, and T. L. Sham: Fracture Mechanics: 12th Conf., ASTM STP 700, ASTM, Philadelphia, PA, 1980, pp. 189-221.

64. K. S. Chan: *Acta. Met.*, vol. 37, 1989, pp. 1217-1226.

65. L. R. F. Rose: *Int. J. Fract.*, 1986, vol. 31, pp. 233-242.

66. R. G. Hoagland and J. D. Embury: *J. Am. Ceram. Soc.*, vol. 63, 1990, pp. 404-410.

67. A. G. Evans and K. T. Faber: "Fracture in Ceramics Materials," A. G. Evans, ed., Noyes Publications, Park Ridge, NJ, 1984, pp. 109-134.

68. J. W. Hutchinson: *Acta Met.*, vol. 35, 1987, pp. 1605-1619.

69. S-C. Huang and D. S. Shih: "Microstructure/Property Relationships in Titanium Aluminides and Alloys," Y-W. Kim and R. R. Boyer, eds., *TMS*, Warrendale, PA, 1991, pp. 105-122.

70. K. S. Chan: *Met. Trans. A*, vol. 23A, 1992, pp. 497-507.

71. K. S. Chan: *Scripta Met.*, vol. 24, 1990, pp. 1725-1730.

72. K. T. Venkateswara Rao, G. R. Odette, and R. O. Ritchie: "Fatigue of Advanced Materials," R. O. Ritchie, R. H. Dauskardt, and B. N. Cox, eds., *MCEP*, Birmingham, UK, 1991, pp. 429-436.

73. M. J. Blackburn and M. P. Smith: AFWAL Technical Report No. AFWAL-TR-82-4086, 1982.

74. W. O. Soboyejo, S. J. Midea, D. S. Schwartz, and M. J. Parzuchowski: "Microstructure/Property Relationships in Titanium Alloys and Titanium Aluminides," Y-W. Kim, R. R. Boyer, and J. A. Hall, eds., *TMS*, Warrendale, PA, 1991, pp. 197-212.

75. W. O. Soboyejo, D. S. Schwartz, and S.M.L. Sastry: *Met. Trans.*, 1990 (submitted).

76. Y-W. Kim: "Microstructure/Property Relationships in Titanium Alloys and Titanium Aluminides," Y-W. Kim and R. R. Boyer, eds., *TMS*, Warrendale, PA, 1991, pp. 91-103.

Table 1

Summary of Important Microstructural and Micromechanical Factors in Various Toughening Mechanisms

Mechanism	Important Factors
Ductile-Phase Blunting	$K_c \propto K_m, V_\beta, \sigma_y^\beta, \varepsilon_f^\beta$
Ductile-Phase Bridging	$K_c \propto K_m, C, \sigma_p, V_p, L$
Ligament Toughening	$K_c \propto K_m, v_l, \Gamma_l, D$
Crack-Path Tortuosity	$K_c \propto K_m, v_l, \Gamma_l, \phi, R_s$
Twin Toughening	$K_c \propto K_m, v_t, \tau_t, \gamma_t^*$
Microcrack Toughening	$K_c \propto K_m$, microcrack density, process zone size
Growing Crack Singularity	$K_c \propto \Omega(= E\varepsilon_{1f} / \sigma_o)$

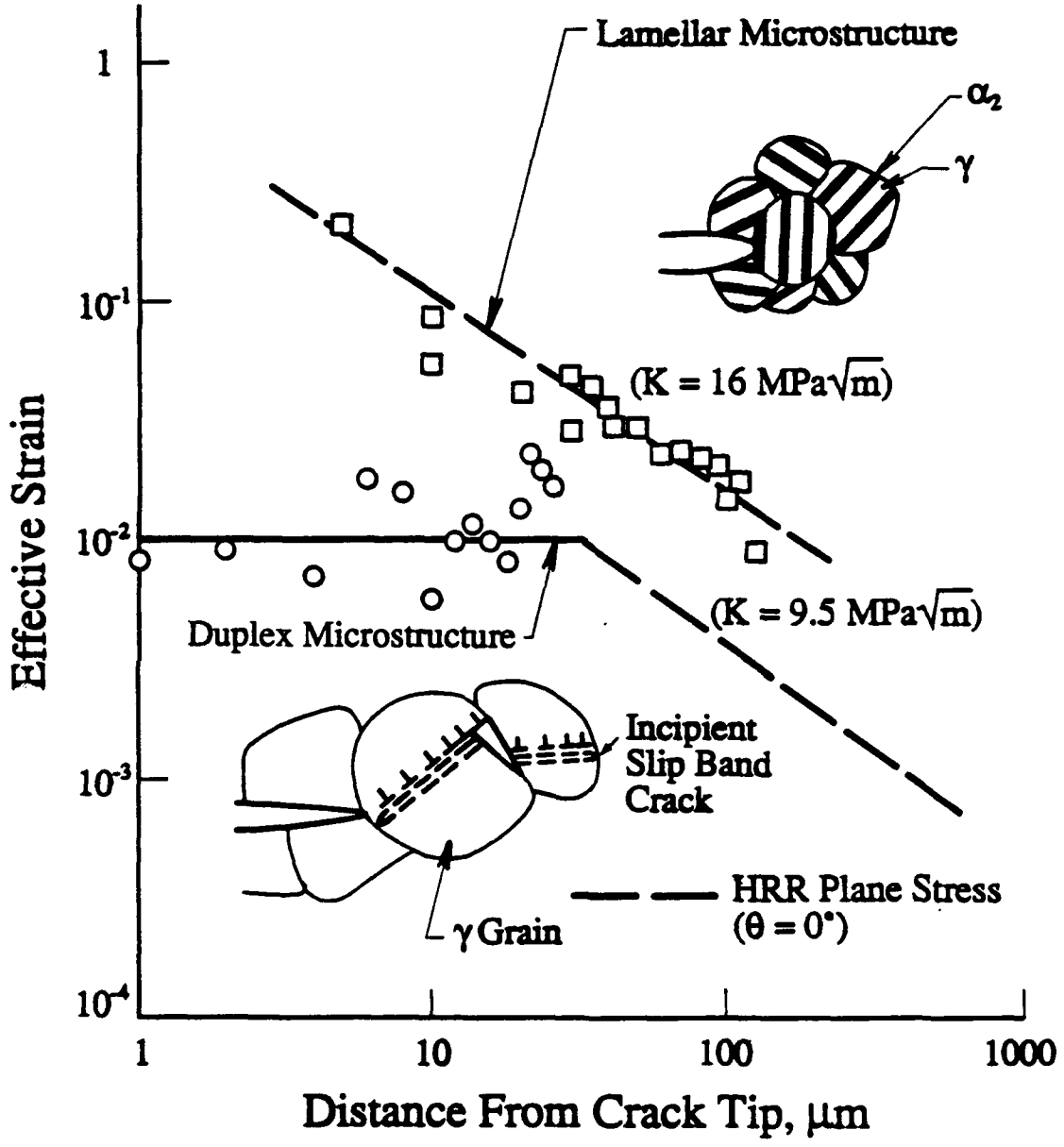

Figure 1. Comparison of near-tip fracture process and strain distribution in the duplex and the lamellar microstructures of the two-phase TiAl-alloy, Ti-47Al-2.6Nb-2(Cr + V), at 25°C.

Ti-24Al-11Nb
Coarse Basketweave Microstructure
25°C

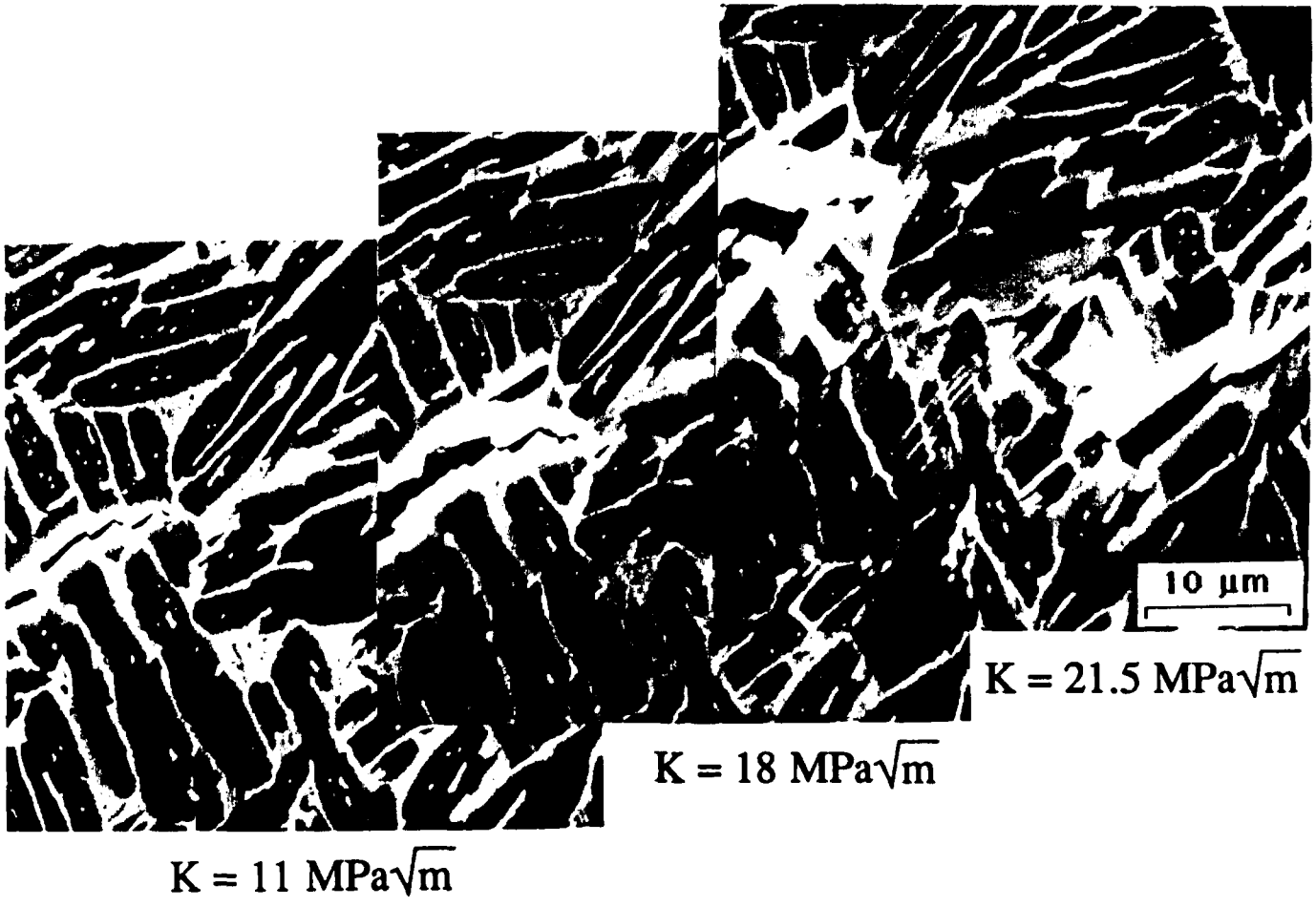

Figure 2. Composite in-situ SEM micrographs show the near-tip fracture process in the coarse basketweave microstructure is characterized by blunting of the tips of the main crack and microcracks by the continuous β phase. The volume of β is 39%.

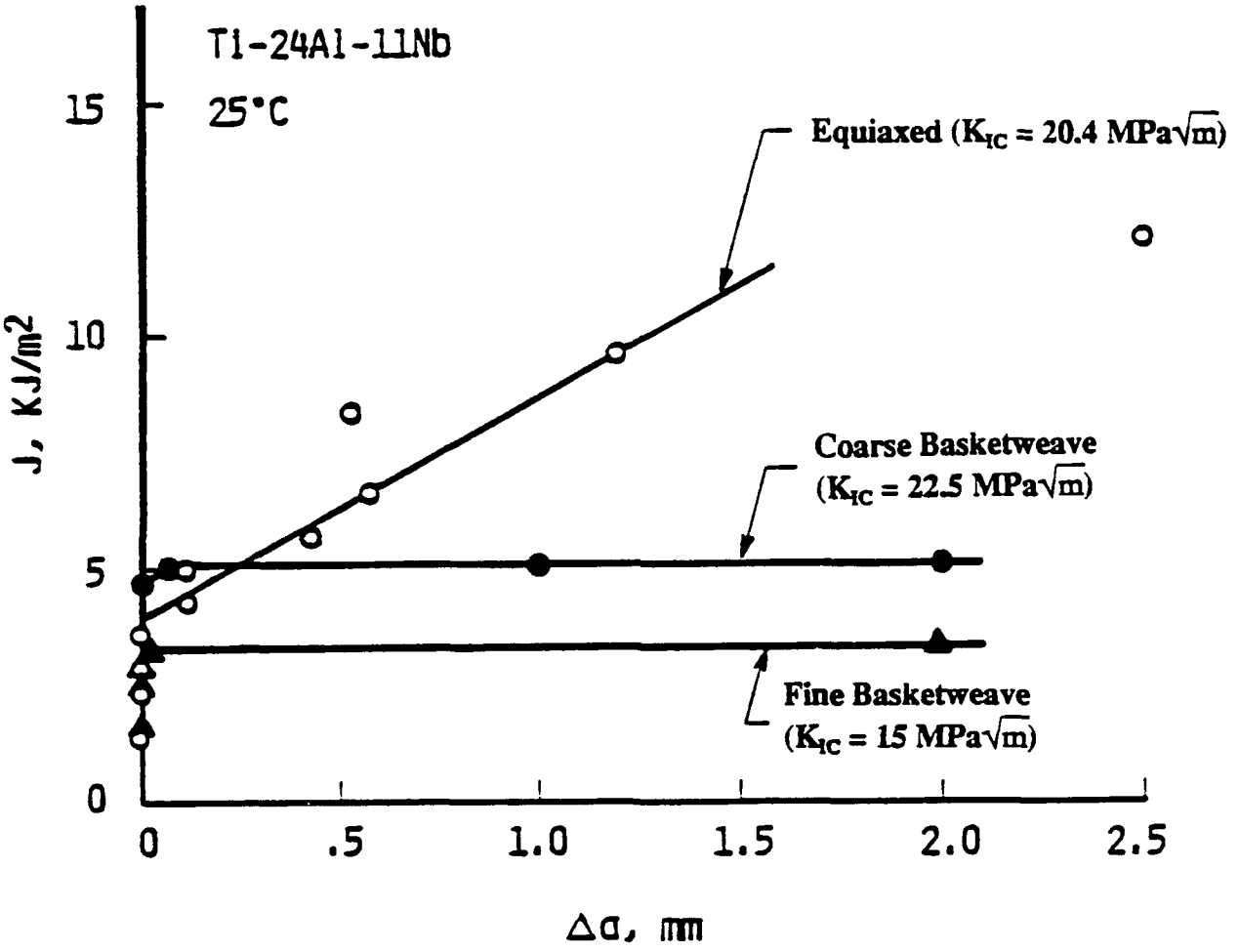

Figure 3. J-resistance curves of the Ti-24Al-11Nb at 25°C indicating a significant microstructural influence on initiation and crack growth toughness. Both the equiaxed $\alpha_2 + \beta$ and the coarse basketweave microstructures contain relatively continuous β, while the fine basketweave contains discontinuous β.

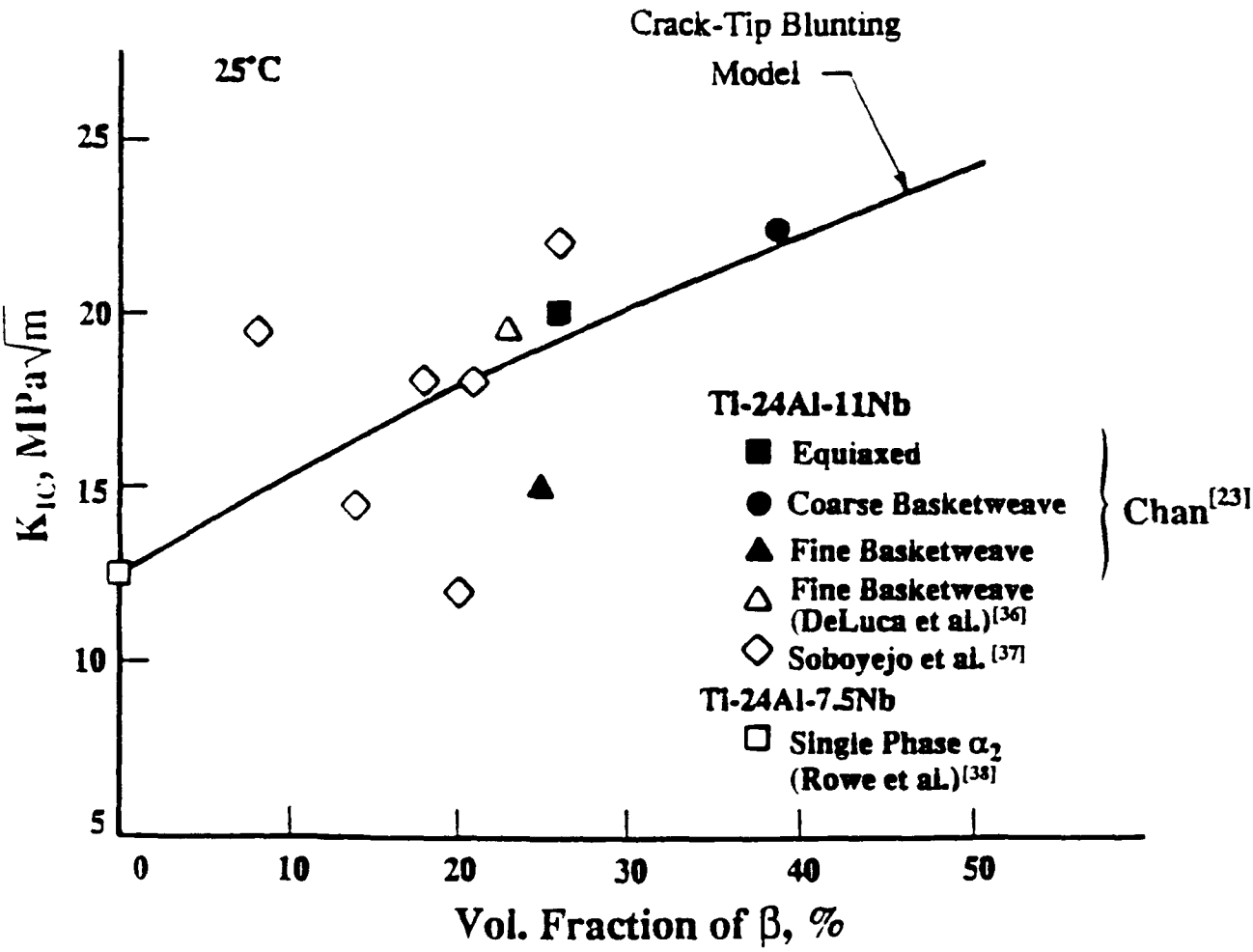

Figure 4. Comparison of the crack-tip ductile-phase blunting model with measured K_{IC} values from Chan,[23] Soboyejo, et al.,[37] and DeLuca, et al.[36] The fracture toughness result for the single phase α_2 Ti-24Al-7.5Nb alloy from Rowe et al.,[38] was used as input data to the model.

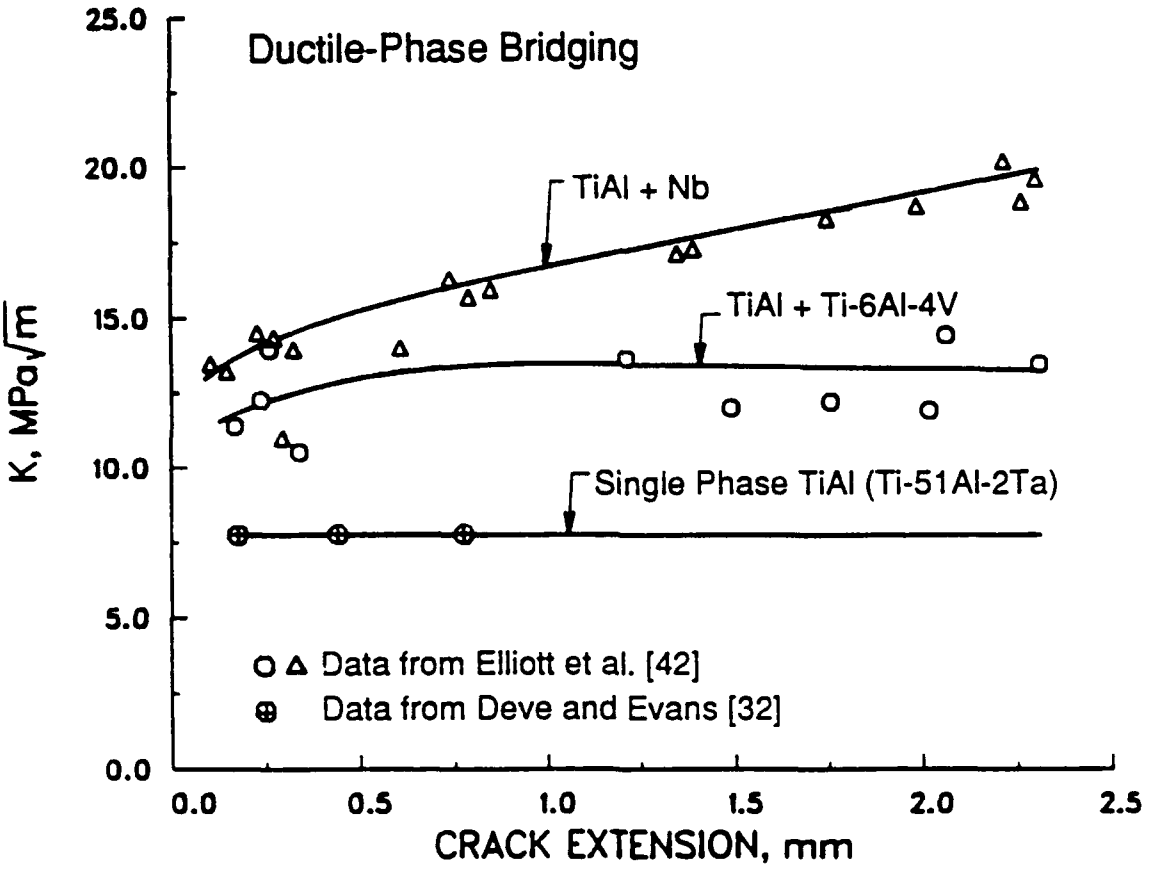

Figure 5. K-resistance curves of TiAl/Nb and TiAl/Ti-6Al-4V particulate composites [42] compared with the single-phase TiAl-alloy, Ti-51Al-2Ta [32].

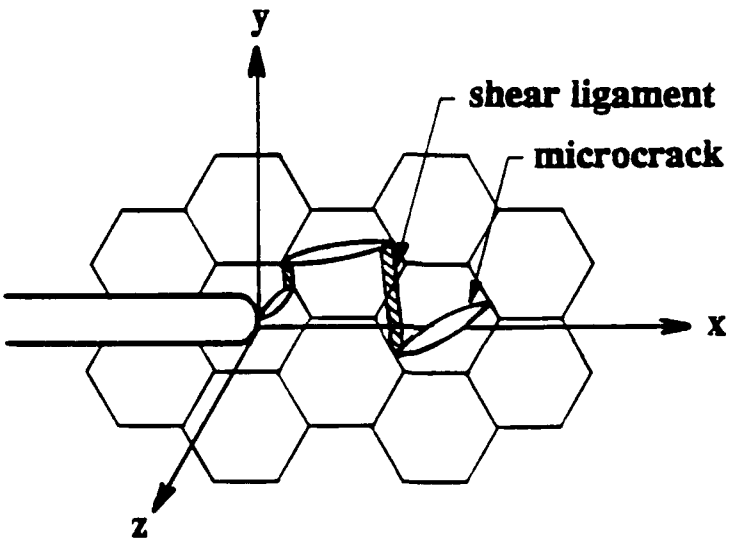

Figure 6. Schematics showing the formation of shear ligaments by mismatched crack planes located ahead of the crack tip in the x-y plane.

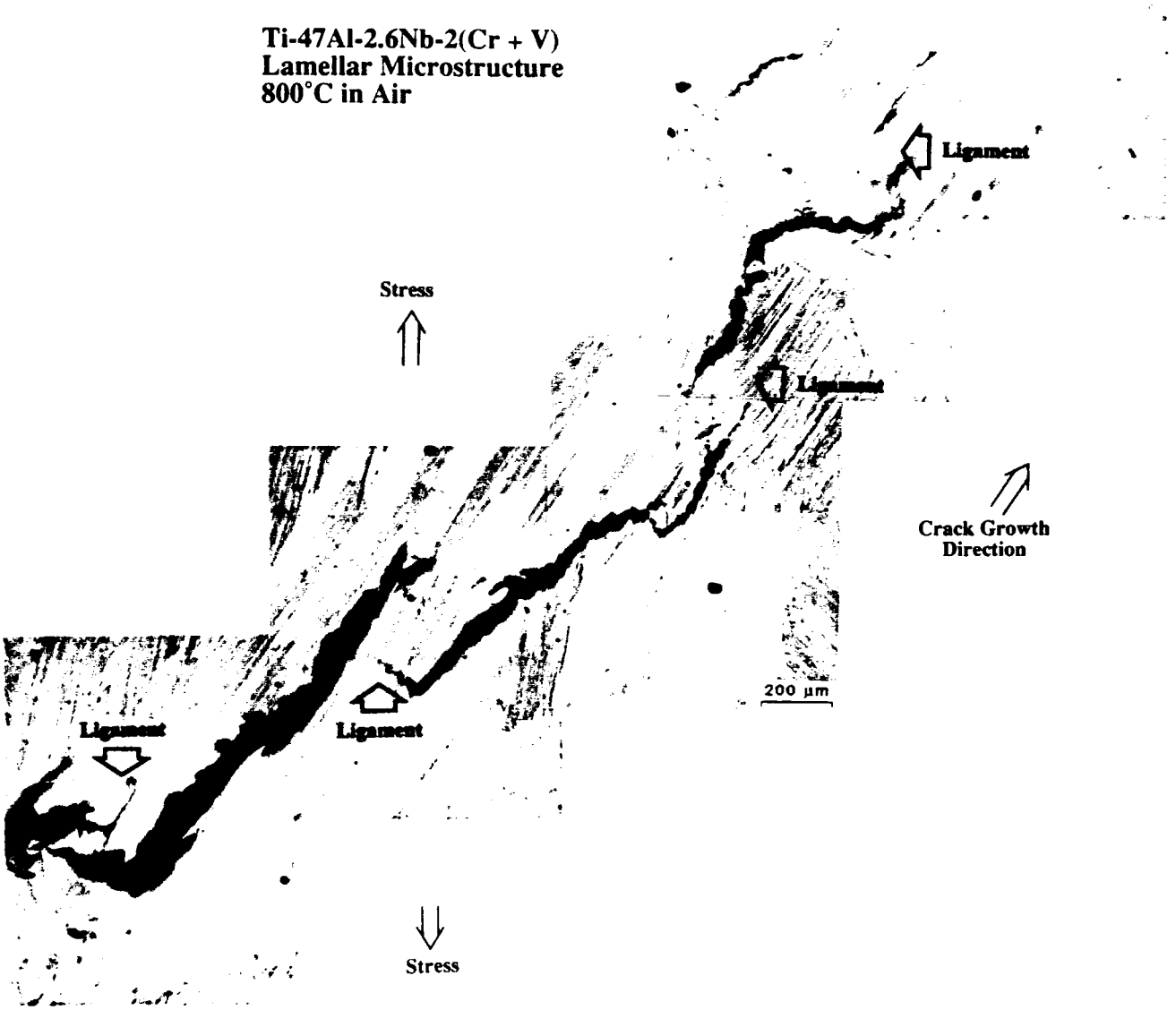

Figure 7. Process zone in the lamellar Ti-47Al-2.6Nb-2(Cr + V) alloy at 800°C showing the presence of five intact ligaments that led to the resistance-curve behavior observed in the material.

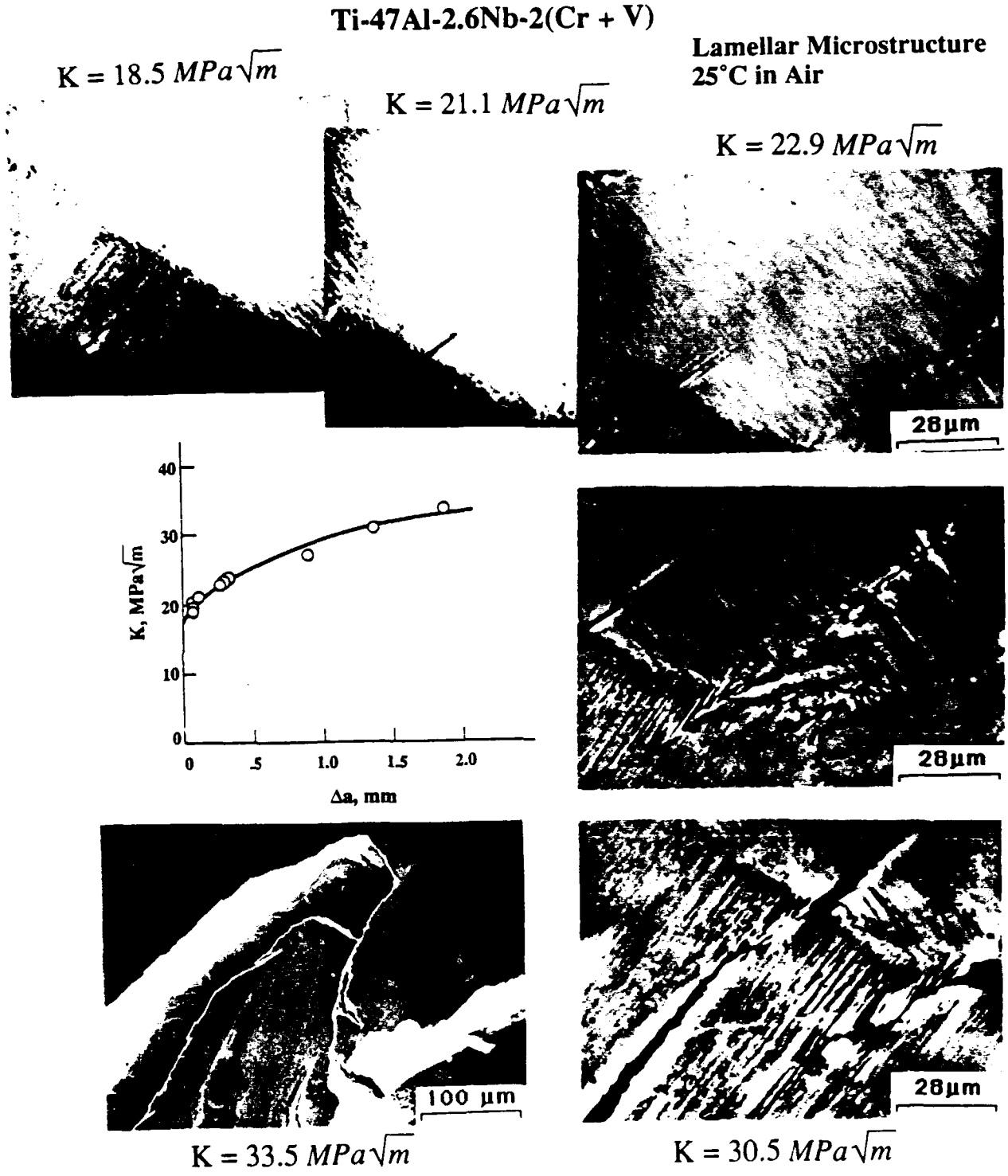

Figure 8. Composite figures showing the process by which shear ligament toughening occurs in a two-phase TiAl-alloy. The shear ligament is formed as the result of the formation of a misaligned microcrack ahead of the crack tip. Fracture of the shear ligament requires additional plastic dissipation leading to a tortuous crack path and a resistance-curve behavior.

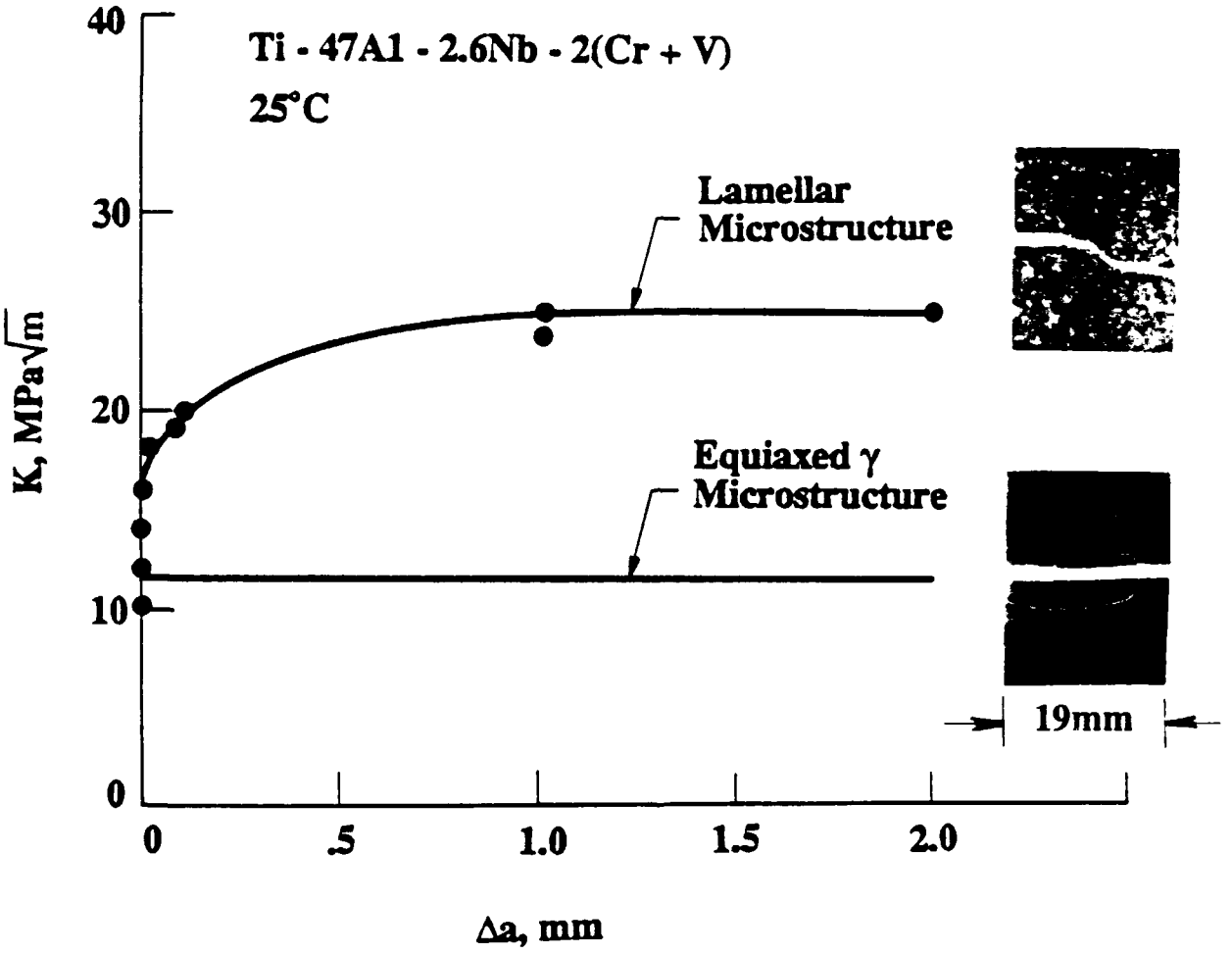

Figure 9. Comparison of K-resistance curves and crack-path tortuosity for the two-phase TiAl-alloy, Ti-47Al-2.6Nb-2(Cr + V), with either a predominantly equiaxed γ grain microstructure or a predominantly lamellar microstructure.

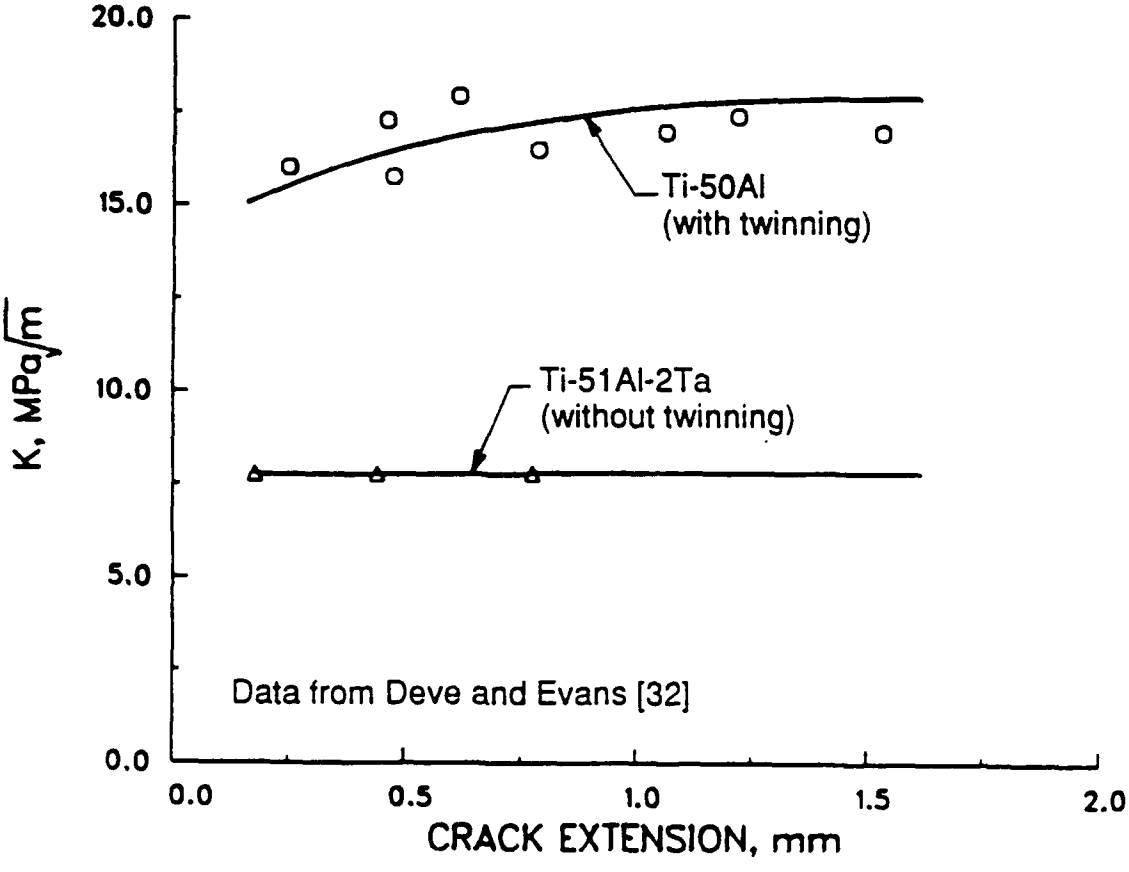

Figure 10. K-resistance curves of single-phase TiAl-alloys with or without twin toughening. Data are from Deve and Evans [32].

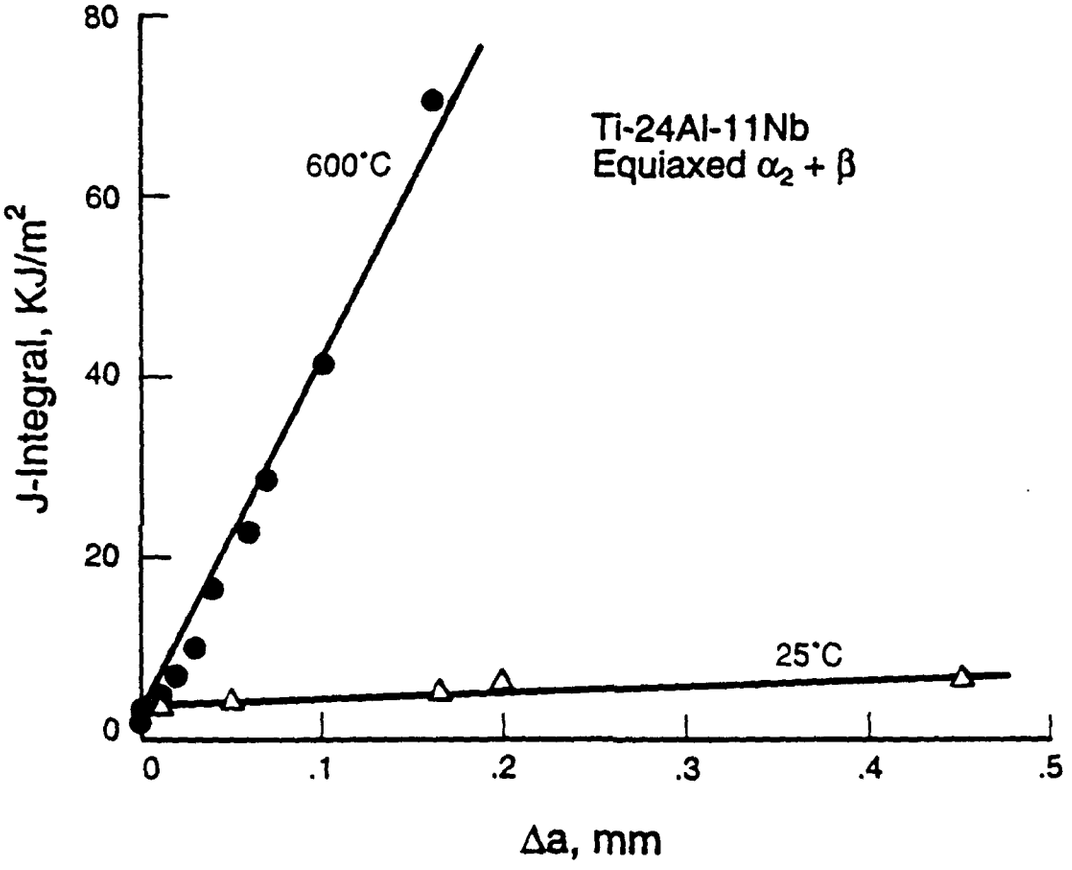

Figure 11. Comparison of J-resistance curves of Ti-24Al-11Nb with the equiaxed $\alpha_2 + \beta$ microstructure for 25 and 600°C.

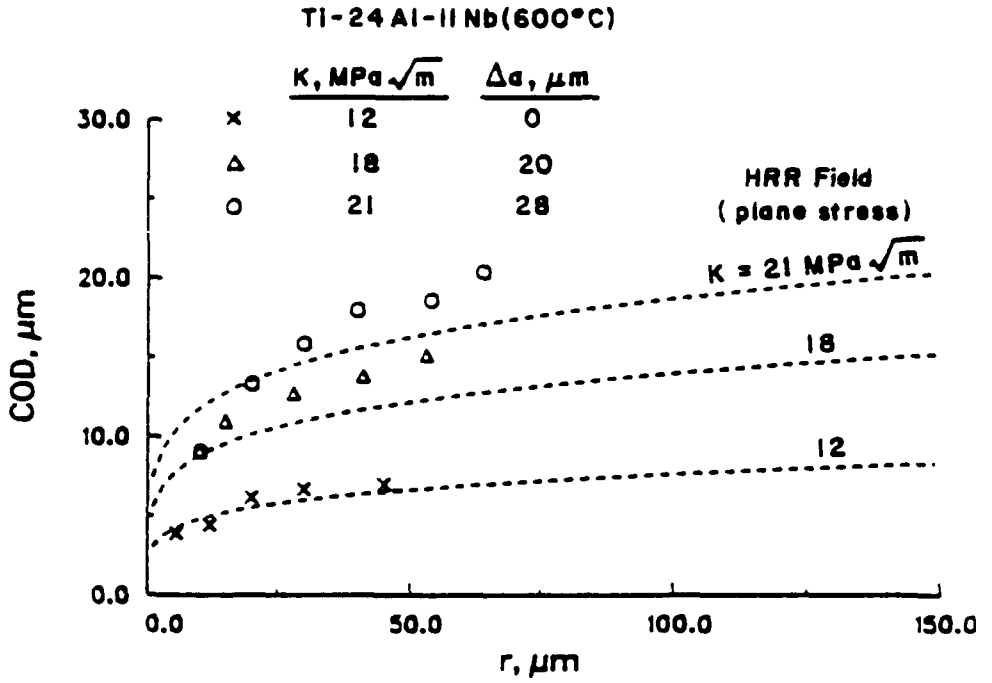

(a)

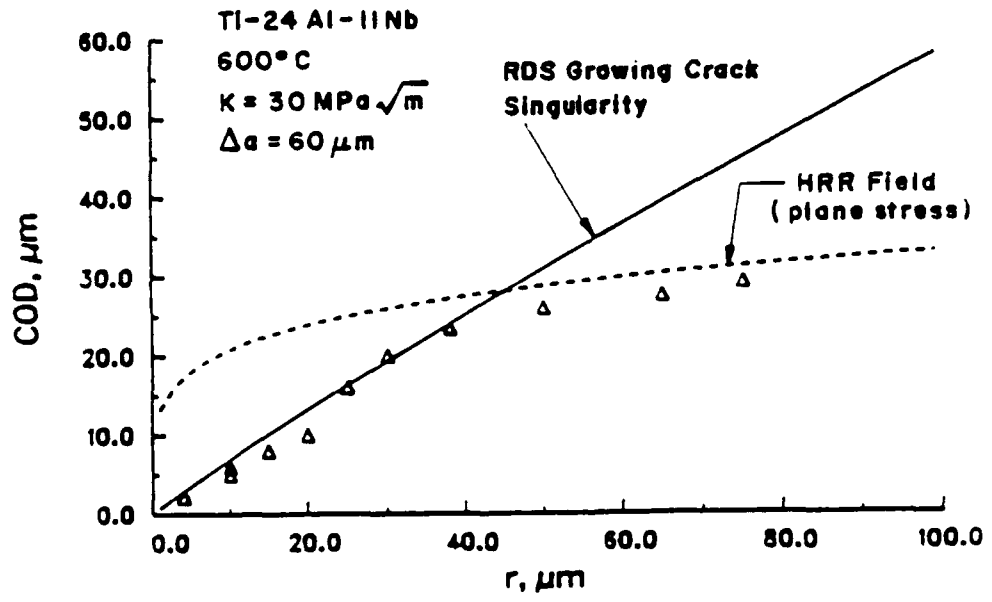

(b)

Figure 12. Measured crack profiles compared to theoretical calculations for various K levels: (a) comparison with the HRR theory for stationary cracks; (b) comparison with the RDS theory for growing cracks in a perfectly plastic material and with the HRR theory.

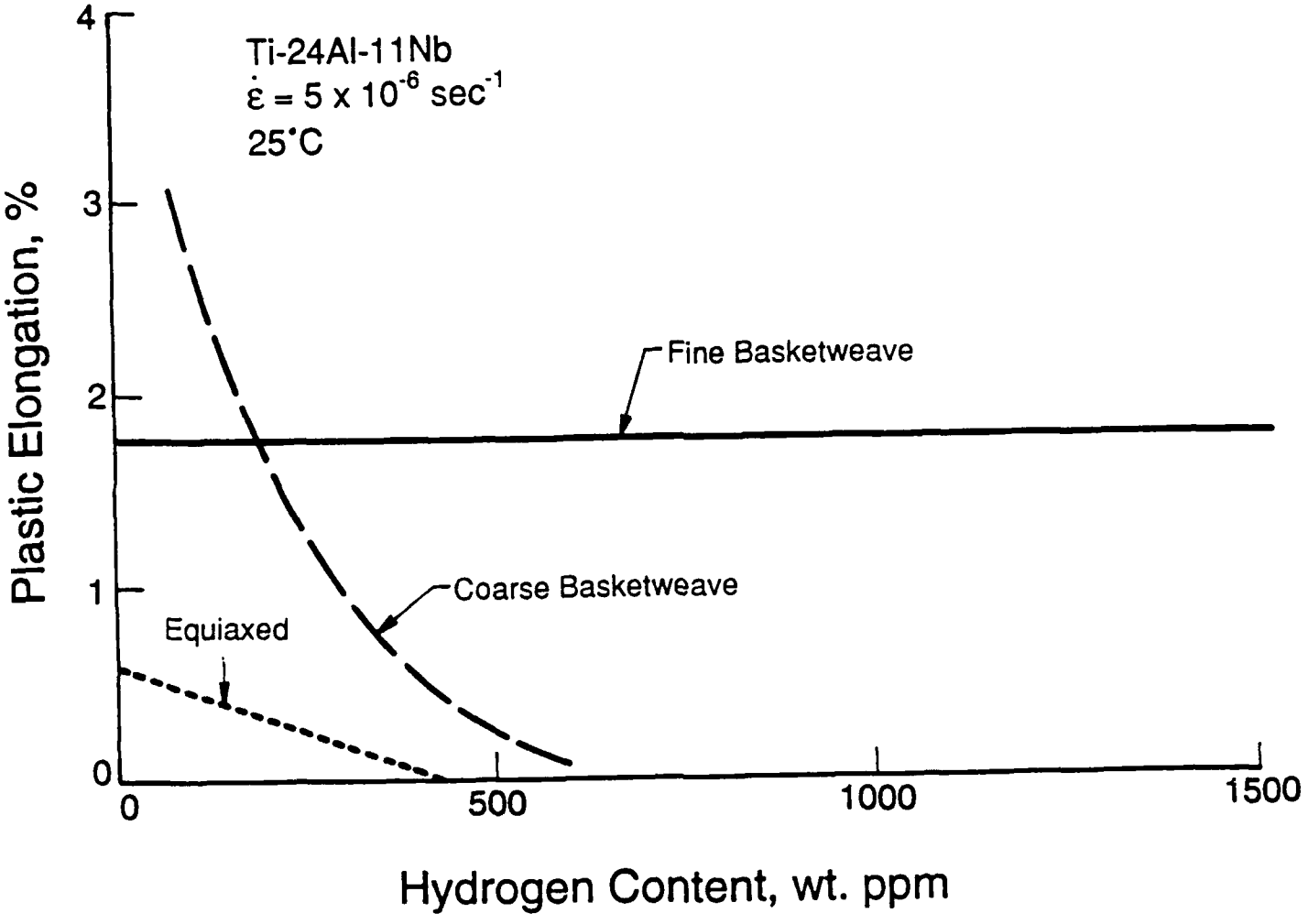

Figure 13. Comparison of plastic elongation as a function of hydrogen contents for Ti-24Al-11Nb with a variety of microstructures. Data from Chan [70].

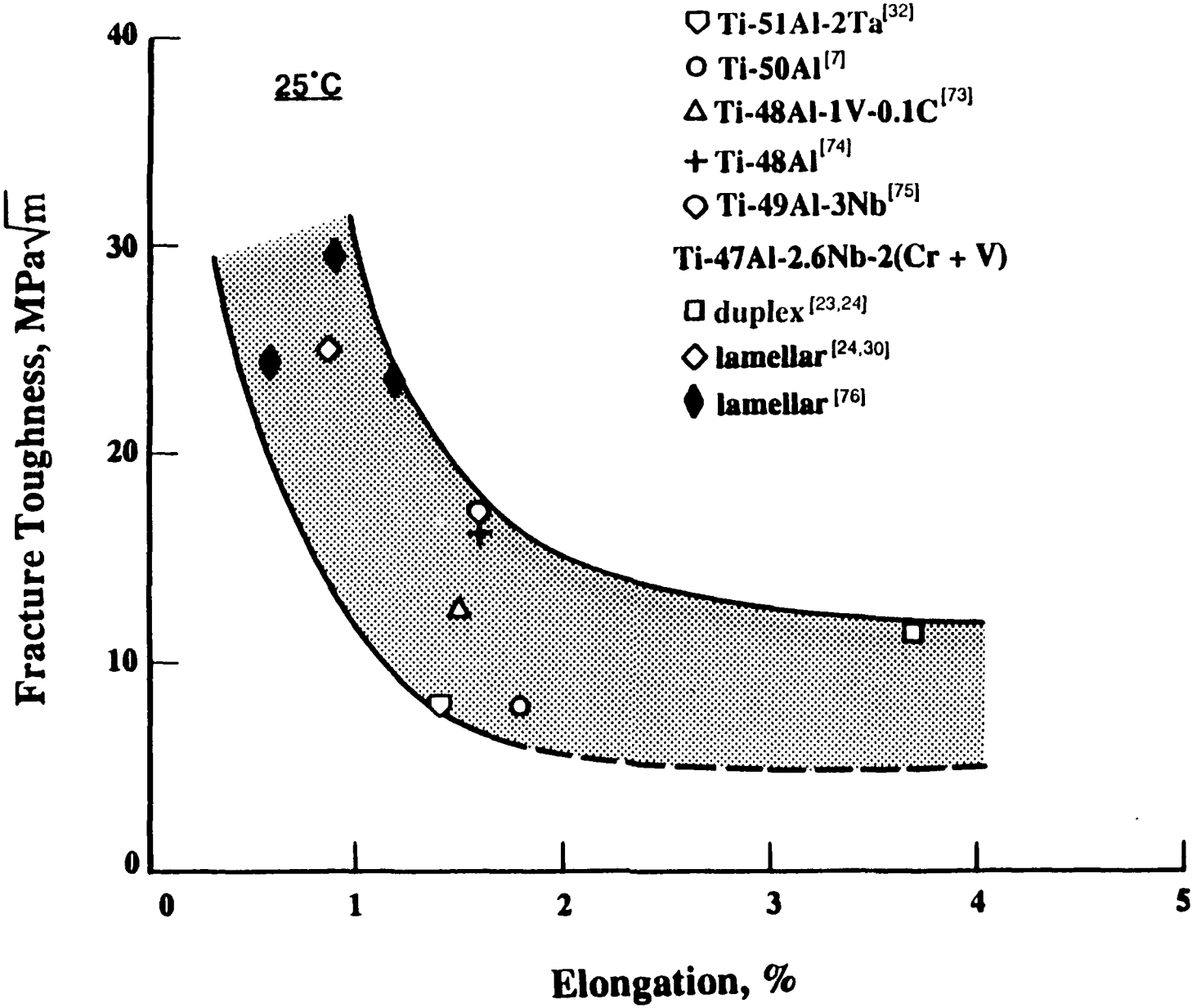

Figure 14. Inverse dependence of fracture toughness on total elongation in TiAl-alloys.

PUBLICATIONS

1. "Fracture and Toughening Mechanisms in an α_2 Titanium Aluminide Alloy," K. S. Chan, *Met. Trans. A*, vol. 21A, 1990, pp. 2687-2699.

2. "Application of Scanning Tunneling Microscopy to Fatigue and Fracture," J. Lankford and M. Longmire, *J. of Mater. Sci.*, vol. 26, 1991, pp. 1131-1136.

3. "Theoretical Analysis of Grain Size Effects on Tensile Ductility," K. S. Chan, *Scripta Metall.*, vol. 24, 1990, pp. 1725-1730.

4. "Fracture Processes in a Two-Phase Gamma Titanium Aluminide Alloy," K. S. Chan and Young-Won Kim, in Microstructure/Property Relationships in Titanium Alloys and Titanium Aluminides, Y-W. Kim and R. R. Boyer, eds., *TMS*, Warrendale, PA, 1991, pp. 179-196.

5. "Micromechanics of Shear Ligament Toughening," K. S. Chan, *Met. Trans. A*, vol. 22A, 1991, pp. 2021-2029.

6. "Influence of Microstructure on Intrinsic and Extrinsic Toughening in an Alpha-Two Titanium Aluminide Alloy," K. S. Chan, *Met. Trans. A*, vol. 23A, 1992, pp. 183-200.

7. "Titanium Alloys: Fatigue Crack Growth Mechanisms and Crack Tip Micromechanics," D. L. Davidson, in Microstructure/Property Relationships in Titanium Alloys and Titanium Aluminides, Y-W. Kim and R. R. Boyer, eds., *TMS*, Warrendale, PA, 1991, pp. 447-461.

8. Fatigue Crack Closure," D. L. Davidson, Engineering Fracture Mechanics, vol. 38, 1991, pp. 393-402.

9. "Micromechanics of Materials Brittle at Ambient Temperature," D. L. Davidson, in Micromechanics of Failure of Quasi-Brittle Materials, S. P. Shah, S. E. Swartz, and M. L. Ming, eds., Elsevier, New York, 1990, pp. 305-314.

10. "Techniques for Microcrack Mechanics," D. L. Davidson, ASTM Workshop on Small Crack Test Methods, J. E. Larsen and J. E. Allison, eds., 1990 (in press).

11. "Fatigue Crack Growth Mechanisms and Mechanics in Metallic and Intermetallic Alloys and Partially Stabilized Zirconia," D. L. Davidson, in Mechanical Fatigue of Advanced Materials, R. O. Ritchie, B. N. Cox, and R. Dauskardt, eds., Met. and Component Eng. Publ. (MCEP), Birmingham, UK, 1991, pp. 33-52.

12. "Influence of Microstructure on Crack-Tip Micromechanics and Fracture Behaviors of a Two-Phase TiAl-Alloy," K. S. Chan and Y-W. Kim, *Met. Trans. A*, 1992 (in press).

13. "Rate and Environmental Effects on Fracture of a Two-Phase TiAl-Alloy," K. S. Chan and Y-W. Kim, *Met. Trans. A*, 1992 (submitted).

14. "Fatigue Crack Growth through the Lamellar Microstructure of an Alloy Based on TiAl at 25 and 800°C," D. L. Davidson and J. B. Campbell, *Met. Trans. A*, 1992 (submitted).

15. "Progress and Limitations in Understanding and Modeling Fracture by Fatigue," D. L. Davidson, in Jaffee Symposium, Electric Power Research Institute, Palo Alto, CA (submitted).

Program Personnel

Name	Title	
Dr. David Davidson	Institute Scientist	
Dr. James Lankford	Institute Scientist	Co-Principal Investigators
Dr. Kwai S. Chan	Principal Engineer	
Mr. Harold Saldana	Staff Technician	
Mr. John Campbell	Senior Technician	
Mr. James Spencer	Sention Technician	

AWARDS

Dr. Kwai S. Chan was the recipient of the Rossiter W. Raymond Memorial Award for 1990 for the paper entitled "Evidence of a Thin Sheet Toughening Mechanism in Al-Fe-X Alloys," which appeared in the January 1989 issue of *Metallurgical Transactions A*. This work was supported by the Air Force office of Scientific Research through Contract No. F49620-86-C-0024. The Raymond Award is an annual award presented by AIME to a young author for the best paper published in one of the ten journals of the four member societies of AIME, which include TMS, SPC, SME, and ISS.

Dr. Kwai S. Chan received the 1991 Alfred Noble Prize from the American Society of Civil Engineers for his paper "Crack Tip Behaviors of Stationary and Growing Cracks in Al-Fe-X Alloys: Part 1. Near-Tip Strain Field," which appeared in the January 1990 issue of *Metallurgical Transactions A*. This work was supported by the Air Force Office of Scientific Research through Contract No. F49620-86-C-0024. This award is presented annually for the best paper published by a member of AIME, ASME, ASCE, IEEE, and WSE.

INTERACTIONS

1. Titanium Review Meeting, Wright-Patterson Air Force Base, Dayton, OH, Jan. 23-25, 1991. K. S. Chan attended the meeting and met with Drs. Y-W. Kim and D. Dimiduk and discussed on-going research on TiAl-alloys and future research efforts on TiAl-base, Cr_2Nb-base, and other intermetallic alloys of interest to the Air Force.

2. TMS Spring Meeting, New Orleans, LA, Feb. 17-21, 1991. K. S. Chan presented a paper entitled "High-Temperature Deformation and Fracture of a Two-Phase γ Titanium Aluminide Alloy."

3. United Technologies Research Center, East Hartford, CT, Apr. 14, 1991. K. S. Chan met with Drs. A. Giamei and D. L. Anton and discussed cooperative research efforts on Cr_2Nb-base and Nb_3Al-base intermetallic alloys.

4. Wright-Patterson Air Force Base, Dayton, OH, May 2, 1991. K. S. Chan visited Dr. Y-W. Kim of Metcut-Materials Research Group at WPAFB and discussed on-going cooperative research efforts on TiAl-alloys. Chan and Kim published three papers jointly on TiAl-alloys.

5. Seminar at University of Texas, Austin, May 21, 1991. K. S. Chan presented a seminar on titanium aluminide alloys and discussed research activities on Cr_2Nb-base intermetallic alloys with Professor J. Tien.

6. TMS Fall Meeting, Cincinnati, OH, Oct. 20-24, 1991. K. S. Chan presented two papers. The first one was entitled "Toughening Mechanisms in Titanium Aluminides," and the second one was entitled "Rate and Environmental Effects on Fracture of a Two-Phase TiAl-Alloy."

7. Wright-Patterson Air Force Base, OH, Jun. 12, 1991. D. L. Davidson visited J. Lassen, D. Miracle, and T. Nicholas. Discussions were held on advanced materials for aerospace applications and a seminar was presented.

8. TMS, Detroit Section Meeting, Mar. 4, 1991. D. L. Davidson presented a seminar entitled "How Fatigue Cracks Grow." A visit to John Allison at Ford Motor Co. was made on Mar. 5, 1991. Part of the discussion concerned the effects of microstructure on the fracture of titanium alloys.